LOW STRESS ACRYLATED HYPERBRANCHED POLYMERS

THÈSE N^{O} 3627 (2006)

PRÉSENTÉE LE 17 NOVEMBRE 2006

À LA FACULTÉ DES SCIENCES ET TECHNIQUES DE L'INGÉNIEUR

Laboratoire de technologie des composites et polymères

SECTION DE SCIENCE ET GÉNIE DES MATÉRIAUX

ÉCOLE POLYTECHNIQUE FÉDÉRALE DE LAUSANNE

POUR L'OBTENTION DU GRADE DE DOCTEUR ÈS SCIENCES

PAR

Lars Erik SCHMIDT

ingénieur en science des matériaux diplômé EPF
de nationalité allemande

acceptée sur proposition du jury:

Prof. H. J. Mathieu, président du jury
Prof. J.-A. E. Månson, Dr Y. Leterrier, directeurs de thèse
Prof. J. Brugger, rapporteur
Prof. S. Lundmark, rapporteur
Prof. M. Sangermano, rapporteur

ÉCOLE POLYTECHNIQUE
FÉDÉRALE DE LAUSANNE

Lausanne, EPFL
2006

Abstract

The objective of this study was to investigate the behavior of highly functional acrylates, during isothermal ultraviolet (UV) curing. The materials included a penta-functional acrylate and two acrylated hyperbranched polymers, one with a stiff polyester core and one with a more flexible polyether core. In particular, the influence of UV intensity and reactive blend composition on structural transitions, such as gelation and vitrification, and on the dynamics of internal stress was considered.

Curing kinetics were studied with photo differential scanning calorimetry. The chemical conversion was analyzed using an autocatalytic model and a criterion for identifying vitrification directly from photocalorimetric experiments was proposed. It was observed that reactive blends containing HBPs had a higher conversion at vitrification, compared to the pure penta-functional acrylate. Strong intensity dependence of the maximum conversion rate and a weak intensity dependence of the ultimate conversion were observed. The latter was found to be controlled by the conversion at vitrification.

The structural transitions and the modulus build-up during UV polymerization were determined by photorheology. A refined data processing algorithm was developed, that allows monitoring the shear modulus over 5 orders of magnitude within a short experimental time scale, with millisecond time resolution. Gelation – the liquid-solid transition – was found to be below 5 % conversion for all acrylates investigated. In contrast, the conversion at vitrification was strongly dependent on the actual monomer and increased with increasing UV intensity. The results of the photo DSC and the photorheology study were synthesized in the form of time-intensity-transformation diagrams.

The dynamics of internal stress and cure shrinkage were studied using beam-bending and an interferometry-based method, respectively. The internal stress of the acrylated HBPs was largely reduced compared to the standard highly functional acrylate monomer. Moreover, in the case of one HBP with a polyester core and a reactive blend of the HBP with the standard highly functional acrylate, the stress reduction was obtained with a combined increase of Young's modulus, which was attributed to retarded modulus build-up and a higher final conversion.

It was found that curing at a lower UV intensity led to earlier vitrification, hence earlier internal stress build-up, but limited maximum conversion thus limited final stress. Curing at a higher intensity led to later stress build-up but higher final stresses.

Polymer microstructures were fabricated from the different acrylates in a photolithographic process and compared to SU-8, an epoxy frequently used for this kind of application. It was shown that the shape accuracy is linked to the process-induced internal stresses: the best result for thick and high aspect ratio microstructures – as used for example for microfluidic devices – was obtained for the acrylated HBP with a polyether core.

Keywords: hyperbranched polymer, UV curing, internal stress, acrylates, gelation, vitrification

Kurzfassung

Zielsetzung dieser Studie war die Untersuchung der Eigenspannungen multifunktionaler Akrylate während der isothermen UV-Polymerisation. Die verwendeten Materialien umfassten ein penta-funktionales Referenzakrylat sowie zwei hochverzweigte Polymere, eines mit einem steifen Polyesterkern und eines mit einem flexibleren Polyetherkern. Der Einfluss der UV-Intensität, des Monomers, der Gelbildung und der Verglasung auf die Entwicklung der Eigenspannungen während der Vernetzung wurde betrachtet.

Der Reaktionskinetik der Polymerisation wurde mittels eines Photo-Differential-Scanning-Kalorimeters gemessen und mit Hilfe eines autokatalytischen Modells analysiert. Ausserdem wurde ein Kriterium zur direkten Identifizierung der Verglasung aus Photo-DSC-Kurven vorgeschlagen. Die Reaktionsgemische, die hochverzweigte Polymere enthielten, wiesen einen höheren Reaktionsumsatz zu Beginn der Verglasung auf. Die maximale Reaktionsgeschwindigkeit stieg mit steigender UV-Intensität stark an. Der finale Reaktionsumsatz stieg ebenfalls, wenn auch weniger stark, und wurde durch den Umsatz zu Beginn der Verglasung kontrolliert.

Gelbildung, Verglasung und die Zunahme des Schermoduls während der UV-Aushärtung wurden mittels Photorheologie ermittelt. Durch einen optimierten Algorithmus zur Datenauswertung wurde es möglich, einen Schermodulanstieg von fünf Grössenordnungen während der raschen UV-Aushärtung mit einer hohen Auflösung (0.001 s) zu messen.

Die Gelbildung aller untersuchten Akrylate lag unterhalb von 5% des Reaktionsumsatzes. Zu Beginn der Verglasung hingegen hing der Reaktionsumsatz stark von dem jeweiligen Monomer ab und erhöhte sich mit steigender UV-Intensität. Die Resultate der photokalorimetrischen und photorheologischen Untersuchung konnten in Zeit-Intensität-Umwandlungs-Diagrammen dargestellt werden.

Durch eine interferometerbasierte Methode wurde die Reaktionsschwindung gemessen. Sie war niedriger für die zwei hochverzweigten Akrylate, verglichen mit dem Referenzakrylat. Die Eigenspannungen, die während der Vernetzung entstanden, wurden aus der Krümmung akrylatbeschichteter Aluminiumlamellen bestimmt. Sie wiesen für die hochverzweigten Acrylate deutlich niedrigere Werte,

verglichen mit dem Referenzmonomer, auf. Für den hochverzweigten Polyester und ein Reaktionsgemisch dessen mit dem Referenzakrylat, wurde die Eigenspannungsreduktion erzielt, ohne an Steifigkeit zu verlieren, was einem verspäteten Steifigkeitsaufbau und einem höheren finalen Reaktionsumsatz zugeschrieben wurde.

Durch stärkere UV Strahlung verzögerte sich die Verglasung, was zu Beginn der Reaktion zu niedrigeren Eigenspannungen führte. Da die höhere UV-Intensität jedoch auch den Reaktionsumsatz steigerte, waren die Eigenspannungen am Ende der Reaktion grösser als bei Proben, die unter schwacher UV-Strahlung ausgehärtet wurden.

In einem photolithographischen Prozess wurden aus den verschiedenen Akrylaten Mikrostrukturen hergestellt und mit denen aus SU-8, einem häufig verwendeten Epoxydharz, verglichen. Die Formtreue nahm mit steigender Eigenspannung ab. Das beste Resultat für dicke Polymerschichten mit hohem Formfaktor, wie sie zum Beispiel für mikrofluidische Systeme verwendet werden, wurde mit dem hochverzweigten Polyether erzielt. Verglichen mit SU-8 war ausserdem die Fabrikationszeit 80% niedriger.

Schlüsselwörter: hochverzweigte Polymere, UV Aushärtung, Eigenspannung, Akrylate, Gelbildung, Verglasung

Acknowledgements

I gratefully acknowledge the provision of funding for the work described in this thesis from the Swiss National Science Foundation.

I would like to thank Prof. Jan-Anders E. Månson, the director of my thesis, for proposing this interesting project at his laboratory and letting my carry out research under such good conditions. I am indebted to Dr. Yves Leterrier, my thesis supervisor, for his excellent scientific guidance and enthusiasm throughout the work.

I am obliged to Prof. Young-Ho Cho at the Korea Advanced Institute of Science and Technology, for hosting me during six month at his laboratory and for letting me profit from his vast experience in micro-engineering. In addition I would like to thank Young-Hyun and Soyeon for the excellent collaboration during that time and their friendship.

I am grateful for excellent support of Dr. Jean-Marc Vesin and Prof. Manfred Wilhelm, for their support with my sometimes difficult rheology measurements.

I must also acknowledge David James, Pia Appelkvist, Eva Gustavsson and Lennart S. Svensson from Perstorp Specialty Chemicals, Dr. André Fuchs from Ciba Specialty Chemicals and Alain Lejeune from GE Silicones for providing me with samples and useful advice throughout this project.

It’s the people who really make the LTC. Thanks’ to those who have left and those who are still here. First of all I should mention my office mates, Chrystèle, Christian and Antonio for always seeing to a good atmosphere.

Without the continuous support of Fabio for solving technical problems, this thesis would have taken three more years. Furthermore I would like to thank Niklas, Steve, Russell, Marlene, Daniel, Eric, Eva, Jerome and Per-Ola, for help with solid mechanics, experiments, proofreading, and the numerous evenings at SAT.

I am also grateful to the members of the IMX workshop for their precise work in building Fabio’s sometimes difficult designs.

A final word should go to those who have done their best to remind me that there is a world outside EPFL and PhD, my old friends, Thomas, Marc and Jörg, and, of course, my parents.

Thanks.

Table of Contents

1 Introduction

During the last decades there has been an increasing demand for functional integration and miniaturization. Especially in the biotechnology domain, there is an increasing need for small structures which are easy to fabricate: Labs-on-a-chip are already used in the pharmaceutical industry for drug discovery and a strong demand for blood-based diagnostics, pathogen detection, and water-safety monitoring is predicted [1]. Other examples of functional integration are organic electronics [2, 3], such as flexible displays, and microelectromechanical systems [4].

A well known problem in these multi-material assemblies is internal or residual stress. This originates, for example, from shrinkage during curing of crosslinked polymers if the polymers are subjected to temperature gradients, and if they are in contact with a rigid material, such as the substrate of a thin film, the reinforcement in a composite, or the encapsulation of an electronic component. In organic coatings for example, these stresses may cause defects such as cracking, bending and delamination [5, 6]. In dental restoration shrinkage provokes tooth deformation, debonding of the filling, enamel crack propagation, and post-operative sensitivity [7]; moreover, it was found to provoke secondary caries in 25% of cases [8]. In bone cement, which is a mixture of liquid methyl methacrylate with powdered polymethyl methacrylate

polymer, the shrinkage during thermal crosslinking leads to porosity at the bone/bone-cement and bone-cement/implant interfaces. Moreover, this phenomenon reduces the ability to transfer stress, which may, for example, lead to loosening of artificial hip joints [9-11]. In addition, in microelectronic packaging internal stresses generated during the assembly process cause delamination or bending of the entire assembly [4, 12] and are responsible for up to three quarters of failures in working parts [13].

As illustrated in Figure 1-1 internal stress is determined by the evolution of the cure shrinkage and the increase of the elastic modulus during curing: In a “high stress” material there is a significant increase in modulus at a low conversion level, that is a low level of shrinkage, and shrinkage proceeds in a stiff material. The development of a “low stress” material should be based on the following property combination: reduced process-induced shrinkage and delayed modulus build-up to high conversion level.

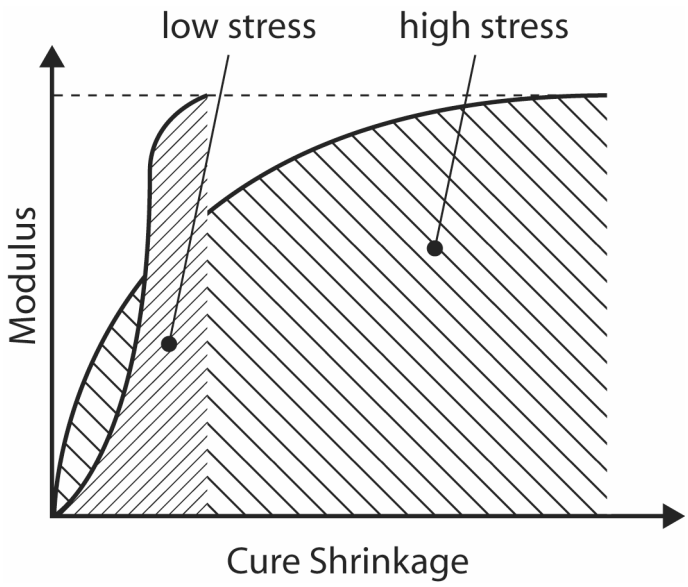

Figure 1-1 Schematic representation of the approach towards low-stress polymers.

Different approaches have been evaluated for shrinkage reduction in crosslinking polymers, for example the introduction of low profile additives [14, 15] and the use of inorganic fillers. To further reduce the stress in the matrix, UV-curing was developed as an alternative to thermal curing, since not only the contraction due to the network formation, but also thermal contraction after cool-down from the reaction temperature is responsible for shrinkage. Other benefits of UV-curing are the absence of hazardous solvents and the short cycle times. Currently, UV curing is mainly used in adhesives, coatings, and dental implants [16]. A recent attempt,

described in very few studies, is the use of hyperbranched polymers (HBP) as modifiers for the polymer matrix [17]: Klee et al. [18] used hyperbranched polymers with methacrylate end groups as a matrix material for dental applications. They obtained a volume shrinkage of 0.5-1.5% compared to 2.5-4% for commercially available dental composites. Kou et al. [19] blended a commercially available bisphenol-A epoxy acrylate oligomer with a hyperbranched acrylated aromatic polyester. This reduced the linear polymerization shrinkage from 10.5 to 2%. For thermosetting similar effects have already been observed. Eom et al. [20] also obtained a remarkable reduction of process-induced stress, by a factor of three, for a tetra glycidyl-4, 4'- diaminadiphenyl-methane epoxy formulation containing 10% epoxy-functionalysed polyester HBP, compared to the pure resin.

Further advantages of incorporating HBPs in crosslinking formulations include increasing toughness [21] without compromising resin stiffness and glass transition temperature [22]. Moreover, depending on the shell chemistry, the miscibility of the HBP-modifier with the matrix could be tailored [23, 24], to control the onset of reaction induced phase separation hence the morphology of the cured thermoset [25].

Recent studies demonstrate the efficiency of HBPs to achieve exfoliation of clay in polymer-nanocomposite formulations, both for thermoset matrices [26] and photosetting polymers [27].

1.1 Objective

The aim of this study is to reduce residual stresses in crosslinked polymers and to understand how different processing parameters influence internal stresses, in order to optimize materials selection and provide solutions with good long-term stability. Mainly acrylate systems are examined, characterized by considerable shrinkage. The focus will be on highly functional acrylates such as di-pentaerythritol hexaacrylate (DPHA, volume shrinkage 17% [28]).

UV curable hyperbranched polymers offer interesting possibilities for improving coating properties. However there are still unanswered questions: Little is known about the influence of UV intensity on overall shrinkage. It has been well established that shrinkage before the liquid to solid transition (gelation) does not cause internal stresses [29], and that shrinkage occurring after vitrification contributes most to internal stresses [30-33]; however, it is very difficult to detect gelation and vitrification in fast curing acrylates [34]. Detection with photorheology is possible, but rather challenging, due to the fast progressing reaction, especially in the case of

low viscosity acrylates [35-37]; therefore it would be an asset to directly identify it from kinetic profiles.

As discussed above, especially for cheap disposable micro-fluidic devices, there will be an increasing demand in the future. However, there is not yet a well-established range of polymers enabling the cheap production of ultra-thick polymer microstructures for these applications.

To address these questions, a systematic approach was used, as depicted in Figure 1-2. The approach consists of the examination of a range of materials with different internal stress levels and understanding what causes these stresses, and how they can be reduced. The investigation is based, on the one hand, on photocalorimetry in order to model network conversion as a function of time and UV intensity, and on the other hand, on photorheology, in order to identify structural transitions. The results from the two approaches are then combined into a time-intensity-transformation diagram, a processing map, for the optimization of UV curing.

The different materials will be used to fabricate polymer microstructures in a photolithographic process, and these will be compared to microstructures fabricated from the frequently used epoxy, SU-8. For this purpose, an understanding of gelation, vitrification and process-induced internal stresses is important: At a conversion above gelation the microstructure will resist the developer solution, and vitrification and internal stresses will control the shape accuracy of the obtained structures. Especially for high aspect ratio structures, internal stresses will lead to large deformations.

1.2 Outline

This report starts with a literature review of important aspects of the work (Chapter 2), such as the evolution of internal stresses in solidifying coatings, radiation curing, kinetics of photopolymerization, and dendritic polymers and their implementation in crosslinked polymers. This is followed by a detailed description of the materials and methods (Chapter 3). The results obtained for the kinetics of photo-polymerization of HBP (Chapter 4), on photorheology (Chapter 5) a novel method for analyzing photocuring, were synthesized into a time-intensity-transformation diagram. The dynamics of internal stress and shrinkage are addressed in Chapter 6, and discussed, in the light of the results from the two preceeding chapters. Based on this knowledge low-stress polymer microstructures were developed as detailed in Chapter 7, and compared with the standard negative photoresist SU-8.

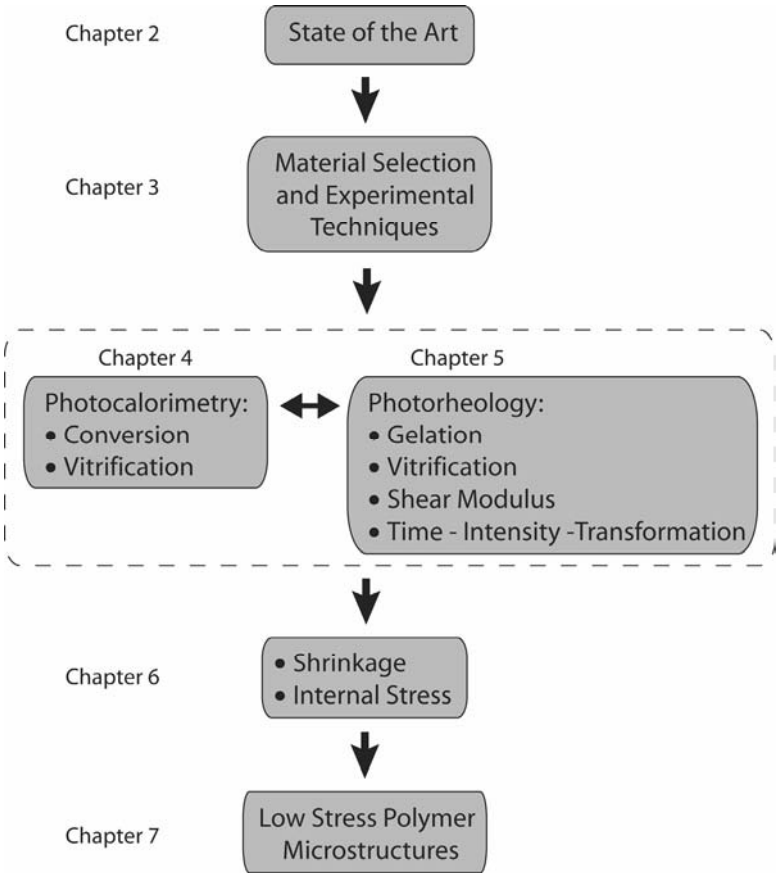

Figure 1-2 Schematic structure of the thesis.

1.3 References

1. Thilmany, J., *Think small: Lab-on-a chip technology shrinks the biological laboratory to the microscale and expands the potential for future applications.* EMBO Reports, 2005. **6**(10): p. 913-916.
2. Lewis, J.S. and M.S. Weaver, *Thin-film permeation-barrier technology for flexible organic light-emitting devices.* IEEE Journal of Selected Topics in Quantum Electronics, 2004. **10**(1): p. 45-57.
3. Leterrier, Y., L. Médico, F. Demarco, J.-A.E. Månson, U. Betz, M.F. Escolà, M. Kharrazi Olsson, and F. Atamny, *Mechanical integrity of transparent conductive oxide films for flexible polymer-based displays.* Thin Sold Films, 2004. **460**: p. 156-166.
4. Spearing, S.M., *Materials issues in microelectromechanical systems (MEMS).* Acta Materialia, 2000. **48**: p. 179-196.
5. Sato, K., *The internal stress of coating films.* Progress in Organic Coatings, 1980. **8**: p. 143-160.
6. Negele, O. and W. Funke, *Internal stress and wet adhesion of organic coatings.* Progress in Organic Coatings, 1996. **28**: p. 285-289.
7. Tantbirojn, D., A. Versluis, M.R. Pintado, R. DeLong, and W.H. Douglas, *Tooth deformation patterns in molars after composite restoration.* Dental Materials, 2004. **20**: p. 535-542.
8. Condon, J.R. and J.L. Ferracane, *Assessing the effect of composite formulation on polymerization stress.* Journal of the American Dental Association, 2000. **131**: p. 497-503.

9. Wijn, J.R.d., F.C.M. Driessens, and T.J.J.H. Slooff, *Dimensional behavior of curing bone cement masses.* Journal of Biomedical Materials Research, 1975. **6**: p. 99-103.
10. Orr, J.F., N.J. Dunne, and J.C. Quinn, *Shrinkage stresses in bone cement.* Biomaterials, 2003. **24**: p. 2933-2940.
11. Roques, A., M. Browne, A. Taylor, A. New, and D. Baker, *Quantitative measurement of the stresses induced during polymerization of bone cement.* Biomaterials, 2004. **25**: p. 4415-4424.
12. Sham, M.-L. and J.-K. Kim, *Evolution of residual stresses in modified epoxy resins for electronic packaging applications.* Composites Part A - Applied Science and Manufacturing, 2004. **35**: p. 537-546.
13. Morrissey, A., G. Kelly, and J. Alderman, *Selection of materials for reduced stress packaging of a microstructure.* Sensors and Actuators A-Physical, 1999. **74**: p. 178-181.
14. Atkins, K.E., *Low-profile additives: shrinkage control mechanisms and applications*, in *Sheet Molding Compounds : Science and Technology*, H.G. Kia, Editor. 1993, Carl Hanser Verlag: Munich. p. 49-78.
15. Bulliard, X., V. Michaud, and J.-A.E. Månson, *Low-profil mechanisms in a PVAc/Polyester Blend.* Polymer Engineering and Science, 2006. **46**: p. 303-313.
16. Davidson, S., *Exploring the science, technology and applications of U.V. and E.B. curing*. SITA Series In Surface Coatings Technology. 1999, London, UK: SITA Technology Limited. 290.
17. Claesson, H., E. Malmström, M. Johansson, A. Hult, M. Doyle, and J.-A.E. Månson, *Rheological behaviour during UV-curing of a star-branched polyester.* Progress in Organic Coatings, 2002. **44**: p. 63-67.
18. Klee, J.E., C. Schneider, D. Hölter, A. Burgath, H. Frey, and R. Mülhaupt, *Hyperbranched polyesters and their application in dental composites: monomers for low shrinking composites.* Polymers for Advanced Technologies, 2001. **12**(6): p. 346-354.
19. Kou, H.-G., A. Asif, and W.-F. Shi, *Hyperbranched acrylated aromatic polyester used as a modifier in UV-curable epoxy acrylate resins.* Chinese Journal of Chemistry, 2003. **21**: p. 91-95.
20. Eom, Y., L. Boogh, V. Michaud, and J.-A.E. Månson, *Internal stress control in epoxy resins and their composites by material and process tailoring.* Polymer Composites, 2002. **23**(6): p. 1044-1056.
21. Mezzenga, R., L. Boogh, and J.-A.E. Månson, *A review of dendritic hyperbranched polymer as modifiers in epoxy composites.* Composites Science and Technology, 2001. **61**: p. 787-795.
22. Boogh, L., B. Pettersson, and J.-A.E. Månson, *Dendritic hyperbranched polymers as toughеners for epoxy resins.* Polymer, 1999. **40**: p. 2249-2261.
23. Plummer, C.J.G., R. Mezzenga, L. Boogh, and J.-A.E. Månson, *Phase separation in epoxy resing-reactive dendritic hyperbranched polymer blends.* Polymer Engineering and Science, 2001. **41**: p. 43-52.
24. Mezzenga, R., A. Luciani, and J.-A.E. Månson, *Phase separation and gelation of epoxy resin/hyperbranched polymer blends.* Polymer Engineering and Science, 2002. **42**(2): p. 249-257.
25. Mezzenga, R., C.J.G. Plummer, L. Boogh, and J.-A.E. Månson, *Morphology build-up in dendritic hyperbranched polymer modified epoxy resins: modelling and characterization.* Polymer, 2000. **42**: p. 305-317.

26. Rodlert, M., C.J.G. Plummer, L. Garamszegi, Y. Leterrier, H.J.M. Grünbauer, and J.-A.E. Månson, *Hyperbranched polymer/montmorillonite clay nanocomposites.* Polymer, 2004. **45**: p. 949-960.
27. Fogelström, L., P. Antoni, E. Malmström, and A. Hult, *UV-curable hyperbranched nanocomposite coatings.* Progress in Organic Coatings, 2006. **55**: p. 284-290.
28. Klang, J.A., *Radiation curable hyperbranched polyester acrylates*. 2006, Sartomer Company, Inc.: Exton, Pennsylvania. p. 1-7.
29. Lange, J., S. Toll, J.-A.E. Månson, and A. Hult, *Residual stress build-up in thermoset films cured above their ultimate glass transition temperature.* Polymer, 1995. **36**(16): p. 3135-3141.
30. Payne, J.A., *Stress Evolution in Solidifying Coatings*, in *Department of Chemical Engineering and Materials Science*. 1998, University of Minnesota: Twin Cities.
31. Wen, M., L.E. Scriven, and A.V. McCormick, *Differential scanning calorimetry and cantilver deflection studies of polymerization kinetics and stress in ultraviolet curing of multifunctional (meth)acrylate coatings.* Macromolecules, 2002. **35**: p. 112-120.
32. Lange, J. and J.-A.E. Månson, *Build-up of structure and viscoelastic properties in epoxy and acrylate resins cured below their ultimate glass transition temperature.* Polymer, 1996. **37**(26): p. 5859-5868.
33. Lange, J., S. Toll, J.-A.E. Månson, and A. Hult, *Residual stress build-up in thermoset films cured below their ultimate glass transition temperature.* Polymer, 1997. **38**(4): p. 809-815.
34. Lange, J., N. Altmann, C.T. Kelly, and P.J. Halley, *Understanding vitrification during cure of epoxy resins using dynamic scanning calorimetry and rheological techniques.* Polymer, 2000. **41**: p. 5949-5955.
35. Lee, S.S., A. Luciani, and J.-A.E. Månson, *A rheological characterisation technique for fast UV-curable systems.* Progress in Organic Coatings, 2000. **38**: p. 193-197.
36. Steeman, P.A.M., A.A. Dias, D. Wienke, and T. Zwartkruis, *Polymerization and network formation of UV-curable systems monitored by hyphenated real-time dynamic mechanical analysis and near-infrared spectroscopy*. Macromolecules, 2004. **37**: p. 7001-7007.
37. Botella, A., J. Dupuy, A.-A. Roche, H. Sautereau, and V. Verney, *Photo-rheometry/NIR spectrometry: An in situ technique for monitoring conversion and viscoelastic properties during photopolymerization.* Macromolecular Rapid Communications, 2004. **25**: p. 1155-1158.

2 State of the Art

UV radiation curing has been successfully used to produce, within seconds, weathering-resistant protective coatings, high-resolution relief images, glass laminates and nanocomposite materials [1]. Acrylates are the photocuring materials that are most widely used for applications such as coating and printing purposes. Compared to their low functional counterparts, highly functional acrylates have the advantage that they cure at a lower light dose, which allows lower photoinitiator concentrations, weaker light sources and faster line speeds [2]. They also have high ultimate glass transition temperatures and form stronger, more impermeable coatings. However their drawback is the extensive amount of polymerization shrinkage [3], leading to high levels of internal stresses and resulting problems in dimensional stability, to defects such as cracking and delamination [4, 5] and to surface wrinkles [6].

2.1 Shrinkage and Internal Stresses in Polymers

Internal or residual stresses in materials are a consequence of shrinkage. Shrinkage occurs, for example, during solidification of polymer coatings as a result of solvent evaporation, phase transformations, chemical reactions and coalescence [7], as illustrated in Figure 2-1.

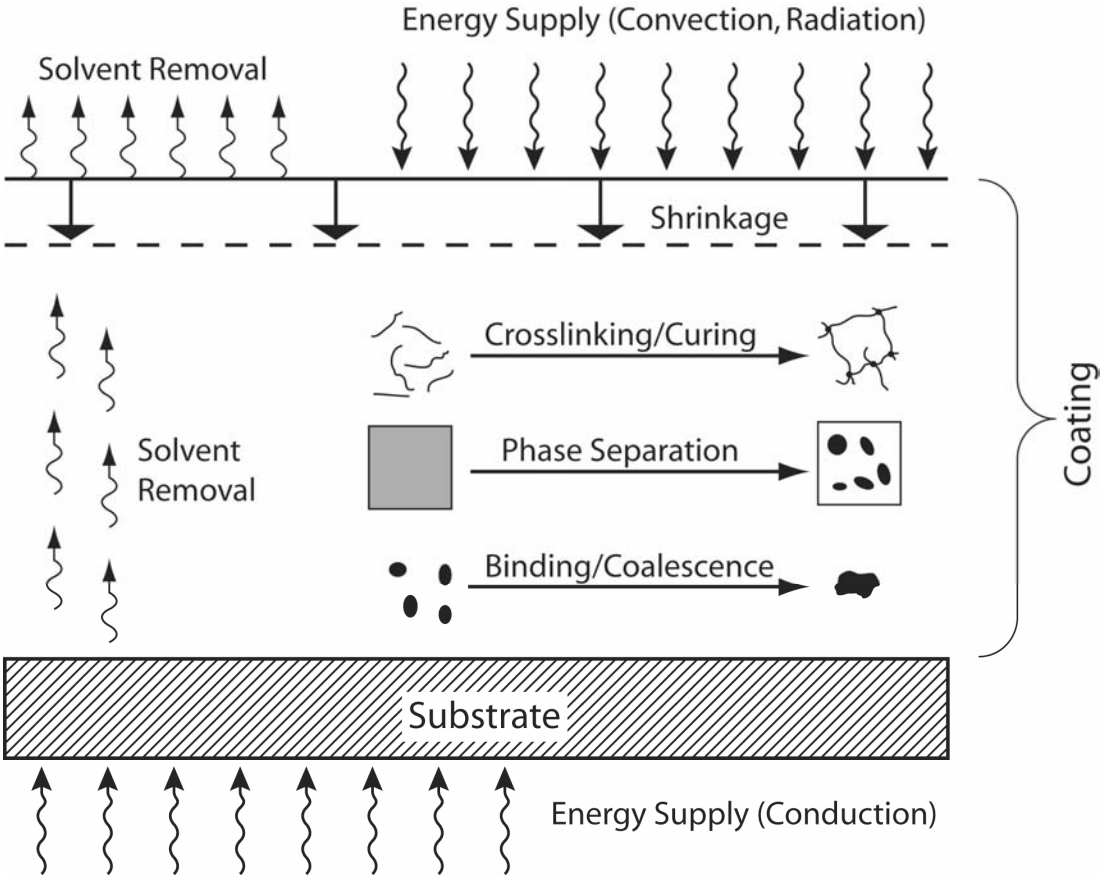

Figure 2-1 Mechanisms contributing to shrinkage during processing of a coating. Redrawn from Payne [7].

If the material undergoing one or several of the above mentioned transitions, is not allowed to shrink freely, but is constrained, for example by a rigid substrate or reinforcement [8], the shrinkage will cause internal stresses to arise.

In the case of polymeric coatings especially, the shrinkage resulting from solvent removal [9] and crosslinking are relevant. Once the relaxation times of the forming polymer become too long to follow the volume change generated by evaporation of the solvent, the volume departs from equilibrium [7]. The amount of internal stress created during solidification will therefore not only depend on the material contraction but also on the rate of contraction and material relaxation.

A similar situation can be encountered for crosslinking coatings: The internal stress depends not only on shrinkage but also on the rate of contraction which, in turn, is strongly dependent on the rate of conversion of the monomer's functional groups. De Boer et al. [10] developed an interferometry-based method for simultaneous measurement of linear shrinkage (that is, the unconstrained shrinkage in the thickness direction of a curing film) and conversion during photopolymerization. For a dimethacrylate monomer, they found that the linear shrinkage increased linearly with

conversion at the beginning of the reaction, whereas at a certain conversion a change of the slope occurred (Figure 2-2). They attributed this change to the onset of vitrification, where the polymer passes from a gel to a glassy state. However vitrification in chain crosslinking systems is not fully understood. There are strong indications that vitrification in chainwise polymerizing systems, such as acrylates, is not a distinct event but a gradual process happening over a wide conversion range, mainly due to the inhomogeneous network formation of chain-wise reacting systems [11]. Therefore vitrification is generally difficult to detect and there is a lack of highly sensitive techniques, which would enable key structural features such as gelation and vitrification to be determined, and the influence of UV intensity and temperature to be investigated.

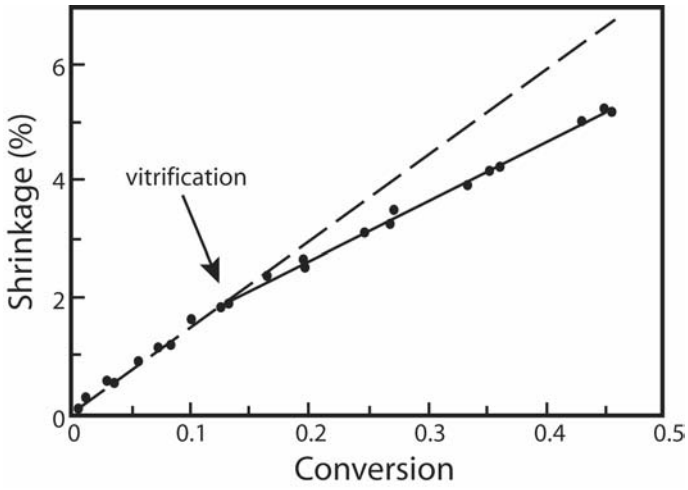

Figure 2-2 Relationship between shrinkage and conversion during the photopolymerization of hydroxy-ethyl-bisphenol A-dimethacrylate (adapted from de Boer et al. [10]).

From the point where vitrification starts, the shrinkage is no longer able to keep up with conversion, and the resulting excess volume allows additional mobility for the reactive chain ends [12]. The faster the rate of polymerization, for example due to higher UV light intensities or temperatures, the more temporary excess volume is formed, leading to higher final maximum attainable conversions and crosslink densities. An understanding of vitrification is crucial to reducing internal stresses, most of which are are formed after the material vitrifies [13].

When a thermoset system is cured at an elevated temperature, it is not only chemical shrinkage, but also thermal contraction during cool-down that contributes to the overall internal stress [14]. In the case of a thin coating cured above its ultimate glass transition temperature and thence not vitrifying during curing, the in-plane

internal stress is written as the sum of a cure shrinkage stress and a thermal stress [15]:

$$\sigma(t) = 2\int_{t_g}^{t_c} G\frac{\partial c}{\partial t}dt + 2\int_{T_c}^{T_f} G\left(\alpha_s + \frac{\partial c}{\partial T}\right)dT \qquad (2.1)$$

where G is the shear modulus, $c(t)$ is the thickness contraction or out of plane strain, and α_s is the linear thermal expansion coefficient. The limits t_g and t_c are the times at gelation and completion of cure. Before the material gels, the material can shrink freely since the coating still behaves like a liquid. The limits T_c and T_f are the temperatures during cure and at the end of the cool-down. In the case of radiation curable coatings polymerized isothermally at T_f, the RHS term of the above equation is usually small, and would result from exothermic effects. The thickness contraction is linked to substrate dilatation and free linear shrinkage, S_L, of the coating having a Poisson's ratio ν_c, throughout:

$$dc = 2\frac{\nu_c}{1-\nu_c}\alpha_s dT + \frac{1+\nu_c}{1-\nu_c}dS_L \qquad (2.2)$$

In the case of curing below the ultimate T_g, the coating first gels and then vitrifies. As a consequence the relaxation times increase significantly, exceeding the experimental time scale. Lange et al. stated that if the material does not follow a complex thermal history, the relaxation behavior can be modeled by choosing a simple Maxwell model with one single relaxation time [16]. As an approximation for the internal stress level for coatings cured below or above their ultimate T_g, the following formula was proposed [16]:

$$\sigma = G_r c_c \qquad (2.3)$$

where G_r is the rubbery modulus, and c_c the thickness contraction after gelation until the end of cure. This approximation was confirmed for crosslinked epoxies and moderately crosslinked acrylates; for very densely crosslinked acrylates, the obtained values were far too high [16].

The volumetric polymerization shrinkage of different materials are listed in Table 2-1. The volumetric shrinkage is determined by the specific reaction mechanisms. Ring-opening in epoxies for example leads to lower shrinkage compared to acrylates, since the two reactive groups have to approach each other less for the covalent bond to be formed.

Table 2-1 Overview of polymerization shrinkage for different materials.

Material	Volumetric Shrinkage	Reference
TGDDM (Epoxy)	~ 10 %	[17]
DPHA (Acrylate)	~ 18 %	[18]
Polydimethylesiloxane	up to 15 %	[19]
Thiol-ene	up to 7 %	[20]

2.2 Strategies for Reducing Shrinkage and Internal Stress

Different approaches exist to reduce shrinkage and internal stress in crosslinking polymers. One possibility, in the case of thermosetting polymers, is to introduce so-called low profile additives (LPA) which do not take part in the reaction and are soluble in the thermoset resin. When crosslinking proceeds, the LPAs become incompatible with the resin and phase separate. Gelation will start in the resin-rich phase and overall macroscopic gelation will be retarded [21, 22].

Secondly, choosing appropriate curing conditions, including curing and cooling rates [23], was shown to influence the internal stress level. Plepys and Farris [24] demonstrated that a temperature ramp cure resulted in lower internal stresses, compared to an isothermal cure. They explained this by the fact that the thermal expansion of the resin during the cure ramp would counteract the polymerization shrinkage. A substantial effort was also made to analyse [25] and model [26-28] internal stresses in composite processing. It was found that skin-core stresses are especially critical leading to voids and cracks.

Thirdly the introduction of inorganic fillers reduces overall polymerization shrinkage. However, little is known about how a dispersed inorganic phase influences internal stress. Sham and Kim [29] incorporated 50 vol.-% of fused silica particles into an epoxy resin, and obtained a stress reduction of 12.5 %. An opposite trend was found by Condon and Ferracane [30] in their work on the influence of filler content on the internal stress level. A linear correlation of internal stress and filler content was explained by an increasing Young's modulus with increasing filler content. The same authors studied the influence of silane-sizings of the nanofillers on the internal stress level. The lowest internal stresses occurred for non-treated nanofiller, which has only a weak adhesion to the matrix. For nanofillers treated with an inert silane sizing, providing improved adhesion, the internal stresses were already higher, and these further increased for a functionalized silane sizing, effectuating covalent bonding

between nanofiller and matrix [31]. In spite of macroscopic stress reduction, one should point out microscopic stress concentrations around the filler particles, which could lead to further problems, such as cracks. Besides contributing to shrinkage reduction, the inclusion of fillers brings further advantages, such as improved mechanical properties, scratch resistance, and barrier properties [32, 33].

Interesting possibilities are offered by recent work on thiol and ene monomers. Compared to acrylates, photopolymerization between thiol and ene monomers leads to mechanically stable, highly crosslinked networks, with the benefit of retarded gelation [34], which is thus expected to lower internal stresses, as explained in Figure 1-1. Characteristics of these systems include a comparatively low amount of polymerization shrinkage, little oxygen inhibition, and self-initiation. It was found that certain thiol-ene copolymerizations happen stochiometrically such as thiol vinyl-ether, whereas others, such as the copolymerization of thiols and acrylates are a combination of step-growth and vinyl homopolymerization [35]. Recently, Carioscia et al. [20] compared the internal stresses of a dimethacrylate monomer, frequently used as a tooth restorative material, with those of a thiol-ene oligomer, and found a reduction of the internal stress of 92%. They attributed the lower internal stress to the step-growth nature of thiol-ene polymerization, delaying gelation of the overall network. These systems, however, suffer from severe instability due to spontaneous dark reactions, which limits their applicability. A recent study showed that introducing a radical scavenger can increase the shelf life of thiol-ene resins from a few hours to a few days [36].

Mention should also be made of the novel approach towards low stress polymers recently promoted by Bowman and co-workers, based on an addition-fragmentation chain transfer mechanism [37]: The thiol-ene resin contained two photoinitiators with non-overlapping absorption spectra, one absorbing blue light and one absorbing in the near UV-range. The resin was photopolymerized with blue light, to ensure residual photoinitiator molecules which would introduce radicals in the polymer network upon a second irradiation. The formed radicals cleaved the polymer network by attacking vinyl groups in the polymer backbone to release internal stress and form a new bond. This addition-fragmentation process leaves the overall network density unchanged. Noticeable stress relaxation was achieved in the rubbery state. Similar effects are claimed for vitreous systems.

Another promising approach specifically investigated in the present work is the use of hyperbranched polymers, as described in the next section. These molecules

have unique features, such as reduced viscosity due to fewer entanglements compared to their liner counterparts [38, 39]. This enables the synthesize of large molecules, carrying reactive groups only on their surface, and still retaining a viscosity which is in an acceptable range for polymer processing (below 100 Pa s) [40]. Because of their high molecular weight, the concentration of reactive groups will be comparatively low, leading to low shrinkage during polymerization. Several studies exist on acrylated or methacrylated hyperbranched polymers as modifiers used in crosslinking systems in order to adjust, for example, the T_g, or the wetting behavior [41, 42], or to reduce polymerization shrinkage [43, 44].

Hyperbranched polymers also proved to be valuable modifiers in epoxy systems, by increasing toughness and reducing internal stress [45, 46]. Of the different approaches towards low stress polymers, a combination of reactive blends, containing hyperbranched polymers [17], with radiation curing should in principle be very effective.

2.3 Hyperbranched Polymers

In contrast to linear polymers, dendritic macromolecules are characterized by a high degree of branching The branching emanates from a core molecule with a functionality of 3 or higher. One can distinguish between dendrimers and hyperbranched polymers (Figure 2-3). Dendrimers have a perfect structure with a polydispersity of one and a degree of branching which is defined as [47, 48]:

$$DB_{Fréchet} = \frac{N_D + N_T}{N_D + N_L + N_T} \quad or \quad DB_{Frey} = \frac{2N_D}{2N_D + N_L} \tag{2.4}$$

where N_D, N_L, N_T are the number of dendritic, linear and terminal units respectively.

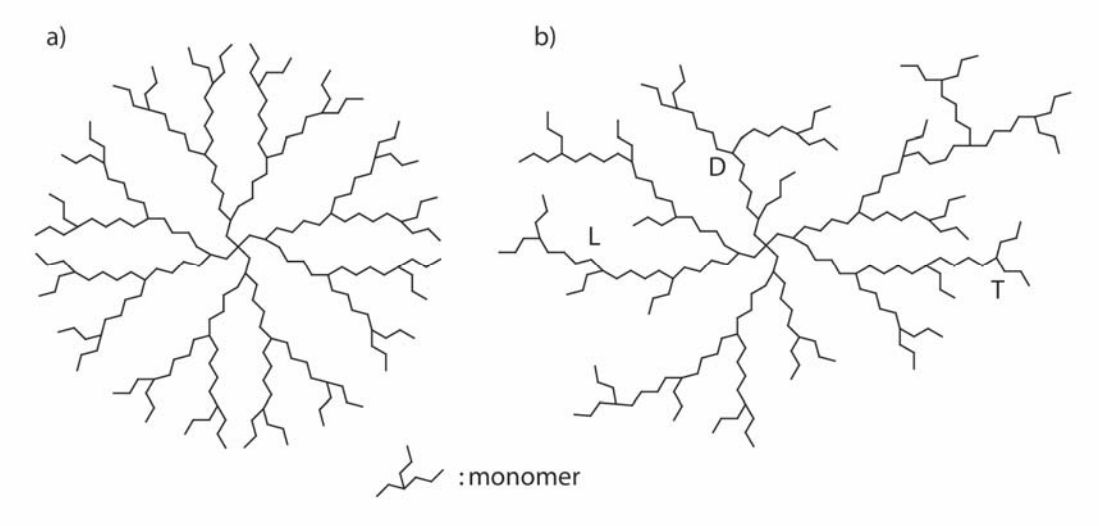

Figure 2-3 Schematic structures of a second generation a) dendrimer and b) hyperbranched polymer. One dendritic, one linear, and one terminal unit D, L, T are indicated. Adapted from Rodlert et al. [49].

Dendrimers are prepared in a step-wise manner including protection and deprotection strategy from AB_x monomers (where x is 2 or greater) with control over the number of generations and the molecular weight. For the synthesis of dendrimers, two different approaches exist [50]: The divergent approach, starting from a multifunctional core and proceeding radially outward, was developed by Tomalia et al. [51] and by Newkome et al. [52]. A newer approach is the convergent approach proposed by Hawker and Fréchet [53, 54], which starts from the periphery, progresses towards the inside, and is followed by coupling of the dendrons to a multifunctional core.

In contrast to dendrimers the synthesis of HBP is easier, leading to less perfect structures with a degree of branching smaller than one. The AB_x-monomers react in through a slow addition in an uncontrolled polycondensation, which allows less control over the numbers of layers and the molecular weight. The degree of branching is an important variable for the characterization of hyperbranched polymers, being normally between 55 and 70 % [55]. A wide range of different structures were synthesized including hyperbranched polyesters [56]; and hyperbranched polyethers [57].

The physical properties of dendrimers and HBPs are mainly dependent on their bulk whereas the chemical properties are controlled by the shell [39, 50]. Therefore phase separation in a polymer-HBP mixture can be controlled by adjusting the amount of polymer matrix compatible end groups [58].

The viscosity of dendrimers is lower than that of their linear counterparts [38] and they behave more like a Newtonian fluid, due to the absence of entanglements [59]. For hyperbranched polymers with a high degree of branching, similar behavior is observed [39]. Figure 2-4 shows the viscosity versus molecular weight of hyperbranched polymers, which is lower compared to that of linear molecules of comparable molecular weight [39], and follows a Rouse-like scaling ($\eta \sim M$) for medium to high molecular weights [60]. The low viscosity enables the synthesis of comparatively high molecular weight photocurable resins, having therefore relatively low concentrations of reactive groups [40].

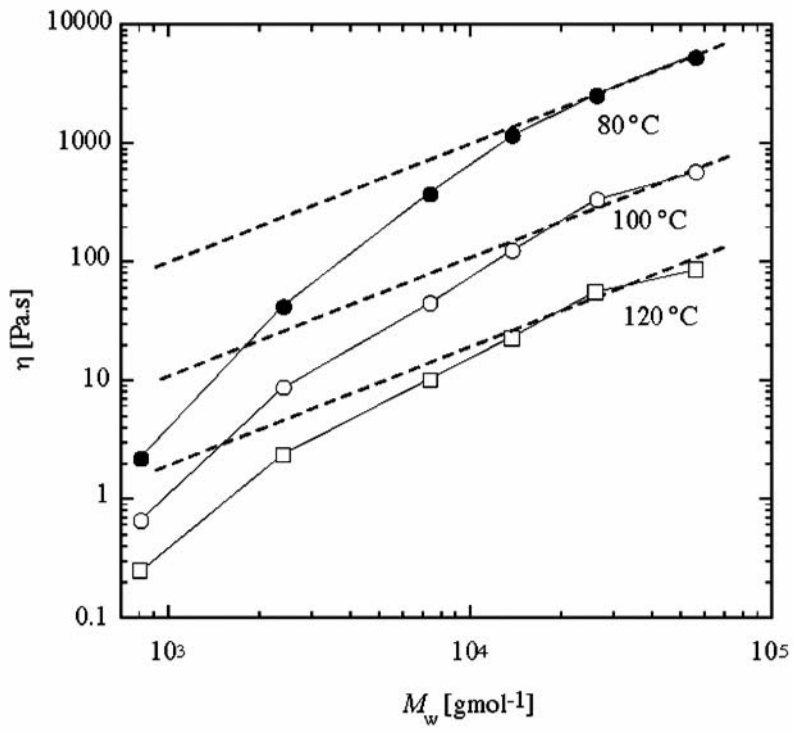

Figure 2-4 Viscosity behavior as a function of molecular weight for hyperbranched polyesters [60]. For medium to high molecular weights Rouse-like scaling, that is $\eta \sim M$, could be observed, shown in the plot by dashed lines (Adapted from [60]).

2.3.1 Hyperbranched Polymers for Shrinkage and Internal Stress Reduction

Hyperbranched polymers have been used as modifiers for stress reduction, both in thermosetting and photosetting systems. Mezzenga et al. [46] reported a stress reduction of one third, by introducing 14 wt.-% epoxy-functional HBP in a tetraglycidyl-4,4'-methylene dianiline (TGMDA) based epoxy resin. The stress reduction was attributed to an increased relaxation capacity of the epoxy network during crosslinking and a stress concentration mechanism at the epoxy/HBP interface.

The increased relaxation capacity was attributed to a delay in modulus build-up due to lower reactivity of the hyperbranched polymers, compared to the resin. During the reaction the hyperbranched polymer phase separates, with retarded solidification of HBP-rich domains. These results were confirmed by a study on process optimization of glass fiber/epoxy composites [17].

HBPs have also been used in UV curable coatings to reduce internal stresses. In methacrylate systems [43], as well as in acrylates [44], polymerization shrinkage was reduced significantly. For these non-phase separating mixtures, it is not yet clear whether hyperbranched polymers exhibit lower internal stresses due to their high acrylate equivalent weight only, or whether other factors, such as their globular shape, play a significant role.

2.4 Radiation Curable Polymers

2.4.1 Free Radical and Cationic Radiation-Induced Polymerization

The two most frequently used radiation curing techniques are ultraviolet (UV) curing and electron beam (EB) curing. UV curing is mainly used for thin, unfilled coatings, whereas EB curing is also applicable to three dimensional filled, or reinforced parts. Table 2-2 gives an overview of the main characteristics of UV and EB curing, and compares them to thermal curing.

Table 2-2 Comparison of UV, EB and thermal curing characteristics [61, 62].

	UV-Curing	**EB-Curing**	**Thermal Curing**
curing time	short	short	long
energy consumption	low	low	high
dimensional stability	good	good	moderate
volatiles	low	low	high
initiator	photoinitiator	non	thermal initiator
resin shelf-life	long	long	medium
oxygen inhibition	medium	high	non
throughput	high	very high	low
type of coatings	clear or lightly pigmented	highly pigmented resins possible	
part geometry	2D	3D	3D
equipment cost	medium	high	

UV curing dates back to the 1940s, when polyester styrene printing inks that polymerise under UV exposure, were developed [63]. In the 1960s the wood industry started to use these systems as varnishes, and this is still one of the most important fields of application for UV-curable resins. Today there are many applications: from protective coatings for all kinds of materials to the making of microelectronic devices. There are two different mechanisms for photopolymerization depending on the monomer and the initiator used [64]: free radical (e.g. acrylates) and cationic polymerisation (e.g. ring-opening reaction of epoxies). Table 2-3 gives an overview of the different characteristics of radiation curing of acrylates and epoxies. The very high curing speed of acrylates, and the wide range of available molecule structures, each having different properties, are together responsible for the predominance of acrylates among all UV curable systems.

Table 2-3 Overview of differences between UV curing of acrylates and epoxies [64-67].

	Acrylates	**Epoxies**
Mechanism	free radical	cationic
Growth	chaingrowth	stepgrowth
Network	heterogeneous	homogeneous
Oxygen inhibition	sensitive	not sensitve
Curing speed	very high	medium
Shrinkage	high	low
Toxicity	low	low
Conversion at Gelation	1-15 %	30-70 %

A UV curing formulation contains two main components [63]: a photoinitiator that effectively absorbs the incident light and generates initiating radicals, and a monomer and/or an oligomer with at least two unsaturations (C=C) that will generate the polymer network.

Acrylates photopolymerize in a chainwise manner, consisting of the following steps: formation of initiator radicals, propagation, and termination. There are numerous studies, investigating the underlying kinetics of crosslinking highly functional acrylates [68].

The complexity of the crosslinking reaction stems from the diffusion-controlled chemistry, including effects such as gelation and vitrification [68]. Kurdikar and Peppas [69] developed a model for diffusion-controlled crosslinking

photopolymerization and verified it for diacrylate monomers: In a first step the increasing viscosity significantly reduces the mobility of the long-chain radical species. Hence it is more unlikely for two radical species to approach each other and recombine. The rate constant for termination drops dramatically [70] and the rate of polymerization increases. The initiation and propagation steps are barely affected because the mobility of the small monomer molecules is still high, even if viscosity of the reaction mixture increases.

During the second stage the reaction rate drops quicker as would be expected from the consumption of monomers only [71] (auto-deceleration) and the polymerization becomes a more and more diffusion-controlled process.

Cook et al. [72] investigated the photopolymerization of bisphenol-A-dimethacrylate and found that the final degree of conversion was largely unaffected by variations in the initiation and polymerization rates, but was dependent on the network mobility and hence on the curing temperature and resin structure. They also stated that the maximum attainable conversion increased with the length and flexibility of the spacer group between the reactive groups, and that full conversion was not obtainable even with a cure at a high temperature. It is well known that not only increasing temperature but also increasing light intensity leads to a higher ultimate conversion [73]. Recently it was proposed that vitrification onset is also shifted to higher conversions for increasing temperature or intensity [74]. However, the interplay between vitrification and ultimate conversion is not yet fully understood.

Experimental techniques most frequently used for measuring the network formation during photopolymerizations include real-time Fourier transform infrared spectroscopy [75], photo differential scanning calorimetry [76], and, more recently, photo rheometry [77, 78]. The first two measure chemical conversion, whereas the latter measures the stiffness build-up during photopolymerization as described below.

2.4.2 Photorheology

The curing of acrylate systems normally takes place within a few seconds [63]. This makes it difficult to analyze network formation during UV polymerization, and to measure corresponding changes in physical and mechanical properties. As far as the rapid change in mechanical properties is concerned, photorheology was developed as a specific kind of chemorheology [79], to enable the occurrence of structural phenomena such as gelation and vitrification to be detected.

One of the first chemorheology studies was performed on UV curing thiol-ene systems by Khan et al. [79]. In this work single UV pulses were used to keep the curing rate low enough for the rheometer to be able to record any changes in rheological properties. Further work showed that this technique was capable of monitoring the structure build-up in UV polymerizing resins, and determining the gel point [80, 81]. These studies were conducted at a low UV intensity (<0.2 mW/cm^2), and the modulus build-up was therefore relatively slow, with a 5 order of magnitude increase in modulus in approximately 500 s. To investigate the fast curing of a polyester acrylate with significantly higher intensities (15 $mW \cdot cm^{-2}$), photorheology was refined by Lee et al. [82]. Since the sampling rate of the equipment was limited to about 1 s, Lee et al. proposed a method whereby the input strain signal and the output stress signal were acquired externally, then split into short time periods (0.2 to 0.5 cycles of excitation), and fitted with sinuoidal functions. Thereby the storage and loss moduli, and the phase shift between stress and strain were calculated. They were able to monitor a three order of magnitude increase in the complex viscosity in 5 s with a time resolution of up to 50 data points per second. However, this technique is not sensitive enough to study monomers with a viscosity lower than about 100 Pa·s.

Steeman et al. [78] combined photorheology with real-time Fourier transform infrared spectroscopy in order to obtain the modulus as a function of double bond conversion, and thus link mechanical data with molecular information. Their study was carried out at a UV intensity of 28 mW/cm^2. Rheological information was obtained by splitting the data into small intervals, and Fourier transformation was performed. A similar study was performed at about the same time by Botella et al. [77], on very thick samples (0.5 mm) cured under low UV intensities (0.15 to 1.36 mW/cm^2). However, these experimental conditions might lead to an important conversion gradient in the sample, inducing a temporal error in the phase angle and stiffness evolution.

2.4.3 Time-Intensity-Transformation

Time-temperature-transformation diagrams (TTT-diagrams) as first proposed by Gillham and Enns [83, 84], are extensively used for the evaluation and design of thermoset curing processes. In these diagrams the physical state of the curing thermoset is plotted as a function of curing time and temperature. These diagrams usually contain information about gelation, vitrification and thermally induced depolymerization. A time-intensity-temperature-transformation diagram was

implemented recently for a UV curing reaction [85]. Understanding the interplay of curing time and UV intensity and its influence on network formation mechanisms helps to optimize processing conditions such as line speed and UV intensity for continuous processes, and ensures that a desired conversion is reached in order to achieve, for example, good mechanical properties, barrier performance, and long-term stability. The study by Lee et al. [85] showed that by increasing light intensities vitrification was shifted to significantly shorter times, whereas for gelation only a slight shift was observed. However, information about conversion as a function of time was not included.

A similar approach, but from a kinetics point of view, was made by Esposito Corcione et al. in the same year [74]. The time-temperature superposition was developed further to a time-irradiation intensity superposition, giving the possibility of identifying vitrification from photo DSC measurements. It was found that increasing temperature and UV intensity shifted the onset of vitrification to higher conversions [74].

2.5 Fabrication of Thick Polymer Microstructures

Processes used for micro-structuring polymer materials for microsystem applications are sketched in Figure 2-5. These include replication methods and direct techniques. A comprehensive description is given by Becker and Gärtner [86]. Replication methods involve a so-called master, whereas in direct techniques no such step is necessary.

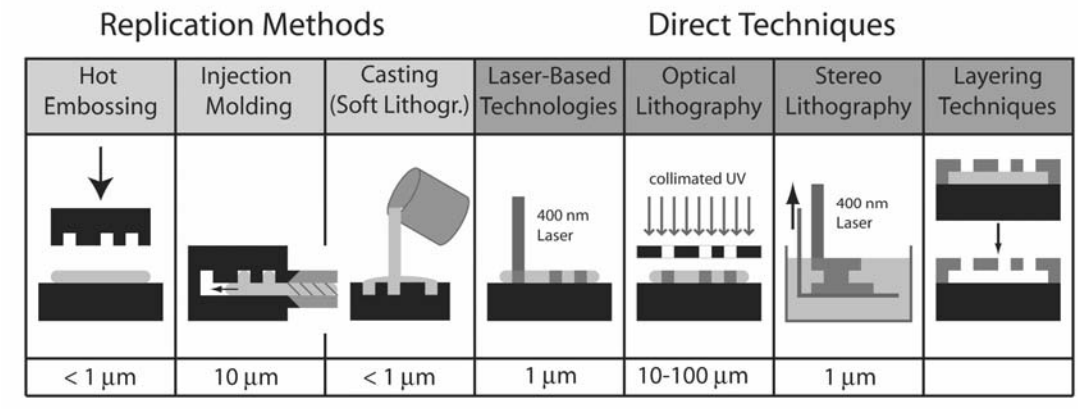

Figure 2-5 Polymer microfabrication methods. The minimum resolution is indicated [86, 87].

The motivation for using polymers for microfluidic applications is the possibility of producing cheap disposable devices. For these applications however,

comparatively thick polymer layers are required. The two materials most widely used are SU-8, an epoxy negative-tone photoresist, and Novolak type negative photoresist. Both materials are in fact limited to a maximum thickness. In a simple single layer process, layer thicknesses up to 100 μm can be reached with Novolak type photoresists and 200 μm in a multilayer process with aspect ratios of up to 10 [88-90]. Thick, high aspect ratio SU-8 structures with layer thicknesses over 200 μm can only be produced in a protracted multilayer process, with fabrication times of over one hour per 100 μm [91, 92], or by using an optimized process cycle with lower backing temperatures [93]. The limiting factor of SU-8 is its comparatively high internal stresses leading to wafer deflection and defects [91], as shown in Figure 2-6. The data from wafer deflection measurements by Lorenz et al. [91] were used to calculate internal stresses by applying the Inoue equation [94]. Stresses above 25 MPa were found and these will be discussed in more detail in Chapter 8.

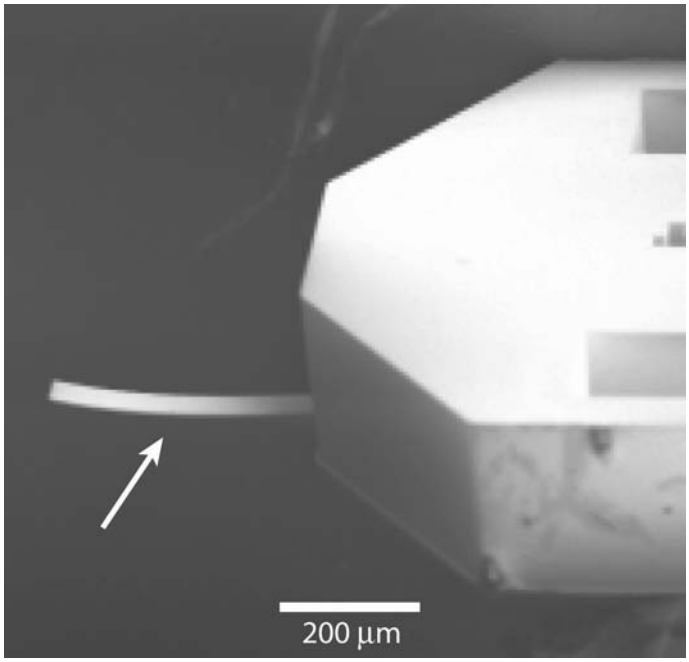

Figure 2-6 Cantilever for use in an atomic force microscope fabricated from SU-8 in a photolithographic process, using a sacrificial Cr and Al layer. The arrow points to the cantilever, which is deflected, due to process-induced internal stresses (Courtesy J. Brugger, LMIS1-EPFL).

2.6 References

1. Decker, C., *Kinetic study and new applications of UV radiation curing.* Macromolecular Rapid Communications, 2002. **23**: p. 1067-1093.
2. Francis, L.F., A.V. McCormick, D.M. Vaessen, and J.A. Payne, *Development and measurement of stress in polymer coatings.* Journal of Materials Science, 2002. **37**: p. 4717-4731.

3. Patel, M.P., M. Braden, and K.W.M. Davy, *Polymerization shrinkage of methacrylate esters.* Biomaterials, 1987. **8**: p. 53-56.
4. Sato, K., *The internal stress of coating films.* Progress in Organic Coatings, 1980. **8**: p. 143-160.
5. Negele, O. and W. Funke, *Internal stress and wet adhesion of organic coatings.* Progress in Organic Coatings, 1996. **28**: p. 285-289.
6. Luciani, A., C.J.G. Plummer, R. Gensler, and J.-A.E. Månson, *Surface pattern formation in UV-curable coatings.* Journal of Coatings Technology, 2000. **72**(909): p. 161-163.
7. Payne, J.A., *Stress Evolution in Solidifying Coatings*, in *Department of Chemical Engineering and Materials Science*. 1998, University of Minnesota: Twin Cities.
8. Eom, Y., L. Boogh, V. Michaud, and J.-A.E. Månson, *A structure and property based process window for void free thermoset composites.* Polymer Composites, 2001. **22**(1): p. 22-31.
9. Lei, H., J.A. Payne, A.V. McCormick, L.F. Francis, W.W. Gerberich, and L.E. Scriven, *Stress development in drying coatings.* Journal of Applied Polymer Science, 2001. **81**: p. 1000-1013.
10. de Boer, J., R.J. Visser, and G.P. Melis, *Time-resolved determination of volume shrinkage and refractive index change of thin polymer films during photopolymerization.* Polymer, 1992. **33**(6): p. 1123-1126.
11. Lange, J. and J.-A.E. Månson, *Build-up of structure and viscoelastic properties in epoxy and acrylate resins cured below their ultimate glass transition temperature.* Polymer, 1996. **37**(26): p. 5859-5868.
12. Kloosterboer, J.G., *Network formation by chain crosslinking photopolymerization and its applications in electronics.* Advances in Polymer Science, 1988. **84**: p. 1-61.
13. Wen, M., L.E. Scriven, and A.V. McCormick, *Differential scanning calorimetry and cantilver deflection studies of polymerization kinetics and stress in ultraviolet curing of multifunctional (meth)acrylate coatings.* Macromolecules, 2002. **35**: p. 112-120.
14. Doyle, M.A., P.-O. Hagstrand, and J.-A.E. Månson, *Process-induced internal stresses in phenol-formaldehyde cellulose composites.* Polymer Composites, 2004. **25**(2): p. 214-228.
15. Lange, J., S. Toll, J.-A.E. Månson, and A. Hult, *Residual stress build-up in thermoset films cured above their ultimate glass transition temperature.* Polymer, 1995. **36**(16): p. 3135-3141.
16. Lange, J., S. Toll, J.-A.E. Månson, and A. Hult, *Residual stress build-up in thermoset films cured below their ultimate glass transition temperature.* Polymer, 1997. **38**(4): p. 809-815.
17. Eom, Y., L. Boogh, V. Michaud, and J.-A.E. Månson, *Internal stress control in epoxy resins and their composites by material and process tailoring.* Polymer Composites, 2002. **23**(6): p. 1044-1056.
18. Klang, J.A., *Radiation curable hyperbranched polyester acrylates*. 2006, Sartomer Company, Inc.: Exton, Pennsylvania. p. 1-7.
19. Govindaraju, A., A. Chakraborty, and C. Luo, *Reinforcement of PDMS masters using SU-8 truss structures.* Journal of Micromechanics and Microengineering, 2005. **15**(6): p. 1303-1309.
20. Carioscia, J.A., H. Lu, J.W. Stansbury, and C.N. Bowman, *Thiol-ene oligomers as dental restorative materials.* Dental Materials, 2005. **21**(12): p. 1137-1143.

21. Li, W. and L.J. Lee, *Shrinkage control of low-profile unsaturated polyester resins cured at low temperature.* Polymer, 1998. **39**(23): p. 5677-5687.
22. Bulliard, X., V. Michaud, and J.-A.E. Månson, *Low-profil mechanisms in a PVAc/Polyester Blend.* Polymer Engineering and Science, 2006. **46**: p. 303-313.
23. Clifford, S.M., N. Jansson, W. Yu, V. Michaud, and J.-A.E. Månson, *Thermoviscoelastic anisotropic analysis of process induced residual stress and dimensional stability in real polymer matrix composite components.* Composites Part A - Applied Science and Manufacturing, 2006. **37**: p. 538-545.
24. Plepys, A.R. and R.J. Farris, *Evolution of residual stresses in three-dimensionally constrained epoxy resins.* Polymer, 1990. **31**: p. 1932-1936.
25. Månson, J.-A.E. and J.C. Seferis, *Process simulated laminate (PSL): a methodology to internal stress characterization in advanced composite materials.* Journal of Composite Materials, 1992. **26**(3): p. 405-431.
26. Prasatya, P., G.B. McKenna, and L.S. Sindee, *A viscoelastic model for prodicting isotropic residual stresses in thermosetting materials: effects of processing parameters.* Journal of Composite Materials, 2001. **35**(10): p. 826-848.
27. Sunderland, P., W. Yu, and J.-A.E. Månson, *A thermoviscoelastic analysis of process-induced internal stresses in thermoplastic matrix composites.* Polymer Composites, 2001. **22**(5): p. 579-592.
28. Kim, B.-S., N. Bernet, P. Sunderland, and J.-A.E. Månson, *Numerical analysis of the dimensional stability of thermoplastic composites using a thermoviscoelastic approach.* Journal of Composite Materials, 2002. **36**(20): p. 2389-2403.
29. Sham, M.-L. and J.-K. Kim, *Evolution of residual stresses in modified epoxy resins for electronic packaging applications.* Composites Part A - Applied Science and Manufacturing, 2004. **35**: p. 537-546.
30. Condon, J.R. and J.L. Ferracane, *Assessing the effect of composite formulation on polymerization stress.* Journal of the American Dental Association, 2000. **131**: p. 497-503.
31. Condon, J.R. and J.L. Ferracane, *Reduced polymerization stress through non-bonded nanofiller particles.* Biomaterials, 2002. **23**: p. 3807-3815.
32. Sangermano, M., G. Malucelli, E. Amerio, A. Priola, E. Billi, and G. Rizza, *Photopolymerization of epoxy coatings containing silica nanoparticles.* Progress in Organic Coatings, 2005. **54**: p. 134-138.
33. Bauer, F., H.-J. Gläsel, U. Decker, H. Ernst, A. Freyer, E. Hartmann, V. Sauerland, and R. Mehnert, *Trialkoxysilane grafting onto nanoparticles for the preparation of clear coat polyacrylate systems with excellent scratch performance.* Progress in Organic Coatings, 2003. **47**: p. 147-153.
34. Okay, O. and C.N. Bowman, *Kinetic modeling of thiol-ene reactions with both step and chain growth aspects.* Macromolecular Theory and Simulation, 2005. **14**: p. 267-277.
35. Cramer, N.B., J.P. Scott, and C.N. Bowman, *Photopolymerization of thiol-ene polymers without photoinitiators.* Macromolecules, 2002. **35**.
36. Kim, Y.B., H.K. Kim, H.C. Choi, and J.W. Hong, *Photocuring of a thiol-ene system based on an unsaturated polyester.* Journal of Applied Polymer Science, 2005. **95**: p. 342-350.
37. Scott, T.F., A.D. Schneider, W.D. Cook, and C.N. Bowman, *Photoinduced plasticity in cross-linked polymers.* Science, 2005. **308**: p. 1615-1617.

38. Mourey, T.H., S.R. Turner, M. Rubinstein, J.M.J. Fréchet, C.J. Hawker, and K.L. Wooley, *Unique behavior of dendritic macromolecules: intrinsic viscosity of polyether dendrimers.* Macromolecules, 1992. **25**: p. 2401-2406.
39. Boogh, L., B. Pettersson, and J.-A.E. Månson, *Dendritic hyperbranched polymers as toughening for epoxy resins.* Polymer, 1999. **40**: p. 2249-2261.
40. Hult, A., M. Johansson, and E. Malmström, *Hyperbranched polymers.* Advances in Polymer Science, 1999. **143**: p. 1-34.
41. Johansson, M. and A. Hult, *Synthesis, characterization, and UV curing of acrylate functional hyperbranched polyester resins.* Journal of Coatings Technology, 1995. **67**: p. 35-39.
42. Johansson, M., T. Glauser, G. Rospo, and A. Hult, *Radiation curing of hyperbranched polyester resins.* Journal of Applied Polymer Science, 2000. **75**: p. 612-618.
43. Klee, J.E., C. Schneider, D. Hölter, A. Burgath, H. Frey, and R. Mülhaupt, *Hyperbranched polyesters and their application in dental composites: monomers for low shrinking composites.* Polymers for Advanced Technologies, 2001. **12**(6): p. 346-354.
44. Kou, H.-G., A. Asif, and W.-F. Shi, *Hyperbranched acrylated aromatic polyester used as a modifier in UV-curable epoxy acrylate resins.* Chinese Journal of Chemistry, 2003. **21**: p. 91-95.
45. Mezzenga, R., C.J.G. Plummer, L. Boogh, and J.-A.E. Månson, *Morphology build-up in dendritic hyperbranched polymer modified epoxy resins: modelling and characterization.* Polymer, 2000. **42**: p. 305-317.
46. Mezzenga, R., L. Boogh, and J.-A.E. Månson, *A review of dendritic hyperbranched polymer as modifiers in epoxy composites.* Composites Science and Technology, 2001. **61**: p. 787-795.
47. Hölter, D., A. Burgath, and H. Frey, *Degree of branching in hyperbranched polymers.* Acta Polymerica, 1997. **48**: p. 30-35.
48. Hawker, C.J., R. Lee, and J.M.J. Fréchet, *One-step synthesis of hyperbranched dendritic polyesters.* Journal of the American Chemical Society, 1991. **113**: p. 4583-4588.
49. Rodlert, M., C.J.G. Plummer, L. Garamszegi, Y. Leterrier, H.J.M. Grünbauer, and J.-A.E. Månson, *Hyperbranched polymer/montmorillonite clay nanocomposites.* Polymer, 2004. **45**: p. 949-960.
50. Inoue, K., *Functional dendrimers, hyperbranched and star polymers.* Progress in Polymer Science, 2000. **25**: p. 453-571.
51. Tomalia, D.A., H. Baker, J. Dewald, M. Hall, J. Ryder, and P. Smith, *A new class of polymers: starburst-dendritic macromolecules.* Polymer Journal, 1985. **17**(1): p. 117-132.
52. Newkome, G.R., Z.-q. Yao, G.R. Baker, and V.K. Gupta, *Cascade molecules: a new approach to micelles. A [27]-Arborol.* The Journal of Organic Chemistry, 1985. **50**: p. 2003-2004.
53. Hawker, C.J. and J.M.J. Fréchet, *Preparation of polymers with controlled molecular architecture. a new convergent approach to dendritic macromolecules.* Journal of the American Chemical Society, 1990. **112**: p. 7638-7647.
54. Hawker, C.J. and J.M.J. Fréchet, *A new convergent approach to monodisperse dendritic macromolecules.* Journal of the Chemical Society-Chemical Communications, 1990. **15**: p. 1010-1014.
55. Newkome, G.R., C.N. Moorefield, and F. Vögtle, *Dendrimers and dendrons*. 2001, Weinheim: WILEY-VCH. 623.

56. Malmström, E., M. Johansson, and A. Hult, *Hyperbranched aliphatic polyesters.* Macromolecules, 1995. **28**: p. 1698-1703.
57. Magnusson, H., E. Malmström, and A. Hult, *Synthesis of hyperbranched aliphatic polyethers via cationic ring-opening polymerization of 3-ethyl-3-(hydroxymethyl)oxetane.* Macromolecular Rapid Communications, 1999. **20**: p. 453-457.
58. Plummer, C.J.G., R. Mezzenga, L. Boogh, and J.-A.E. Månson, *Phase separation in epoxy resing-reactive dendritic hyperbranched polymer blends.* Polymer Engineering and Science, 2001. **41**: p. 43-52.
59. Luciani, A., C.J.G. Plummer, T.Q. Nguyen, L. Garamszegi, and J.-A.E. Månson, *Rheological and physical properties of aliphatic hyperbranched polyesters.* Journal of Polymer Science Part B-Polymer Physics, 2004. **42**: p. 1218-1225.
60. Plummer, C.J.G., A. Luciani, T.-Q. Nguyen, and L. Garamszegi, *Rheological characteristics of hyperbranched polyesters.* Polymer Bulletin, 2002. **49**: p. 77-84.
61. Fengmei, L., B. Jianwen, C. Xiangbao, B. Huaying, and W. Huiliang, *Factors influencing EB curing of epoxy matrix.* Radiation Physics and Chemistry, 2002. **63**: p. 557-561.
62. Läuppi, U.V., *Radiation curing - an overview.* Radiation Physics and Chemistry, 1990. **35**(1-3): p. 30-35.
63. Decker, C., *UV-curing chemistry: past, present, and future.* Journal of Coatings Technology, 1987. **59**(751): p. 97-106.
64. Davidson, S., *Exploring the science, technology and applications of U.V. and E.B. curing*. SITA Series In Surface Coatings Technology. 1999, London, UK: SITA Technology Limited. 290.
65. Pappas, S.P., *Radiation curing : science and technology*. Topics in Applied Chemistry, ed. A.R. Katritzky and G.J. Sabongi. 1992, New York: Plenum Press.
66. Golden, R., *Safety and handling of UV/EB curing materials.* Journal of Coatings Technology, 1997. **69**(871): p. 83-89.
67. Lange, J., M. Johansson, C.T. Kelly, and P.J. Halley, *Gelation behaviour during chainwise crosslinking polymerization of methacrylate resins.* Polymer, 1999. **40**: p. 5699-5707.
68. Andrzejewska, E., *Photopolymerization kinetics of multifunctional monomers.* Progress in Polymer Science, 2001. **26**: p. 605-665.
69. Kurdikar, D.L. and N.A. Peppas, *A kinetic model for diffusion-controlled bulk cross-linking photopolymerizations.* Macromolecules, 1994. **27**: p. 4084-4092.
70. Hayden, P. and S.H. Melville, *The kinetics of the polymerization of methyl methacrylate. II. The crosslinked and heterogeneous reaction.* Journal of Polymer Science, 1960. **43**: p. 215-227.
71. Dietz, E.J. and N.A. Peppas, *Reaction kinetics and chemical changes during polymerization of multifunctional (meth)acrylates for the production of highly crosslinked polymers used in information storage systems.* Polymer, 1997. **38**(15): p. 3767-3781.
72. Cook, W.D., *Photopolymerization kinetics of dimethacrylates using the camphorquinone / amine initiator system.* Polymer, 1992. **33**(3): p. 600-609.
73. Decker, C., D. Decker, and F. Morel, *Light intensity and temperature effect in photoinitiated polymerization*, in *Photopolymerization: fundamentals and application*, A.B. Scranton, C.N. Bowman, and R.W. Pheiffer, Editors. 1997, American Chemical Society: Washington. p. 63-80.

74. Esposito Corcione, C., A. Greco, and A. Maffezzoli, *Time-temperature and time-irradiation intensity superposition for photopolymerization of an epoxy based resin.* Polymer, 2005. **46**: p. 8018-8027.
75. Decker, C. and K. Moussa, *A new method for monitoring ultra-fast photopolymerizations by real-time infra-red (RTIR) spectroscopy.* Die Makromolekulare Chemie, 1988. **189**: p. 2381-2394.
76. Wight, F.R. and G.W. Hicks, *Applications of differential scanning calorimetry to photocurable polymer systems.* Polymer Engineering and Science, 1978. **18**(5): p. 378-381.
77. Botella, A., J. Dupuy, A.-A. Roche, H. Sautereau, and V. Verney, *Photo-rheometry/NIR spectrometry: An in situ technique for monitoring conversion and viscoelastic properties during photopolymerization.* Macromolecular Rapid Communications, 2004. **25**: p. 1155-1158.
78. Steeman, P.A.M., A.A. Dias, D. Wienke, and T. Zwartkruis, *Polymerization and network formation of UV-curable systems monitored by hyphenated real-time dynamic mechanical analysis and near-infrared spectroscopy.* Macromolecules, 2004. **37**: p. 7001-7007.
79. Khan, S.A., I.M. Plitz, and R.A. Frantz, *In situ technique for monitoring the gelation of UV curable polymers.* Rheologica Acta, 1992. **31**: p. 151-160.
80. Chiou, B.-S., R.J. English, and S.A. Khan, *Rheology and photo-cross-linking of thiol-ene polymers.* Macromolecules, 1996. **29**: p. 5368-5374.
81. Chiou, B.-S., R.J. English, and S.A. Khan, *UV cross-linking of thiol-ene polymers: a rheological study*, in *Photopolymerization: fundamentals and application*, A.B. Scranton, C.N. Bowman, and R.W. Pheiffer, Editors. 1997, American Chemical Society: Washington. p. 150-166.
82. Lee, S.S., A. Luciani, and J.-A.E. Månson, *A rheological characterisation technique for fast UV-curable systems.* Progress in Organic Coatings, 2000. **38**: p. 193-197.
83. Enns, J.B. and J.K. Gillham, *Time-temperature-transformation (TTT) cure diagram: Modeling the cure behaviour of thermosets.* Journal of Applied Polymer Science, 1983. **28**: p. 2567-2591.
84. Gillham, J.K., *The time-temperature-transformation (TTT) state diagram and cure*, in *The Role of the Polymeric Matrix in the Processing and Structural Properties of Composite Materials*, J.L. Seferis and L. Nicolais, Editors. 1983, Plenum Press: New York. p. 127-145.
85. Lee, K.J., J.Y. Choi, and B.S. Lim, *Time-Temperature-Intensity-Transformation Cure Diagram for Visible Light Curable Dimethacrylate Resins.* Polymer Journal, 2003. **35**(10): p. 778-784.
86. Becker, H. and C. Gärtner, *Polymer microfabrication methods for microfluidic analytical applications.* Electrophoresis, 2000. **21**: p. 12-26.
87. Sun, C., N. Fang, D.M. Wu, and X. Zhang, *Projection micro-stereolithography using digital micro-mirror dynamic mask.* Sensors and Actuators A - Physical, 2005. **121**: p. 113-120.
88. Löchel, B., A. Maciossek, H.-J. Quenzer, B. Wagner, and G. Engelmann, *Magnetically driven microstructures fabricated with multilayer electroplating.* Sensors and Actuators A-Physical, 1995. **46-47**: p. 98-103.
89. Roth, S., L. Dellmann, G.-A. Racine, and N.F. de Rooij, *High aspect ratio UV photolithography for electroplated structures.* Journal of Micromechanics and Microengineering, 1999. **9**: p. 105-108.
90. Conédéra, V., B.L. Goff, and N. Fabre, *Potentialities of a new positive photoresist for the realization of thick moulds.* Journal of Micromechanics and Microengineering, 1999. **9**: p. 173-175.

91. Lorenz, H., M. Despont, N. Fahrni, J. Brugger, P. Vettiger, and P. Renaud, *High-aspect-ratio, ultrathick, negative-tone near-UV photoresist and its applications for MEMS.* Sensors and Actuators A-Physical, 1998. **64**: p. 33-39.
92. Williams, J.D. and W. Wang, *Study on the postbaking process and the effects on UV lithography of high aspect ratio SU-8 microstructures.* Journal of Microlithography Microfabrication and Microsystems, 2004. **3**(4): p. 563-568.
93. Kubenz, M., U. Ostrzinski, F. Reuther, and G. Gruetzner. *Challenges of processing thick and ultra-thick photoresist films*. in *Advances in Resist Technology and Processing XX*. 2003: SPIE.
94. Inoue, Y. and Y. Kobatake, *Mechanics of adhesive joints Part III. Evaluation of residual stress.* Applied Scientific Research, 1958. **A7**: p. 314-324.

3 Materials and Experimental Methods

3.1 Materials

3.1.1 Monomers

Figure 3-1 depicts the structures of the different acrylate monomers studied, and Table 3-1 gives an overview of their physical and chemical properties. Di-pentaerythritol penta/hexaacrylate (DPHA, UCB Chemicals) is an acrylate monomer with, theoretically, 6 functional groups but on average 4.7 functional groups as measured using a bromination method [1] to determine the unsaturation level. Two hyperbranched polymers (HBP) were also examined and one sample branch is shown in Figure 3-1, since every single HBP molecule has a different structure. The first HBP was based on a 16-hydroxyl functional 2nd generation hyperbranched polyester (Boltorn® H20, Perstorp AB, Sweden) giving a 13-functional polyester acrylate (called Acrylated Boltorn H20). The second one was based on a 3rd generation hyperbranched polyether polyol (synthesized by Perstorp AB, Sweden) giving a 29-functional polyether acrylated (called Acrylated Polyether HBP).

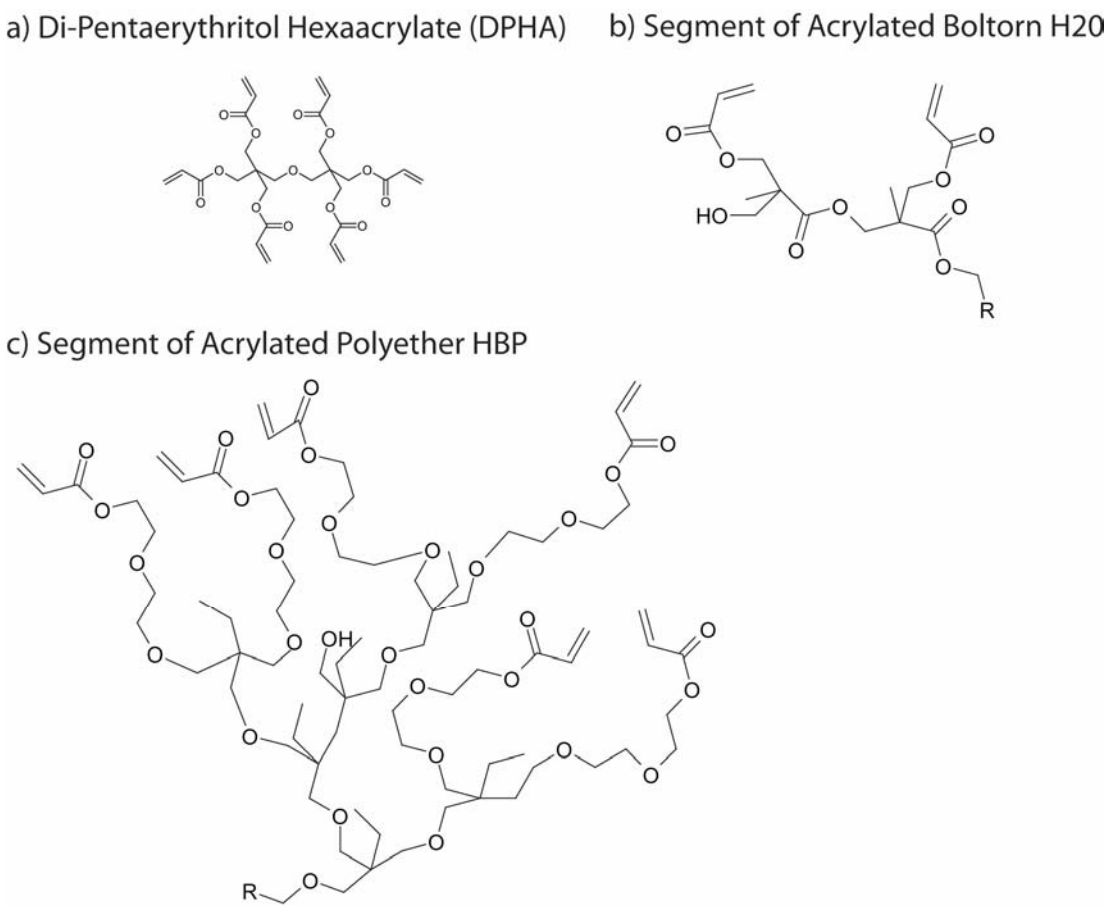

Figure 3-1 Structures of the acrylate monomers studied. For the hyperbranched polymers, only one sample branch is shown. R denotes the tetrafunctional core molecule, from out of which grow four branches.

The polyester HBP was derived from a condensation of 2,2 bis-hydroxymethyl propionic acid (bis-MPA) [2]. The polyether HBP was synthesized by ring-opening polymerization of alkoxylated TMPO derivatives (3-ethyl-3-(hydroxymethyl)-oxetane, Perstorp AB, Sweden) [3]. Acrylation was carried out according to the conventional preparation of acrylic esters by condensation of the polyol with acrylic acid.

Although both syntheses led to imperfect branching and significant polydispersity, HBPs conserved the essential features of dendrimers, that is, high end-group functionality and a globular architecture. The number of acrylate functions per monomer, and the molecular weight, were according to the specifications of the suppliers. The degree of branching was taken respectively from the work of Rodlert et al. on hyperbranched aliphatic polyesters/montmorillonite clay nanocomposites [4], and from that of Magnusson et al. on hyperbranched aliphatic polyether [3].

3.1.2 Photoinitiator

The photoinitiator was 1-hydroxy-cyclohexyl-phenyl-ketone (Irgacure® 184, Ciba Specialty Chemicals, CAS 947-19-3, M=204.26 g/mol, Figure 3-2 a), at a concentration equal to 1 wt.-%. Compared to other photoinitiators such as Irgacure 819 or Irgacure 369 it showed much better solubility in the acrylate monomers.

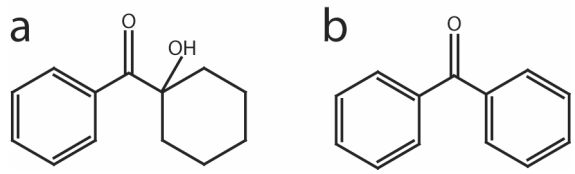

Figure 3-2 Photoinitiator a) 1-hydroxy-cyclohexyl-phenyl-ketone and b) benzophenone.

The relatively small amount of photoinitator should have assured a relatively homogeneous cure throughout the sample thickness. According to the Beer-Lambert equation, the intensity absorbed *I(z)* at a depth *z* is:

$$I(z) = I_0(1 - e^{-2.3\varepsilon_t[PI]z}) \tag{3.1}$$

where I_0 is the incident intensity, [*PI*] the photoinitiator concentration, and ε_t the molar extinction coefficient found to be equal to 74 $L \cdot mol^{-1}cm^{-1}$ at 313 nm for Irgacure 184 [5]. The absorption calculated according to equation 3.1 for Irgacure 184 is shown as a function of photoinitiator concentration and coating thickness in Figure 3-4. For a typical film thickness of 0.1 mm, and a photoinitiator concentration of 0.0563 $mol \cdot L^{-1}$ (i.e., 1wt.-%), only 9% of the UV light at this peak was absorbed throughout the sample thickness. At medium to high intensities, a reaction took place at a similar rate within the sample; for lower intensities, the reactions slowed down drastically, increasing the gradient of cure in the sample.

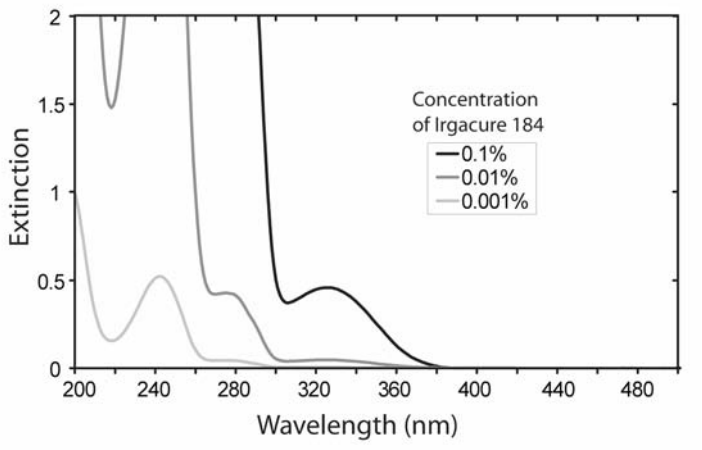

Figure 3-3 Extinction of Irgacure 184 in Acetonitril for different concentrations (adapted from the technical data sheet from Ciba Specialty Chemicals).

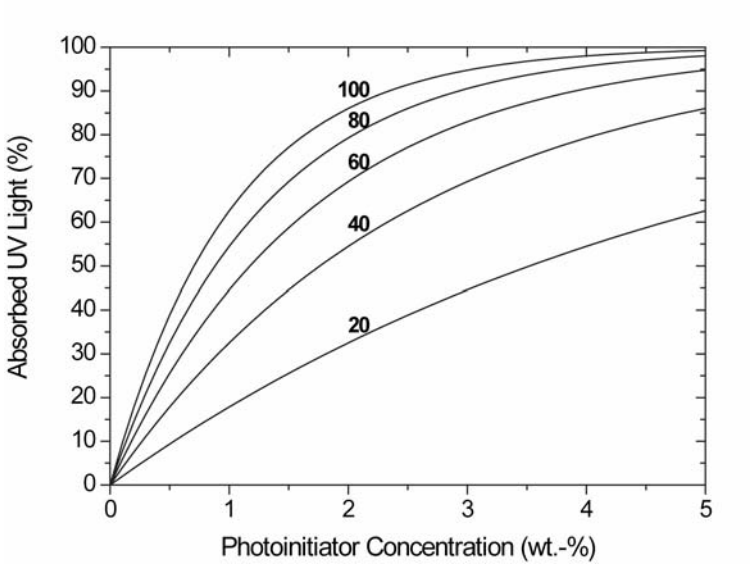

Figure 3-4 Absorption of UV light as a function of photoinitiator concentration (Irgacure 184) for different coating thicknesses indicated in the graph (μm).

3.1.3 Materials for Polymer Microstructures

The three different acrylates with different degrees of polymerization shrinkage were compared to SU-8, an epoxy-based material frequently used in microtechnology. It was developed at the IBM Research center in the ‘80s [6] and introduced in the ‘90s as a so-called negative tone photoresist [7, 8]; it is nowadays used especially for thick polymer microstructures with high aspect ratios.

The SU-8 material was SU-8 2100 (Microchem, US) which is a solution of an epoxy resin (CAS 28906-96-9) in gamma butyrolacetone and propylene carbonate. The monomer and a monomer unit in the crosslinked polymer are depicted in Figure 3-5. The formulation contains a mixture of hexafluoroantimonate salts (CAS 89452-37-9 and 71449-78-0) to initiate the cationic photopolymerization Figure 3-6.

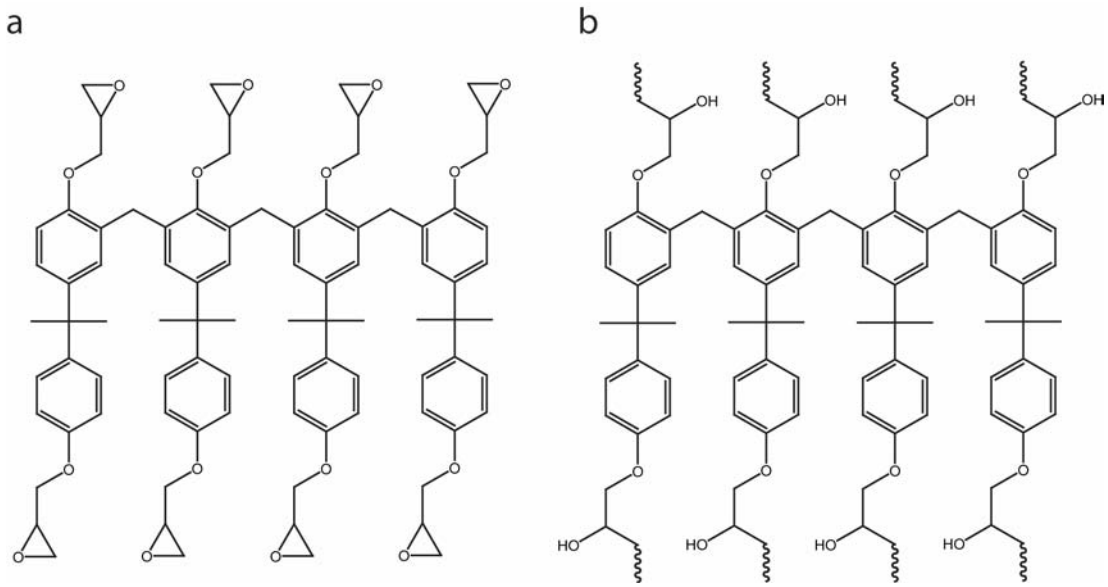

Figure 3-5 Molecular structure of a) the SU-8 monomer and b) the monomer unit in the crosslinked polymer (adapted from Genolet [9]).

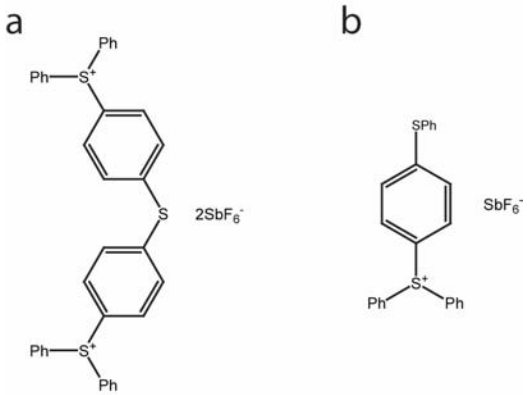

Figure 3-6 Structures of the photoinitiators for cationic polymerization of SU-8 a) Sulfonium, (thiodi-4,1-phenylene)bis[diphenyl-, bis[(OC-6-11)-hexafluoroantimonate(1-)] b) Sulfonium, diphenyl[4-(phenylthio)phenyl]-, (OC-6-11)-hexafluoroantimonate(1-).

The photoinitiator used was Irgacure 500 (a mixture of equal parts of 1-hydroxy-cyclohexyl-phenyl-ketone (Figure 3-2 a, CAS 947-19-3, M=204.26 g/mol) and benzophenone (Figure 3-2 b, CAS 119-61-9, M=182.22 g/mol), supplied by Ciba Specialty Chemicals), at a concentration equal to 2 wt.-%. It was blended with the acrylate monomer at a temperature of 85 °C to facilitate mixing.

Irgacure 500 was chosen instead of Irgacure 184 since it is liquid, and hence easier to blend with the acrylate because it has a higher absorption in the UV-A range (320-400 nm) and was therefore better adapted to the spectrum of the Hg-lamp than Irgacure 184.

3.2 Basic Material Characterization

3.2.1 Acrylates

The viscosity of the monomers was measured with the ARES rheometer, using 25 mm diameter parallel plates, at ambient temperature and an excitation frequency of 1 Hz. The viscosity was found to be Newtonian and equal to 6 Pa·s for the Acrylated Polyether HBP, 26 Pa·s for the DPHA, and 365 Pa·s for the Acrylated Boltorn H20 (polyester HBP). The viscosity of the Acrylated Boltorn H20 was therefore in a comparable range to the materials studied by Lee et al. [10]. The corresponding viscosity for DPHA and the Acrylated Polyether HBP was already significantly lower, and therefore rheological analysis using the standard set-up was not possible.

The glass transition temperature of the monomers was measured by means of differential scanning calorimetry (TA Instruments Q100) at a heating rate of 10 K/min under N_2 atmosphere. The glass transition temperature of the polymers cured under UV light (240 mW/cm^2) was determined doing three-point bending tests on rectangular samples in a Rheometric Scientific RSA dynamic mechanical analyzer. Tests were performed at an excitation frequency of 1 Hz and a heating rate of 10 K/min, and the T_g was determined from the peak of tan(δ) [11]. The samples were produced using a 1 mm thick steel plate with a 52x12 mm^2 cut-out between two glass plates. After a short irradiation the samples were demolded whilst still in a rubber-like state, so as to be able to shrink freely during the subsequent irradiation. The T_g of DPHA (73% conversion) was found to be equal to 68 °C (Figure 3-7); the T_g of Acrylated Boltorn H20 (73% conversion) equalled 126 °C (Figure 3-8); and the T_g of Acrylated Polyether HBP (83% conversion) equalled 26 °C (Figure 3-9). For the Acrylated Boltorn H20 (Figure 3-8) a very broad tan δ peak was found, spanning over more than 100°C, indicating an inhomogeneous network [11, 12].

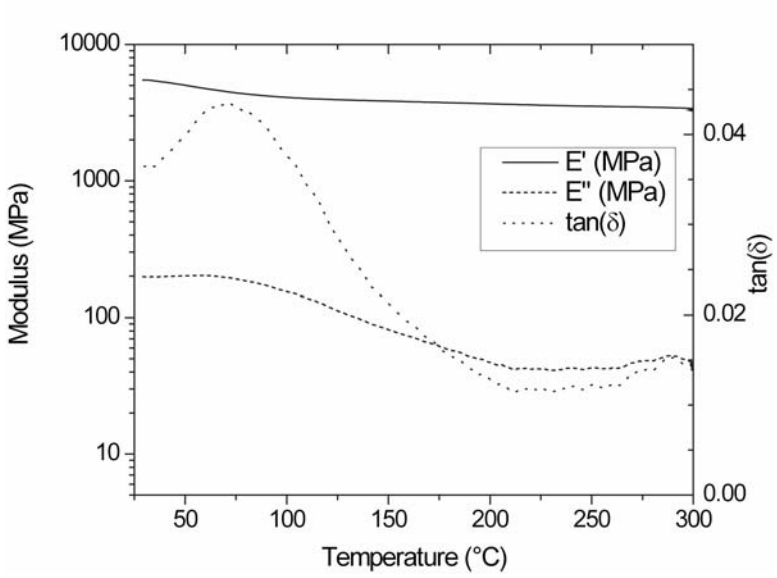

Figure 3-7 Storage modulus, loss modulus, and tan(δ) for UV cured DPHA measured in a 3-point-bending test. (73% conversion). Excitation frequency: 10 Hz.

The tan δ peaks of DPHA and the Acrylated Polyether HBP were not as broad indicating a more homogeneous network. Anseth et al. [12] studied the influence of the molecular structure on the glass transition temperature of different acrylates. Their study confirmed, that the tan δ peaks of acrylates typically span up to 100°C, due to the extreme heterogeneity of the acrylate network.

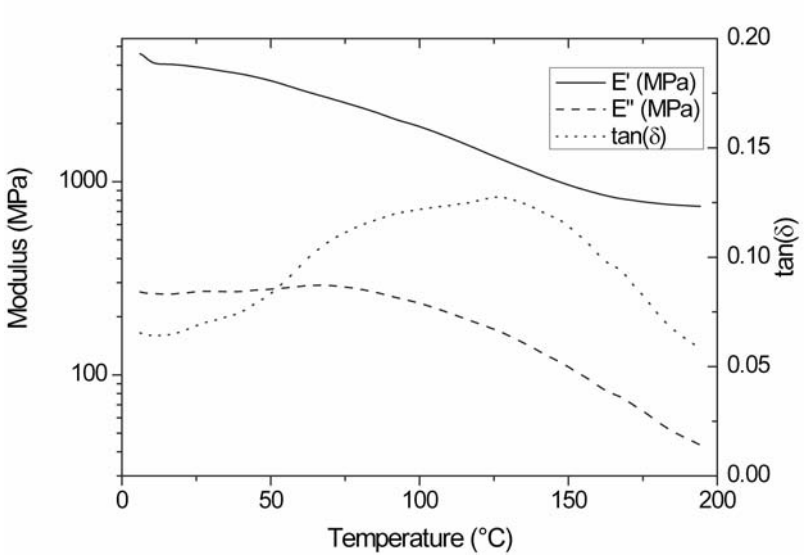

Figure 3-8 Storage modulus, loss modulus, and tan(δ) for UV cured Acrylated Boltorn H20 measured in a 3-point-bending test. (73% conversion). Excitation frequency: 10 Hz.

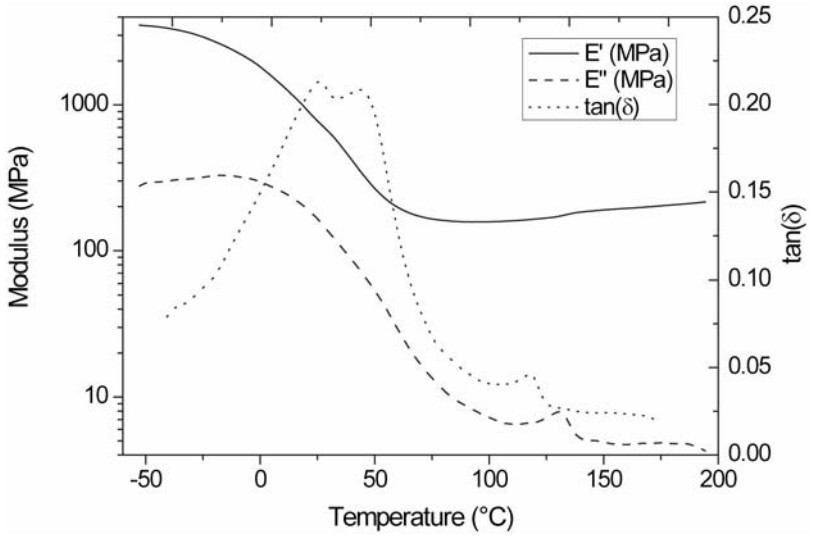

Figure 3-9 Storage modulus, loss modulus, and tan(δ) for UV cured Acrylated Polyether HBP measured in a 3-point-bending test. (73% conversion). Excitation frequency: 10 Hz.

There were also substantial differences in the magnitude of the tan δ peaks, which are a further indication of the damping capacity of the material. For the DPHA the tan δ value was about 0.045, whereas for the Acrylated Boltorn H20 it was 0.125 and for the Acrylated Polyether HBP 0.22. The HBPs therefore lie one order of magnitude above the values found by Anseth et al. [12] for highly functional acrylates.

The conversion of cured samples was determined by Fourier transform infrared spectroscopy (Nicolet Magna IR 560, attenuated total reflection mode). An attempt was also made to determine the T_g by differential scanning calorimetry (DSC), but this turned out to be not possible for most of the samples. Due to the inhomogeneous network formed in chainwise reacting acrylates, the T_g spans over a large temperature range, making it difficult to determine with DSC.

The Young's modulus was measured on rectangular specimens (20 x 4 x 0.15 mm3) using a miniature tensile tester (Minimat, Rheometric Scientific), equipped with video-extensometry, with strain resolution better than 0.001.

Table 3-1 Physical properties of the examined monomers. Mn: number molecular weight; Mw: mass molecular weight; AEW: acrylated equivalent weight; DB: degree of branching. Here the functionality denotes how many functions a monomer carries. Per one acrylate function, two bonds can be formed.

Property	**Unit**	**DPHA**	**Acr. Boltorn H20**	**Acr. Polyether HBP**
core		aliphatic	polyester HBP	polyether HBP
theor. functionality		6	16	32
actual functionality		5	13	29
M_n	[g/mol]	< 520	1434	3577
Newtonian viscosity	[Pa·s]	26	365	6
AEW	[g/mol]	104	316	294
DB (Fréchet)		-	0.43	0.4
T_g monomer	[°C]	-36	-26	-55
T_g polymer / at conversion	[°C]	68 / 73%	126 / 73%	28 / 83%
E_c	[GPa]	3.2	3.9	1.1
Acrylate Concentration	[mmol/g]	8.0	4.8	3.4
Heat for 100% Conversion	[J/g]	643.2	385.9	273.4

3.2.2 SU-8 – Engineering material for microfabrication

The physical properties of SU-8 are listed in Table 3-2. The fabrication consisted of a combination of thermal and UV curing and included the following steps: softbaking prior to UV-curing in order to remove the solvent (at 65 and 95 °C), post-exposure baking (PEB) after UV exposure (at 65 and 95 °C), and finally development. Sometimes a so-called hardbaking at a higher temperature (200 °C) was carried out. The duration of the following steps depends on the SU-8 layer thickness. A detailed description for a 100 µm layer can be found in Chapter 7.

Table 3-2 Mechanical properties of microstructures produced from SU-8.

Property	**Processing**	**Value**	**Ref.**
Young's modulus	after PEB at 95 °C	2.6 - 4.02 GPa	[13-16]
	after hardbake at 200 °C	2.7 - 4.95 GPa	[16, 17]
yield stress		34 MPa (after hardbake at 200 °C)	[17]
T_g (monomer)		~ 50 °C	[7]
T_g (polymer)		> 200 °C	[7]

3.3 Experimental Methods

The different experimental methods used for measuring a property change during UV curing are summarized in Table 3-3.

Table 3-3 Overview of real-time experimental methods to characterize photopolymerizations.

Experimental Method	Measured Property	Derived Property	Time Resolution	Film Thickness (mm)	UV Intensity Range (mW/cm^2)
Photo DSC	heat	conversion	0.2 s	< 0.5 mm	2-20
Photo Rheology	stress	modulus, phase angle	1 ms	< 0.1 mm	8-80
Beam Bending	deflection	internal stress	1 ms	< 0.3 mm	20-40
Interferometry	refractive index	conversion, shrinkage	1 ms	< 0.5 mm	5-500

3.3.1 Ultraviolet Source

An EFOS Novacure N2000 spotcure UV lamp was used to cure the samples in photorheology, photo DSC, and interferometry experiments, whereas a Dymax Flood Lamp PC-2000 was used in beam-bending experiments, and to cure larger films for tensile and three-point-bending test. The UV-B fraction (280-320 nm) of the EFOS spotcure lamp was about 22% and for the Dymax flood lamp 25% as determined via integration (Figure 3-10). Irgacure 184 reached its absorption peak at 320 nm, which meant that the photoinitiator could not tap the full spectra radiated from the lamps. The UV intensity was measured using the Sola-Check (Solatell, UK), and was found to vary by less than 20% between two illuminations.

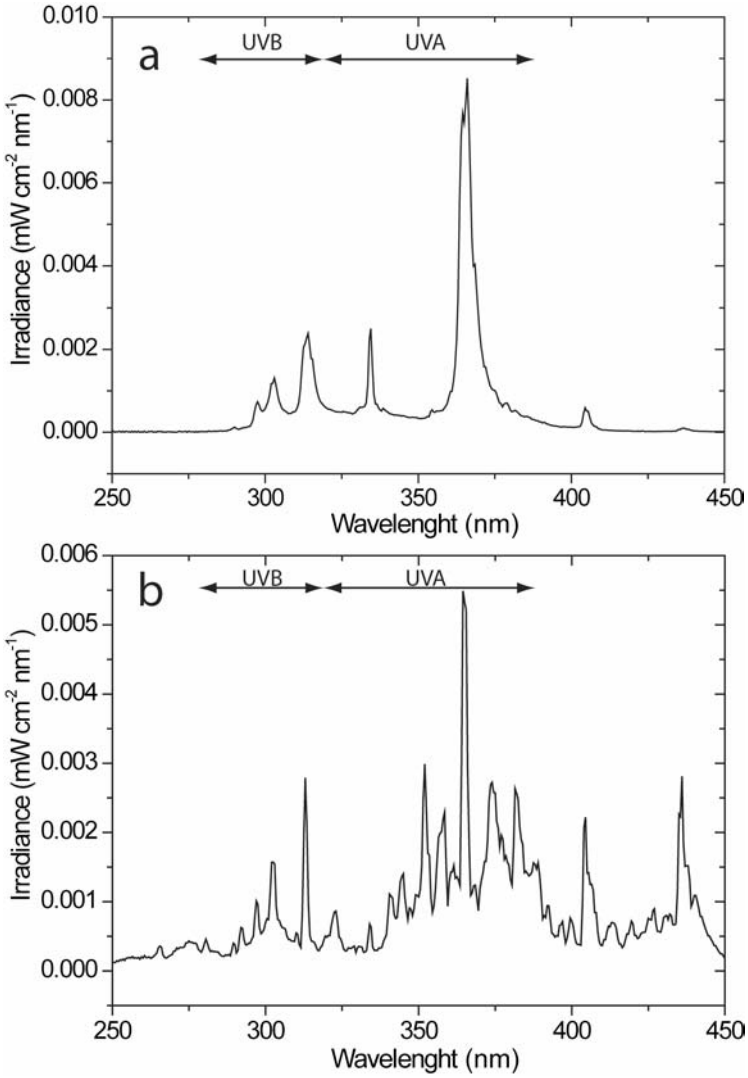

Figure 3-10 Spectrum of the a) EFOS Novacure N2000 spotcure lamp, and of the b) Dymax flood lamp PC-2000 measured with the spectrally resolved Sola-Scope 2000 (Solatell, UK).

3.3.2 Photo Differential Scanning Calorimetry and Fourier Transform Infrared Spectroscopy

The two methods mainly used for the characterization of the kinetics of a polymerization reaction are differential scanning calorimetry (DSC) and Fourier transformed infrared spectroscopy (FTIR). Both techniques are adapted for photopolymerizations. FTIR was enhanced to analyze photopolymerizations and to record the progression of the photocuring reaction with exposure time [18-20].

The heat of the photopolymerization reaction was measured by means of photo-differential scanning calorimetry [21-23] (photo-DSC, Perkin Elmer DSC7). The extent of conversion was therefore determined by relating the obtained heat of reaction to the theoretical heat of reaction for complete conversion. Open aluminum pans were used and a special cell for UV experiments. The cell comprised a lens,

which focused the UV light onto the sample pans. The sample-pan holders were sealed with windows which let the UV light pass through to the sample and the reference. An IR filter was used to cut out the IR part of the lamp spectrum. The sample space was flushed with nitrogen. To measure the UV intensity the Solatell Sola-Check^{TM} sensor was used. Tests were carried out isothermally mostly at room temperature. Several tests were performed on a TA Instruments DSC Q100 at 79 °C isothermally, which was the upper temperature limit of the equipment.

To obtain a reference value for full conversion, the concentration of acrylated functions per weight, determined via bromine titration [1], was multiplied by a reference value of 80.4 kJ/mol [24]. For DPHA a heat of 643.2 J/g, for the Acrylated Boltorn H20 a heat of 385.9 J/g, and for Acrylated Polyether HBP a heat of 273.4 J/g was determined (Table 3-1). This method was preferred to measuring the conversion with FTIR for each sample cured in the DSC, since a gradient in cure in the sample might induce an error.

3.3.3 Photorheology

The curing of acrylate systems normally takes place within a few seconds [25]. One possibility of monitoring the stiffness build-up during cure is the so-called UV rheology. It was shown that this technique is capable of monitoring the structure build-up in fast UV polymerizing resins, and of determining the gel point [26, 27].

Photorheological measurements were carried out on a controlled strain dynamic rotational rheometer (ARES, Rheometrics Scientific), combined with a UV-light generator equipped with an IR (or heat) filter. As depicted in Figure 3-11 a special upper fixture was designed to allow coupling with the UV source, the upper plate being made of quartz to ensure the transmittance of UV light. The sample was inserted between the quartz plate and a parallel steel plate, both with a diameter of 8 mm. All experiments were conducted at ambient temperature, under air. The onset of illumination was synchronized with the rheological data acquisition by sending an electric signal to the acquisition system while switching on the lamp. Since the current equipment was limited to one measurement per second, which was not sufficient to follow the fast curing of acrylates, a refined methodology is proposed and described in detail in Chapter 5.

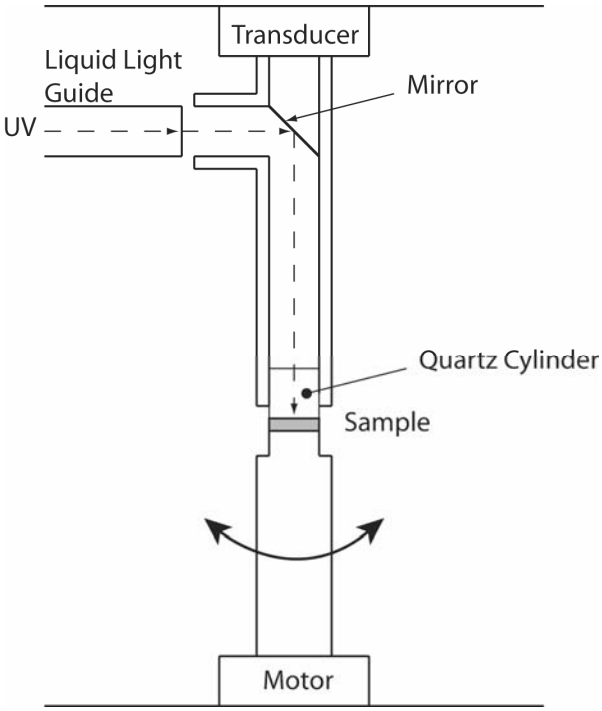

Figure 3-11 Photorheology set-up, redrawn from [10].

3.3.4 Internal Stress Measurement – Beam Bending

The in-plane internal stress of acrylate coatings was determined from the curvature of coated aluminum beams, and calculated according to the models of Stoney [28] and Inoue [29].

The most common method used to evaluate internal stress states in a coating is to measure the curvature or deflection of a coated elastic substrate (e.g. wafer, disk, strip, cantilever) [30]. In the beam-bending method [31], a thin layer of resin is coated onto a strip of metallic foil and cured. The curvature of the strip is a measure of the internal stress in the coating. Different models exist to calculate the internal stress σ_i, depending on coating and substrate thickness, starting with the classic expression derived by Stoney [28]:

$$\sigma_i = -\frac{E_s h_s^2}{6 r h_c} \tag{3.2}$$

where E_s is the Young's modulus of the substrate, h_c, h_s the thickness of coating and substrate respectively and r the radius of curvature. Refinements can be found in a number of studies [30, 32-35]. To calculate the internal stresses, the Inoue model was used, including correction for in-plane strain [29]:

$$\sigma_{\mathrm{i}} = -\frac{E_s h_s^2}{6 r h_c}\left(\frac{(1-ab^2)^3(1-a)+(ab(b+2)+1)^3+a(ab^2+2b+1)^3}{2(1+b)(1+ab)^3}\right) \tag{3.3}$$

where $a=E_c/E_s$, (E_c is the Young's modulus of the coating), and $b=h_c/h_s$.

A test set-up was developed that enabled the internal stress to be measured as a function of time: It was equipped with a capacitive deformation sensor and a UV sensor, which enabled the deformation to be recorded as a function of time, and the onset of illumination to be detected (Figure 3-12). The radius of curvature r was calculated as:

$$r = \frac{4g^2 + L^2}{8g} \approx \frac{L^2}{8g} \tag{3.4}$$

where L is the distance between the bearings (150 mm), and g is the measured deflection.

The deformation sensor weighed 0.5 grams, causing a deformation of approximately 1.5 mm. The initial deformation was subtracted from the final deformation, by setting the deformation sensor to zero before starting the measurement. This induced an error in the final stress calculation, which was below 1%. The system was calibrated, by locating it on different predefined positions; it showed an accuracy of +/- 2 μm. A nitrogen chamber was built around the set-up to avoid oxygen inhibition. It was flushed with N_2 prior to the experiment. The nitrogen chamber had a quartz window on top to let the UV-light pass through without changing its spectrum. The quartz surface was roughened in order to homogenize the UV intensity by scattering the UV light. The UV intensity was 40 mW/cm^2 and could be reduced to 6 mW/cm^2 by placing a small-meshed metallic grid above the quartz window.

As a substrate, 0.5 mm thick aluminum strips with a length of 180 mm and width of 8 mm were degreased and treated with a silane compound (2-Propenoic acid, 2-methyl-, 3-(trimethoxysilyl)propyl, Silquest A-174, GE Silicones) in order to promote adhesion of the acrylate coating: Therefore a solution of 3 wt.-% of Silquest A-174 in 4:1 isopropanol / distilled water was made and the pH was adjusted to 4.5 using acetic acid. The aluminum strips were immersed for 60 min in this solution, and subsequently the solvent was evaporated at 180 °C in an oven.

The acrylate was diluted in THF, applied onto the aluminum strip and the solvent was evaporated during 2h at 80 °C. The samples were produced in a nitrogen atmosphere (see Chapter 3).

In order to estimate the maximum deflection, for the strain to remain in the linear elastic range (0.2%), the following extreme case of an acrylate coating having the same thickness as the Al substrate (0.3 mm) and a Young’s modulus of 5 GPa (Al:

70 GPa) was considered: The neutral axis was calculated to be at a distance y_0 of 0.28 mm from the lower side of the Al beam from [36]:

$$y_0 = \frac{E_s h_s^2 + 2E_c h_s h_c + E_c h_c^2}{2\left(E_s h_s + E_c h_c\right)} \tag{3.5}$$

The maximum strain in the Al beam was calculated as:

$$\varepsilon = \frac{y_0}{r} = \frac{8 g y_0}{L^2} \tag{3.6}$$

Hence, the maximum tolerable deflection is 20 mm.

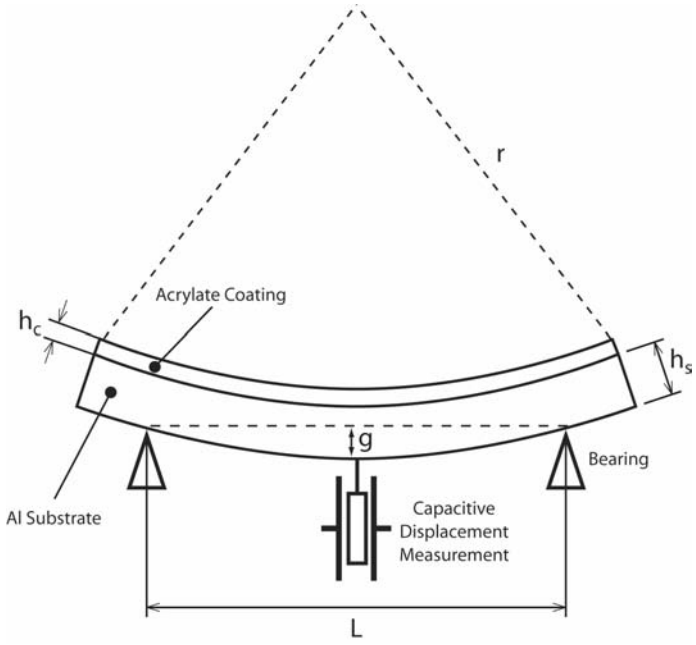

Figure 3-12 Schematic of beam-bending device.

3.3.5 Shrinkage Measurement

Polymerization shrinkage is an important parameter controlling the level of process induced internal stresses. In thermosets curing, it was measured, based on the density change of the resin during crosslinking [37]. In UV curing, the measurement is more challenging [38], due to the fast reaction. In 1992 de Boer et al. [39] proposed a laser based method which allowed the simultaneous measurement of shrinkage and refractive index change, during photopolymerization, with good time resolution.

Principle

The principle is similar to a Michelson interferometer (Figure 3-13). The following discussion is a summary of the detailed treatment given in de Boer's article.

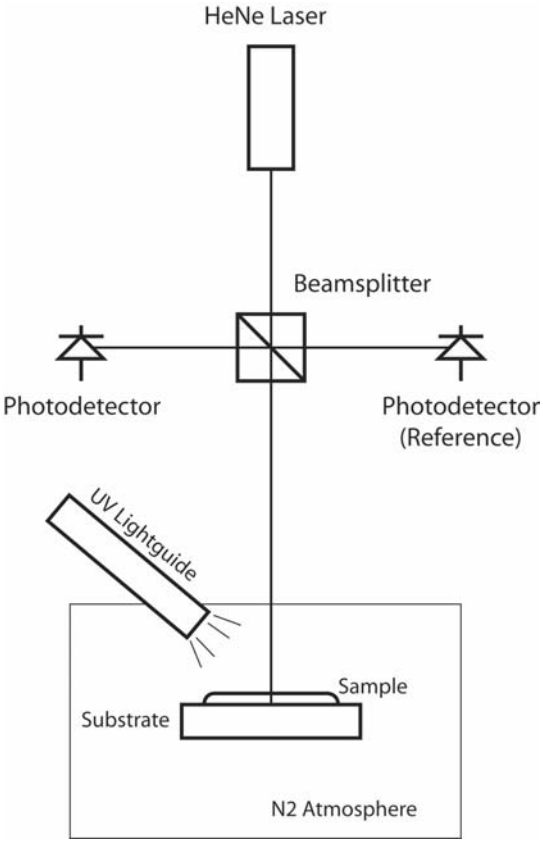

Figure 3-13 Experimental set-up for measuring polymerization shrinkage and change of refractive index during photopolymerization. Adapted from [39].

The laser, emitted at a wavelength λ of 632.8 nm, is split by the beamsplitter into two parts, one going to a reference detector and one going to the sample. One part is reflected at the sample surface and a second reflection happens at the sample/substrate interface. The wave coming to the photodetector is therefore a superposition of these two monochromatic planar reflected waves, having a phase difference of:

$$\Delta\delta = \frac{2\pi 2h_c(t)n_c(t)}{\lambda_L} \tag{3.7}$$

where h_c is the sample thickness, n_c its refractive index. The thickness is multiplied by 2 due to the dual passage of the wave through the polymer layer. The intensity of this superposed wave is:

$$I(t) = I_O + I_m \cos\left(\frac{2\pi 2h_c(t)n_c(t)}{\lambda_L}\right) \tag{3.8}$$

where I_O is the offset of the signal, and I_m its amplitude. The intensity of the reflected light is proportional to the squared magnitude of the ratio of the reflected to the incident amplitude of light [40, 41]:

$$|r_e|^2 = \frac{r_c^2 + r_s^2 + 2r_c r_s \cos(2\delta)}{1 + r_c^2 r_s^2 + 2r_c r_s \cos(2\delta)} \tag{3.9}$$

where δ is the phaseshift, and r_c and r_s are the Fresnel reflection coefficients:

$$r_c = \frac{1 - n_c}{1 + n_c} \qquad r_s = \frac{n_c - n_s}{n_c + n_s} \tag{3.10}$$

with n_c and n_s being the reflective index of the polymer coating and the substrate, respectively. Figure 3-14 shows the squared magnitude of the ratio of the reflected to the incident amplitude of light $|r_e|^2$ as a function of the phaseshift δ_1 and the reflective index of the polymer sample for an arbitrarily chosen refractive index n_s equals 4. It is obvious, that for a refractive index $n_c < n_s$ the maxima are independent of n_c, whereas for $n_s < n_c$ the minima are independent of n_c having the value:

$$|r_e|^2 = \left(\frac{n_s - 1}{1 + n_s}\right)^2 \tag{3.11}$$

One can calculate the change of refractive index of the sample by monitoring the change in amplitude.

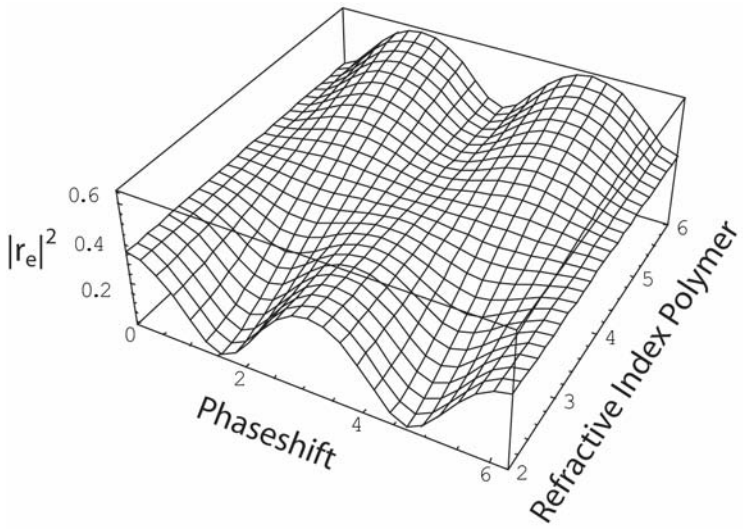

Figure 3-14 Squared magnitude of the ratio of reflected to incidental amplitude of light |re|2.as a function of the phase shift between the incoming and reflected wave, and of the refractive index The refractive index n2 of the substrate was set to 4.

The refractive index of the sample changes due to a change in the polarizability $\alpha(t)$ of the sample, as expressed in the Lorentz-Lorenz equation. The molar refraction R_{LL} changed proportionally with $\alpha(t)$ [42]:

$$R_{LL}(t) = \frac{n_c(t)^2 - 1}{n_c(t)^2 + 2} \frac{M}{\rho(t)} = \frac{4\pi N_A \alpha(t)}{3} \tag{3.12}$$

where M is the molecular weight of the monomer, $\rho(t)$ is the density at a time t, and N_A is Avogadro's number.

De Boer assumes a linear relationship between polarizability $\alpha(t)$ and the degree of double bond conversion $x(t)$:

$$\alpha(t) = \frac{\alpha_m + x(t)(\alpha_p - \alpha_m)}{1 - S_V(t)} \tag{3.13}$$

where α_m is the polarizability of the momomer, α_p is the polarizability of the polymer, and S_V is the volume shrinkage of the polymer. For small values of S_V this equation can be approximated by:

$$\alpha(t) = \alpha_m + x(t)(\alpha_p - \alpha_m) + S_V(t)\alpha_m \tag{3.14}$$

Substituting the Lorentz-Lorenz equation into the above equation leads to:

$$\frac{n_c(t)^2 - 1}{n_c(t)^2 + 2}\frac{M}{\rho(t)} = C\alpha_m + x(t)C(\alpha_p - \alpha_m) + x(t)C\alpha_m \tag{3.15}$$

with $C = 4\pi N_A / 3$ and $\rho(t) = \rho_m(1 + S_V(t))$, where ρ_m is the density of the monomer plus the initiator. Substituting the values $S_V(t)$ and $n_c(t)$ of a sample of known conversion $x(t)$ yields the unknown α_p. Measurement of the reflected intensity now enables the refractive index, shrinkage and conversion during polymerization to be calculated.

Set-up

Figure 3-15 and Figure 3-16 show the front and side views of the shrinkage device. The sample holder was placed on top of a bolt carrying a conical receiver. The micrometer screws pressed on this bolt, and were used to accurately position the sample at a right angle to the incident laser beam by maximizing the measured intensity at photodetector 1. The sample chamber was closed and flushed with nitrogen prior to and during the UV polymerization, and the measured signal at the photodetectors was set to 5 V using the variable gain adjustment of the photodetector unit.

The signals from photodetector 1 and 2 were acquired using a National Instruments NI 6052E card. The UV intensity was about 300 mW/cm^2 and could be reduced down to 9 mW/cm^2 using a tube to extend the distance between the sample and the UV light guide. The onset of illumination was synchronized with the data acquisition by sending an electric signal to the acquisition system while switching on

the lamp. The typical sampling frequency was 200 Hz. To evaluate the polymerization shrinkage the minima and maxima were detected.

The change in sample thickness h_c between a minimum and a maximum corresponds to:

$$\Delta h_c = \frac{\lambda_L}{4n_c(t)} = \frac{635nm}{4n_c} \tag{3.16}$$

where λ_L is the wavelength of the laser (635 nm), and n_c the refractive index of the coating. Using a standard refractometer the refractive indices of the different monomers were determined as 1.483 for DPHA, 1.486 for Acrylated Boltorn H20, and 1.478 for the Acrylated Polyether HBP at 20°C. The refractive index of the coating is a function of time but changes by less than 2% and can therefore be disregarded if one only wants to measure the linear shrinkage S_L during photopolymerization. It is calculated as:

$$S_L = \frac{N_{MM}\Delta h_c}{h_{c,fi} + N_{MM}\Delta h_c} \tag{3.17}$$

where N_{MM} is the number of maxima and minima. The volumetric shrinkage S_V is related to the linear shrinkage S_L as:

$$S_V = 3S_L - 3S_L^2 + S_L^3 \approx 3S_L \tag{3.18}$$

This simplification holds, since the linear shrinkage is usually smaller than 0.1.

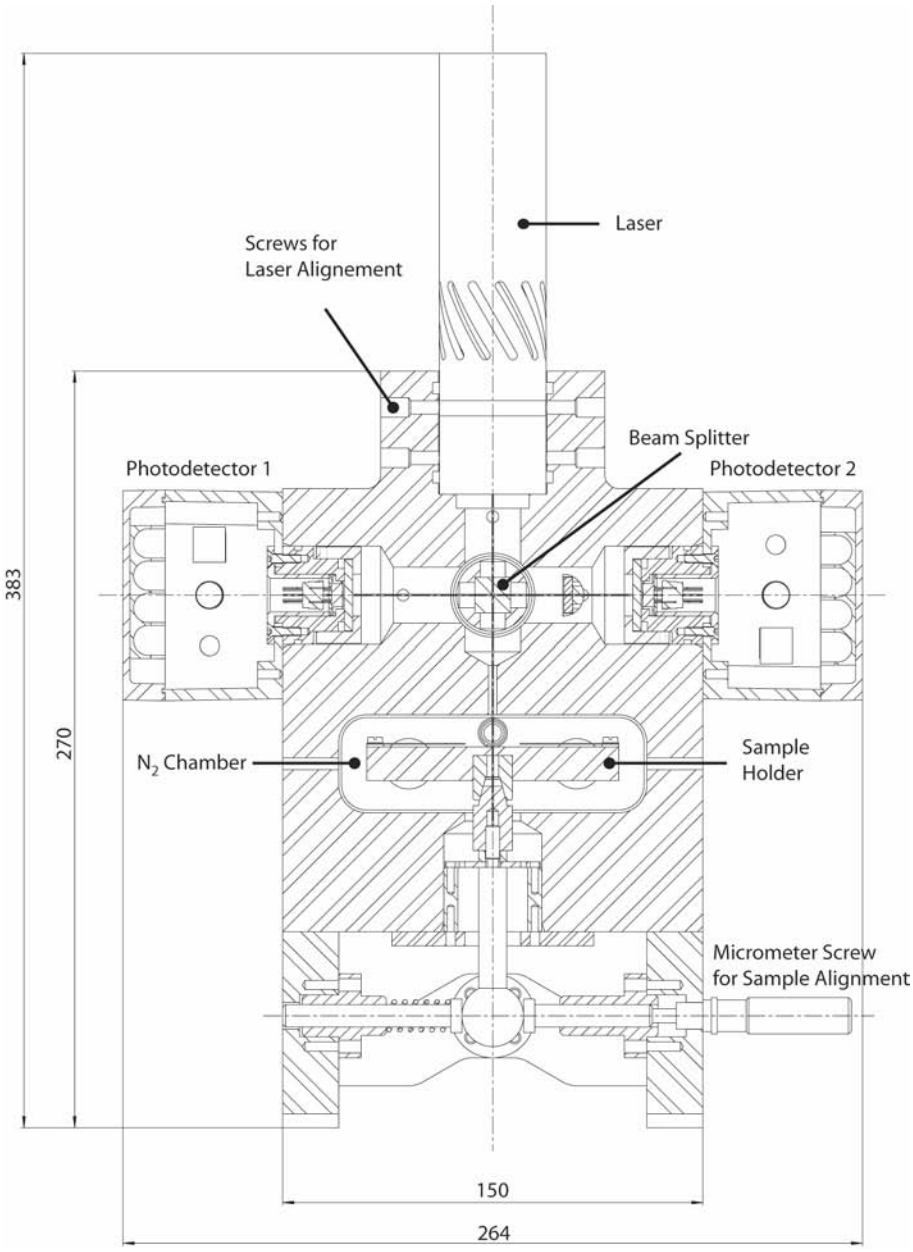

Figure 3-15 Front view of the shrinkage measurement device.

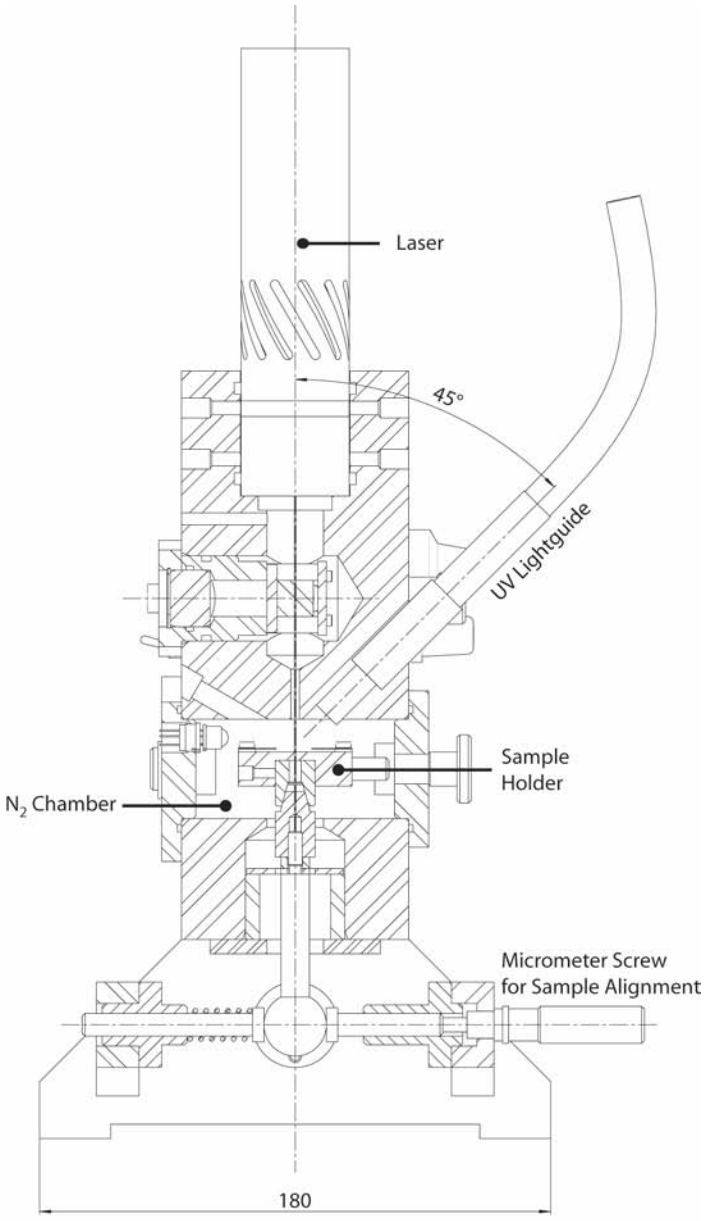

Figure 3-16 Side view of the shrinkage measurement device.

Test Procedure

A 100 µm layer of resin was spread on a laboratory glass slide using a doctor blade. The sample was allowed to flow for two hours. Subsequently it was fixed on the sample holder, and the sample holder was placed in the reaction chamber. The reaction chamber was closed and flushed with N_2 for two minutes, and the sample position was adjusted as described above. Once the acquisition was started, the UV exposure was triggered. After completion of the test the sample thickness was measured using a caliper, and the shrinkage was back-calculated. Since the exact incident position of the laser beam could not be marked on the liquid sample, the

thickness measurement induced a certain error into the calculation that was assumed to be about ±10%.

3.4 References

1. Kratochbil, B., P.K. Chattopadhyay, and R.D. Krause, *Determination of olefins by direct titration with bromine in propylene carbonate.* Analytical Chemistry, 1976. **48**(3): p. 568-570.
2. Malmström, E., M. Johansson, and A. Hult, *Hyperbranched aliphatic polyesters.* Macromolecules, 1995. **28**: p. 1698-1703.
3. Magnusson, H., E. Malmström, and A. Hult, *Synthesis of hyperbranched aliphatic polyethers via cationic ring-opening polymerization of 3-ethyl-3-(hydroxymethyl)oxetane.* Macromolecular Rapid Communications, 1999. **20**: p. 453-457.
4. Rodlert, M., C.J.G. Plummer, L. Garamszegi, Y. Leterrier, H.J.M. Grünbauer, and J.-A.E. Månson, *Hyperbranched polymer/montmorillonite clay nanocomposites.* Polymer, 2004. **45**: p. 949-960.
5. Scherzer, T. and U. Decker, *Kinetic investigations on UV-induced photopolymerization reactions by real-time FTIR-ATR spectroscopy: the efficiency of photoinitiators at 313 nm and 222 nm.* Nuclear Instruments and Methods in Physics Research B, 1999. **151**: p. 306-312.
6. Gelorme, J.D., R.J. Cox, and S.A.R. Gutierrez, *Photoresist composition and printed circuit boards made therewith.* 1987: European Union.
7. La Bianca, N. and J.D. Gelorme. *High aspect ratio resist for thick film application.* in *Advances in Resist Technology and Processing XII*. 1994. Bellingham, WA: The International Society for Optical Engineering (SPIE).
8. Lee, K.Y., N. La Bianca, S.A. Rishton, S. Zolgharnain, J.D. Gelorme, J. Shaw, and T.H.-P. Chang, *Micromaching applications of a high resolution ultrathick photoresist.* Journal of Vacuum Science and Technology B, 1995. **13**(6): p. 3012-3016.
9. Genolet, G., *New photoplastic fabrication techniques and devices based on high aspect ratio photoresist*, in *Département de Microtechnique*. 2001, Ecole Polytechnique Fédérale de Lausanne: Lausanne. p. 1-138.
10. Lee, S.S., A. Luciani, and J.-A.E. Månson, *A rheological characterisation technique for fast UV-curable systems.* Progress in Organic Coatings, 2000. **38**: p. 193-197.
11. Hill, L.W., *Dynamic mechanical and tensile properties*, in *Paint and coating testing manual*, K. J.V., Editor. 1995, ASTM: Philadelphia. p. 534-546.
12. Anseth, K.S., C.N. Bowman, and N.A. Peppas, *Dynamic mechanical studies of the glass transition temperature of photopolymerized multifunctional acrylates.* Polymer Bulletin, 1993. **31**: p. 229-233.
13. Lorenz, H., M. Despont, N. Fahrni, N. La Bianca, P. Renaud, and P. Vettiger, *SU-8: a low-cost negative resist for MEMS.* Journal of Micromechanics and Microengineering, 1997. **7**: p. 121-124.
14. McAleavey, A., G. Coles, R.L. Edwards, and J.W.N. Sharpe. *Mechanical properties of SU-8*. 1999: Materials Research Society.
15. Feng, R. and R.J. Farris, *The characterization of thermal and elastic constants for an epoxy photoresist SU8 coating.* Journal of Materials Science, 2002. **37**: p. 4793-4799.

16. Feng, R. and R.J. Farris, *Influence of processing conditions on the thermal and mechnical properties of SU8 negative photoresist coatings.* Journal of Micromechanics and Microengineering, 2003. **13**: p. 80-88.
17. Dellmann, L., S. Roth, C. Beuret, G.-A. Racine, H. Lorenz, M. Despont, P. Renaud, P. Vettiger, and N.F. de Rooij. *Fabrication process of high aspect ratio elastic structures for piezoelectric motor applications*. in *1997 International Conference on Solid-State Sensors and Actuators (Transducers '97)*. 1997. Chicago: IEEE.
18. Collins, G.L., D.A. Young, and J.R. Costanza, *Reactions of UV curable resin formulations and neat multifunctional acrylics: I. apparatus and procedure*. Journal of Coatings Technology, 1976. **48**: p. 48-51.
19. Decker, C. and K. Moussa, *A new method for monitoring ultra-fast photopolymerizations by real-time infra-red (RTIR) spectroscopy*. Die Makromolekulare Chemie, 1988. **189**: p. 2381-2394.
20. Decker, C. and K. Moussa, *Kinetic investigation of photopolymerizations induced by laser beams.* Die Makromolekulare Chemie, 1990. **191**: p. 963-979.
21. Wight, F.R. and G.W. Hicks, *Applications of differential scanning calorimetry to photocurable polymer systems.* Polymer Engineering and Science, 1978. **18**(5): p. 378-381.
22. Flammersheim, H.J., N. Eckardt, and W. Kunze, *The deconvolution of DSC-curves in the experimental time domain.* Thermochimica Acta, 1991. **187**: p. 269-274.
23. Höhne, G.W.H., W. Hemminger, and H.-J. Flammersheim, *Differential scanning calorimetry: and introduction for practitioners*. 1996, Berlin, Heidelberg: Springer-Verlag. 222.
24. Hoyle, C.E., *Calorimetric analysis of photopolymerization*, in *Radiation Curing: Science and Technology*, S.P. Pappas, Editor. 1992, Plenum Press: New York. p. 57-133.
25. Decker, C., *UV-curing chemistry: past, present, and future.* Journal of Coatings Technology, 1987. **59**(751): p. 97-106.
26. Chiou, B.-S., R.J. English, and S.A. Khan, *Rheology and photo-cross-linking of thiol-ene polymers.* Macromolecules, 1996. **29**: p. 5368-5374.
27. Chiou, B.-S., R.J. English, and S.A. Khan, *UV cross-linking of thiol-ene polymers: a rheological study*, in *Photopolymerization: fundamentals and application*, A.B. Scranton, C.N. Bowman, and R.W. Pheiffer, Editors. 1997, American Chemical Society: Washington. p. 150-166.
28. Stoney, G.G., *The tension of metallic films deposited by electrolysis.* Proceedings of the Royal Society of London Series A-Mathematical and Physical Sciences, 1909. **82**(P Roy. Soc. A-Math. Phy.): p. 172-175.
29. Inoue, Y. and Y. Kobatake, *Mechanics of adhesive joints Part III. Evaluation of residual stress.* Applied Scientific Research, 1958. **A7**: p. 314-324.
30. Francis, L.F., A.V. McCormick, D.M. Vaessen, and J.A. Payne, *Development and measurement of stress in polymer coatings.* Journal of Materials Science, 2002. **37**: p. 4717-4731.
31. Dannenberg, H., *Determination of stresses in cured epoxy resins.* SPE Journal, 1965. **21**: p. 669-675.
32. Corcoran, E.M., *Determining stresses in organic coatings using plate beam deflection.* Journal of Paint Technology, 1969. **41**(538): p. 635-640.
33. Timoshenko, S.P. and J.N. Goodier, *Theory of elasticity*. Third edition ed. 1970, Singapore: McGraw-Hill Book Co. 567.

34. Benabdi, M. and A.A. Roche, *Mechanical properties of thin and thick coatings applied to various substrates. Part I. An elastic analysis of residual stresses within coating materials.* Journal of Adhesion Science and Technology, 1997. **11**: p. 281-299.
35. Stolov, A.A., T. Xie, J. Penelle, and S.L. Hsu, *An analysis of photopolymerization kinetics and stress development in multifunctional acrylate coatings.* Polymer Engineering and Science, 2001. **41**(2): p. 314-328.
36. Clifford, S.M., *Fracture behaviour of metal-composite joints*, in *St. Catharine's College*. 2002, University of Cambridge: Cambridge. p. 170.
37. Eom, Y., L. Boogh, V. Michaud, P. Sunderland, and J.-A.E. Månson, *Stress-initiated void formation during cure of a three-dimensionally constrained thermoset resin.* Polymer Engineering and Science, 2001. **41**(3): p. 492-503.
38. Jakubiak, J. and L.-Å. Lindén, *Contraction (shrinkage) in polymerization: Part I. Fundamentals and measurement.* Polimery, 2001. **46**(7-8): p. 522-528.
39. de Boer, J., R.J. Visser, and G.P. Melis, *Time-resolved determination of volume shrinkage and refractive index change of thin polymer films during photopolymerization.* Polymer, 1992. **33**(6): p. 1123-1126.
40. Heavens, O.S., *Optical properties of thin solid films*. 1965, New York: Dover Publications. 55-62.
41. Heimann, P.A., *Optical etch-rate monitoring using active device areas: lateral interference effects.* Journal of the Electrochemical Society, 1985. **132**: p. 2003-2006.
42. van Krevelen, D.W., *Properties of polymers: their correlation with chemical structure; their numerical estimation and prediction from additive group contributions*. 3rd ed. 1997, Amsterdam: Elsevier. 290-296.

4 Kinetics of Network Formation

In this Chapter the UV curing behavior of highly functional acrylate systems is investigated paying particular attention to the influence of intensity and reactive blend composition, and a criterion for identifying vitrification from photo DSC measurements is proposed.

4.1 Photocalorimetry Analysis

Figure 4-1 a to Figure 4-3 a show the double bond conversion as a function of time and UV intensity for DPHA, Acrylated Boltorn H20 (polyester HBP), and Acrylated Polyether HBP, respectively. After a short induction time (less than 5 s), which was attributed to the formation of initiator-derived radicals and the inhibiting effect of dissolved oxygen, the reaction took off and within a few seconds reached a conversion of about 30% to 50%, after which it considerably slowed down, eventually reaching a plateau value. The final conversion increased in intensity: This was explained by the fact that the shrinkage lagged back behind the conversion, the more so, the higher the intensity [1, 2]. Therefore at higher intensities there was an excess mobility which enabled higher ultimate conversions to be reached. In the following,

the maximum conversion is defined as the conversion for which the polymerization rate was smaller than 1% of the maximum polymerization rate [3].

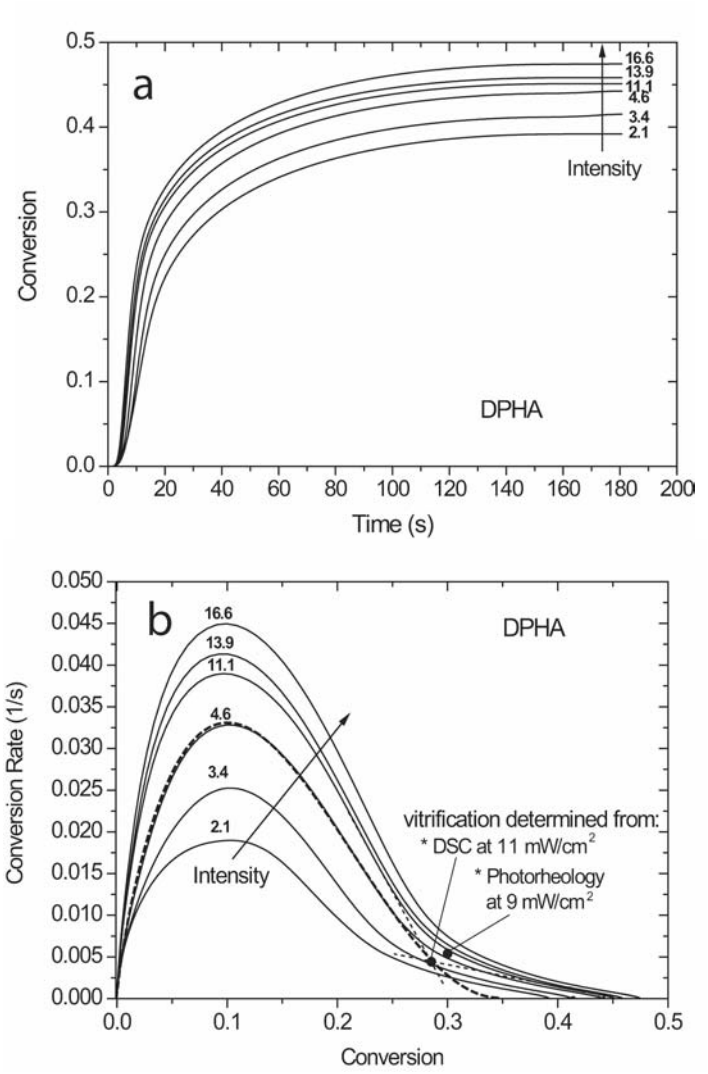

Figure 4-1 (a) Double bond conversion as a function of time, and (b) conversion rate as a function of conversion for DPHA cured under different UV intensities (mW/cm^2). The onset of vitrification is indicated. The autocatalytic model is also compared to the conversion rate data for an intensity of 4.6 mW/cm^2. The model was fitted to the data up to the onset of vitrification and extrapolated beyond vitrification onset back to a zero conversion rate.

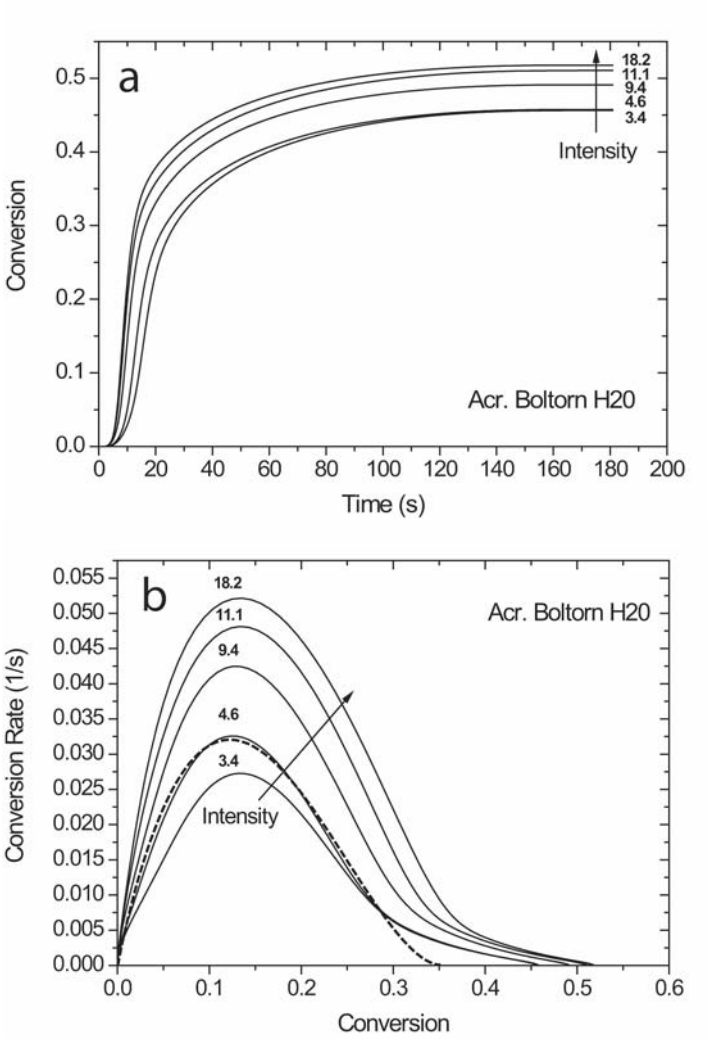

Figure 4-2 (a) Double bond conversion as a function of time, and (b) conversion rate as a function of conversion for Acrylated Boltorn H20 cured under different UV intensities (mW/cm^2).

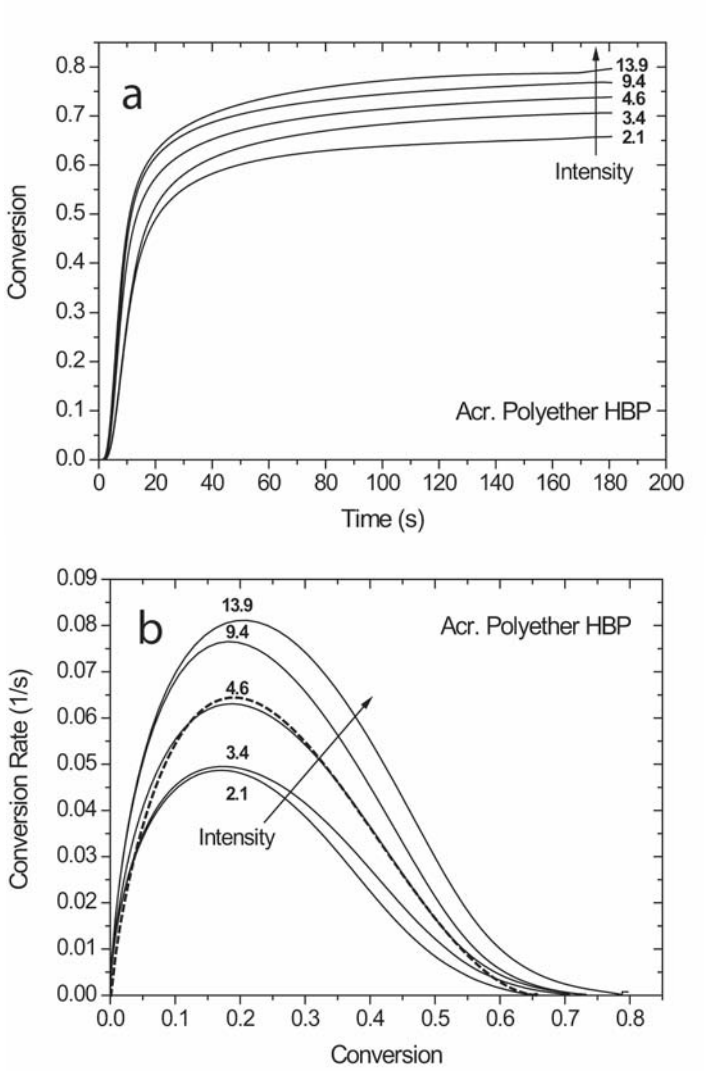

Figure 4-3 (a) Double bond conversion as a function of time, and (b) conversion rate as a function of conversion for Acrylated Polyether HBP cured under different UV intensities (mW/cm^2).

Comparing the three different monomers, it is evident that DPHA reached the lowest final conversion, followed by Acrylated Boltorn H20, and then Acrylated Polyether HBP which achieved the highest final conversion. Two main factors contributed to these differences in final conversion. Firstly, higher ultimate T_g implies lower conversion at vitrification during an isothermal cure below the ultimate T_g, and hence a lower final conversion. The T_g of DPHA was found to be 40°C above the cure temperature (at 73% conversion), whereas in Acrylated Boltorn H20 it was 100°C above the cure temperature (also at 73% conversion). This also explains why vitrification of DPHA could be identified as a distinct event by means of photorheology [4], whereas in Acrylated Boltorn H20 vitrification was a gradual process starting right after gelation. In the cured state, Acrylated Polyether HBP had a lower T_g compared to that of Acrylated Boltorn H20 because the polyether core of

Acrylated Polyether HBP is more flexible compared to the polyester core of Acrylated Boltorn H20 [5].

Secondly, compared to DPHA, Acrylated Boltorn H20 has an acrylate equivalent weight that is three times higher, which also contributed to its higher final conversion compared to that of DPHA. This result is supported by the work of Cook, who found that the rate of the propagation reaction decreased with decreasing length of the spacer group between methacrylate units [6].

4.1.1 The Three Stages in Acrylate Conversion

Figure 4-1 also shows the conversion rate as a function of double bond conversion for the three materials. In all cases, three main polymerization stages were identified: At the beginning of the reaction there was a notable sharp increase in the rate of polymerization, which corresponded to gelation or autoacceleration. In this first stage, no steady state could be identified, in which the conversion rate stayed constant before autoacceleration set in. This does not agree with the findings of Kurdikar and Peppas [7], who developed a model for diffusion-controlled photopolymerizations for diacrylate monomers. In the early stages of the reaction the increasing viscosity significantly reduced the mobility of the long-chain radical species. Hence it was more unlikely for two radical species to approach each other and recombine. The rate constant for termination dropped dramatically [8], and the rate of polymerization increased. The initiation and propagation steps were barely affected because the mobility of the small monomer molecules was still high, even though viscosity of the reaction mixture was increasing.

The second stage started after going through a maximum rate of polymerization (reaction peak). In the case of DPHA and Acrylated Boltorn H20, conversion at the reaction peak was equal to ca. 10% and 13% respectively, and was found to be independent of intensity. In the case of the Acrylated Polyether HBP the conversion at the reaction peak shifted from ca. 17% ($I = 2.1\ mW/cm^2$) to 22% ($I = 13.9\ mW/cm^2$).

During the second stage, the reaction rate dropped quicker as would be expected from the consumption of monomers only [9] (autodeceleration), and the overall reaction became purely diffusion controlled. For Acrylated Boltorn H20 (Figure 4-2 b), the maximum reaction rates were about 0.06 s^{-1} higher compared to those of DPHA (Figure 4-1 b); and for Acrylated Polyether HBP (Figure 4-3 b) they were 0.35 s^{-1} higher than for Acrylated Boltorn H20. Again, the different molecular structures were responsible for that behavior: The kinetics of bulk photopolymerizations is a

largely diffusion-controlled process. The more flexible core of Acrylated Polyether HBP, compared to that of Acrylated Boltorn H20, facilitated diffusion.

In the third stage, which is clear for DPHA (Figure 4-1 b) and Acrylated Boltorn H20 (Figure 4-2 b), and less pronounced for Acrylated Polyether HBP (Figure 4-3 b), the reaction continued at a very low rate. This 3rd stage may be attributed to vitrification, following a study by Yu et al. [10]. A criterion for vitrification onset is proposed from the present results. It is defined as the crossover point, x_{vi}, of the tangent at the inflection point in the second stage, and the tangent to the third stage when the conversion rate *dx/dt = 0.001/s*. This criterion matches the photorheology analysis of these acrylate systems: In the case of DPHA, and under an intensity of 9 mW/cm^2, vitrification was measured after 17 s, corresponding to a conversion of 29% [4]. At 11 mW/cm^2, vitrification was determined at a conversion of 28.5% according to the present criterion.

Figure 4-4 shows the conversion behavior of the three monomers cured at 79°C, which was the maximum achievable temperature in the photo-DSC apparatus. Increasing the temperature will provide additional mobility to the reactive species in the curing network leading to higher ultimate conversion and also to a higher T_g. Setting the curing temperature to 79 °C (which is well above the ultimate T_g for Acrylated Polyether HBP (28 °C at 83% conversion) and slightly above the T_g for DPHA (68 °C for 73% conversion) but well below the T_g of Acrylated Boltorn H20 (126 °C for 73%) increases the ultimate conversion for DPHA from 48.5% to 65%, for Acrylated Boltorn H20 from 52.5% to 74%, and for Acrylated Polyether HBP from 80.5% to 87%: This suggests, that the higher the final T_g, the higher the measured increase in conversion, compared to isothermal curing at room temperature.

From Figure 4-4 b it is clear that the third stage in the rate profile is less pronounced when the curing temperature is increased. This result confirms that the third stage is controlled by vitrification, in the case of curing below the ultimate glass transition temperature of the acrylate.

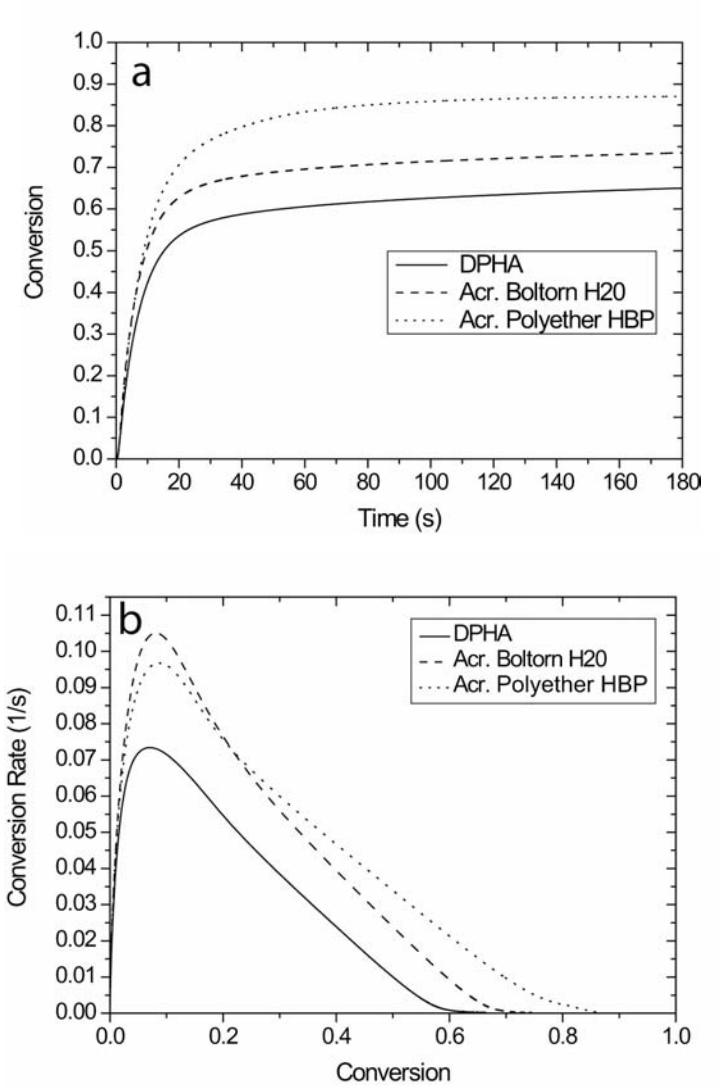

Figure 4-4 a) Conversion as a function of time, and b) Conversion rate as a function of conversion for the three different monomers cured at 79°C at an intensity of 20 mW/cm^2.

4.1.2 Conversion of DPHA / HBP Reactive Blends

The conversion profiles for reactive blends of DPHA with the two different HBPs are reproduced in Figure 4-5 to Figure 4-8. Similar behavior, compared to that of pure products, is evident. Vitrification onset was systematically at higher conversion rates for the DPHA/HBP blends, compared to pure DPHA.

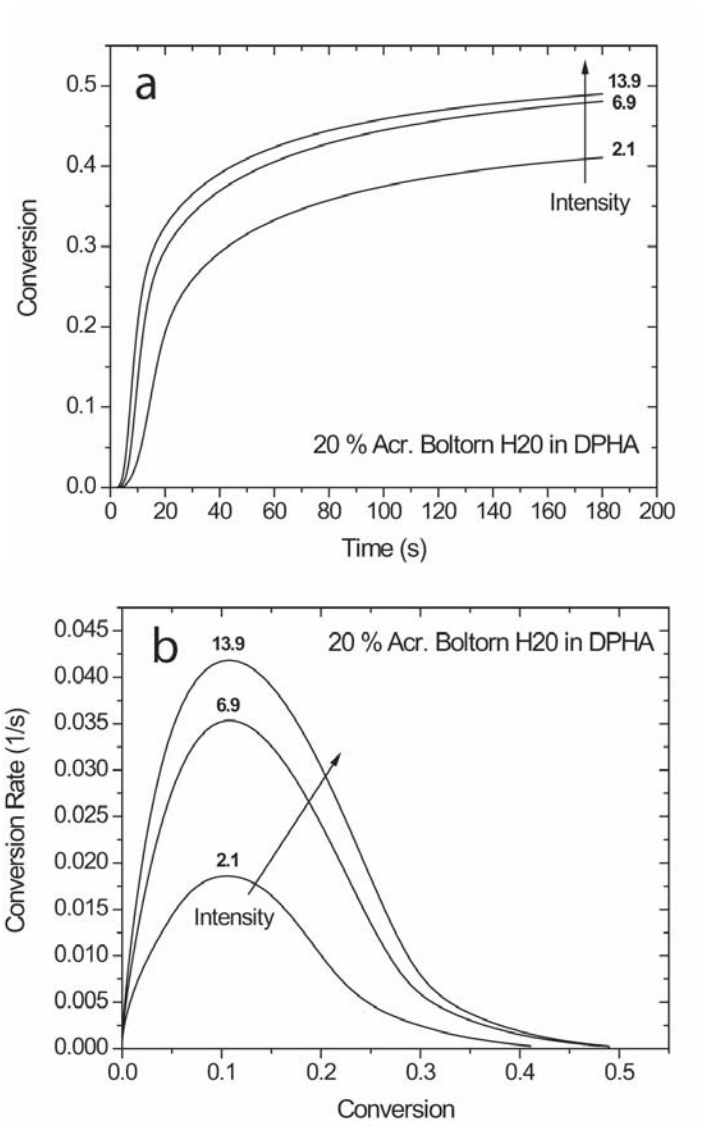

Figure 4-5 (a) Double bond conversion as a function of time, and (b) conversion rate as a function of conversion for 20 wt.-% Acrylated Boltorn H20 in DPHA cured under different UV intensities (mW/cm^2).

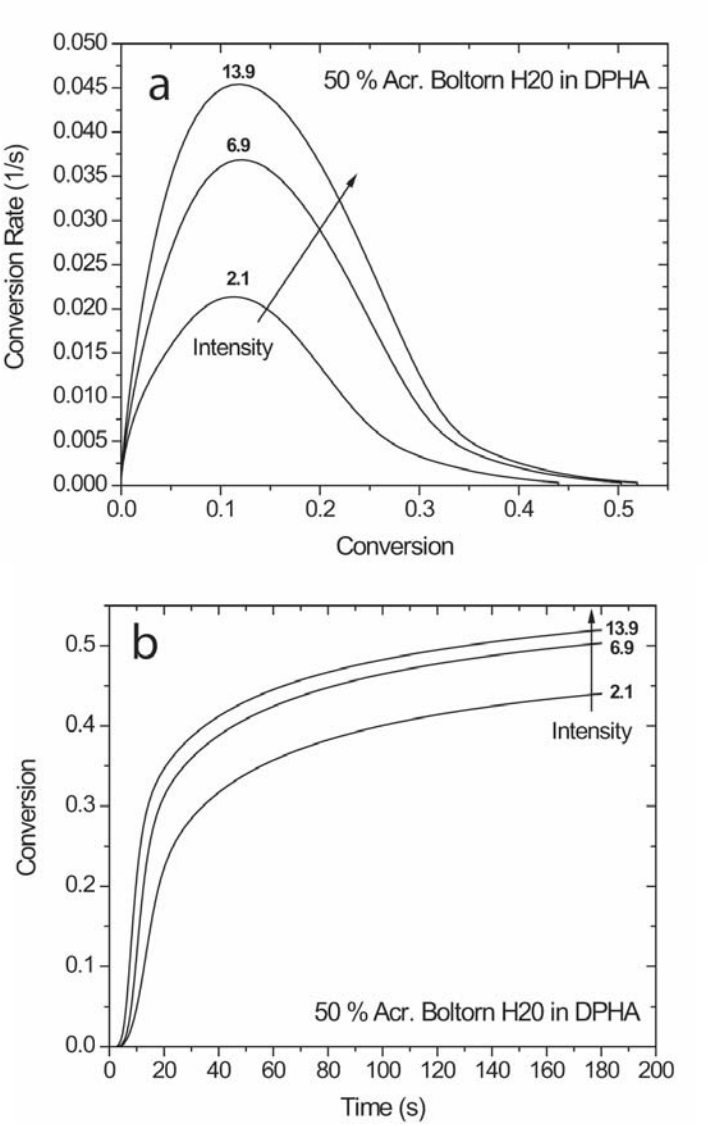

Figure 4-6 (a) Double bond conversion as a function of time, and (b) conversion rate as a function of conversion for 50 wt.-% Acrylated Boltorn H20 in DPHA cured under different UV intensities (mW/cm^2).

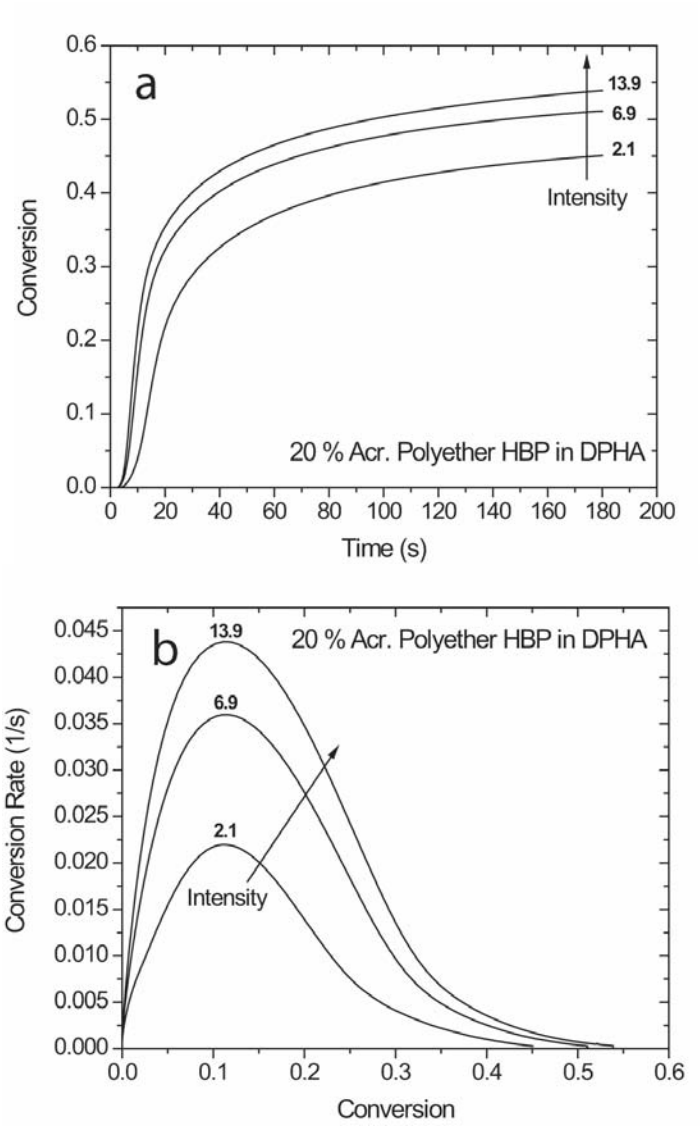

Figure 4-7 (a) Double bond conversion as a function of time, and (b) conversion rate as a function of conversion for 20 wt.-% Acrylated Polyether HBP in DPHA cured under different UV intensities (mW/cm^2).

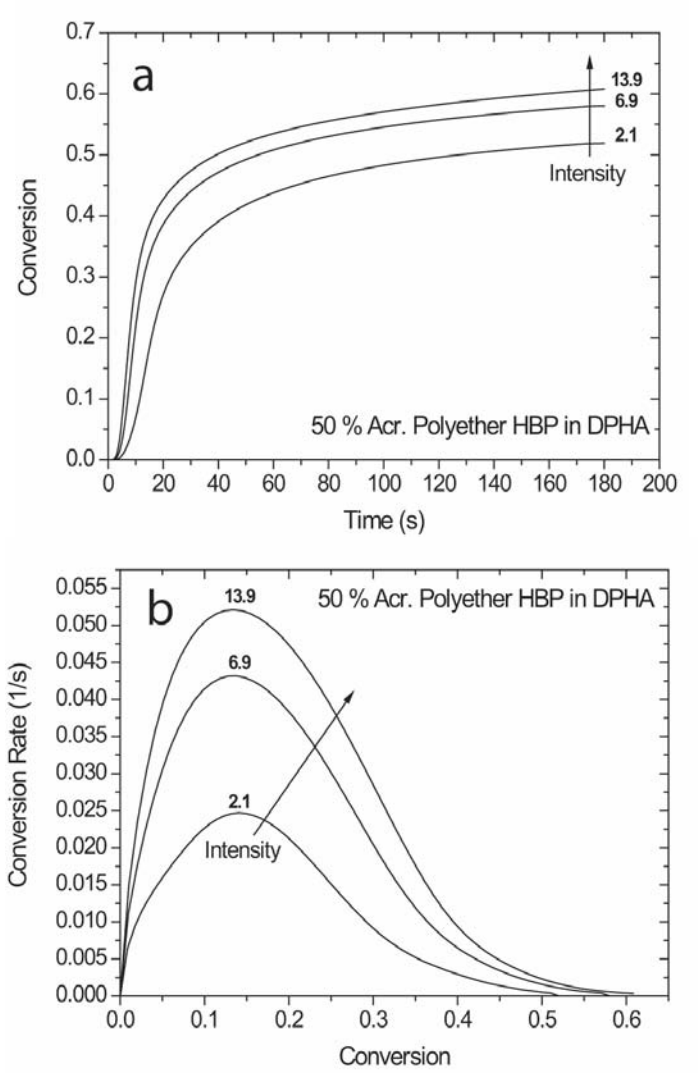

Figure 4-8 (a) Double bond conversion as a function of time, and (b) conversion rate as a function of conversion for 50 wt.-% Acrylated Polyether HBP in DPHA cured under different UV intensities (mW/cm^2).

The influence of intensity and composition on the kinetics of photopolymerization will be discussed in detail in the following section, with particular attention paid to the onset of vitrification.

4.2 Conversion Modeling

Conversion data obtained with Fourier transform IR spectroscopy (FTIR) or photo DSC can be analyzed using mechanistic or phenomenological models. Mechanistic models, which take into account the processes leading up to polymerization of the system, include the diffusion-controlled nature of the polymerization of highly functional monomers [7]. Phenomenological models are more general and only look at the overall reaction. They are used, for example, when the termination mechanism is not known.

One phenomenological model successfully applied to the UV curing of acrylates was the autocatalytic model [11-13], closely related to the Kamal model for thermoset curing [14, 15]:

$$\frac{dx}{dt} = K\left(1 - \frac{x}{x_m}\right)^p \left(\frac{x}{x_m}\right)^q \tag{4.1}$$

where x is the conversion, x_m represents the maximum conversion obtained in isothermal cure, K is a rate constant, p the reaction order and q the autocatalytic exponent, which stands for the auto-acceleration of the UV reaction [16], i.e. the immobilization of the reactive chain ends due to an increase in viscosity, resulting in a drop of the termination rate. This model was derived from the autocatalytic Kamal model [17], which was developed for the thermal cure of polyesters. Although the photopolymerization of acrylates is not autocatalytic but auto-accelerated, these models are well suited for describing this class of reactions providing that the system does not vitrify. After vitrification the volume relaxation is retarded with respect to chemical conversion, providing excess volume for diffusion, which is not accounted for in this model. Therefore, the measured conversion profiles were only modeled from zero conversion to conversion at vitrification onset x_{vi}. A model conversion curve is compared with measured conversion data in Figure 4-1 b.

The influence of intensity I on the reaction rate K, the conversion at vitrification $x_{vi,}$ and the maximum conversion x_m ,was modeled assuming power law behavior:

$$K(I) \sim I^{\beta_1} \tag{4.2}$$

$$x_{vi}(I) \sim I^{\beta_2} \tag{4.3}$$

$$x_m(I) \sim I^{\beta_3} \tag{4.4}$$

where the exponent β_1 is related to the termination mechanism; β_2 and β_3 are empirical constants. For $\beta_1 < 0.5$, second order and primary radical termination is predominant (reaction of an initiator radical with a radical site on the evolving polymer). For $\beta_1 = 0.5$ second order termination is predominant (reaction of two radical polymer sites). For $0.5 < \beta_1 < 1$ first order (e.g. trapping of the radical end in the forming network, or recombination with oxygen) and second order terminations happen in parallel. For $\beta_1 = 1$, first order termination is predominant [1, 18].

4.3 Influence of Composition

The influence of the blend composition on rate constant, conversion at vitrification, and maximum conversion is shown in Figure 4-9 and Figure 4-10. Since

DPHA and Acrylated Boltorn H20 react in a similar manner, and both vitrifying during UV polymerization, the rate constant varies only to a small extent. The reaction order and autocatalytic exponents are found to be close to 2 and 1, respectively, so that the overall reaction order is approximately 3, in agreement with previous analysis of dimethacrylate oligomers [16].

For the maximal conversion reached, the value of 50% Acrylated Boltorn H20 concentration in DPHA lies above the value for the pure product (Figure 4-9). This result explains why the Young's modulus of the 1/1 Acrylated Boltorn H20/DPHA blend (5.0 GPa) was found to be higher than that of either pure DPHA (3.2 GPa) or pure Acrylated Boltorn H20 (3.9 GPa) [19]. The higher conversion of the blend results from the combined synergetic action of increased network mobility and related lower unsaturation concentration compared to DPHA, and reduced viscosity compared to Acrylated Boltorn H20. A similar trend was found for a reactive blend of an acrylated HBP with TMPTA [20] and for HBP-containing epoxy formulations [21].

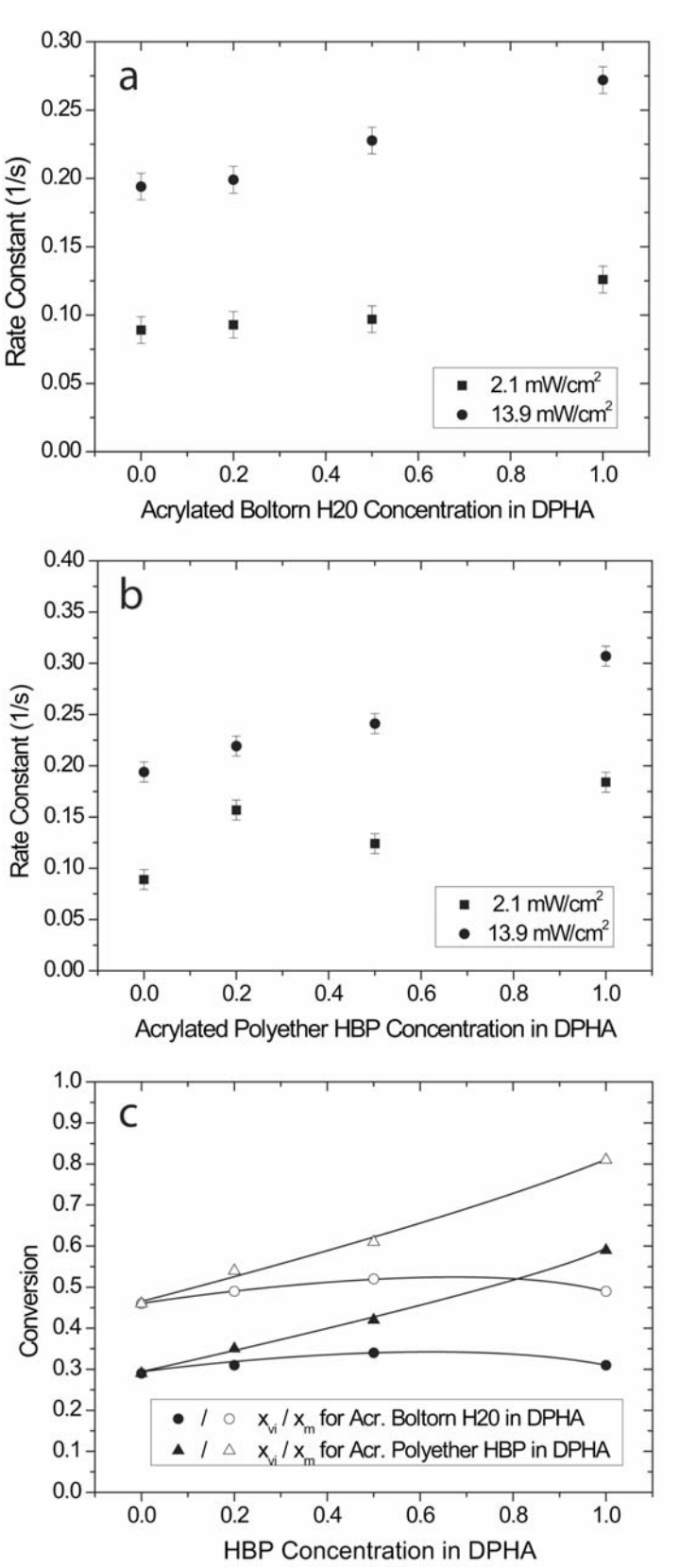

Figure 4-9 Dependence of the rate constant K on (a) the Acrlylated Boltorn H20 concentration in DPHA, and (b) the Acrylated Polyether HBP concentration in DPHA at an intensity of 2.1 mW/cm^2 and 13.9 mW/cm^2, and dependence of the conversion at vitrification and maximum conversion (c) on the HBP concentration in DPHA (6.8 mW/cm^2). Lines are guides for the eye.

For the reactive blend of DPHA with Acrylated Polyether HBP, an increase in the rate constant and an increase in the maximum attainable conversion were observed. Once again this increase results from a reduction in viscosity of the monomer blend, compared to that of pure DPHA.

Interestingly, for all investigated compositions, the maximum conversion was systematically 0.16 higher than the conversion at vitrification (Figure 4-9 c).

4.4 Influence of Intensity

Figure 4-10 displays the influence of UV intensity on the reaction order and autocatalytic exponents, and on the conversion at vitrification and maximum conversion of all acrylate materials. The reaction order and the autocatalytic exponents are independent of intensity within experimental scatter. As listed in Table 4-1, for all three pure materials, the intensity exponents, $\beta 1$,for the reaction rate were found to be smaller than 0.5. This result is in agreement with a similar study [22] on multifunctional acrylates, thus indicating the predominance of primary radical termination (reaction of radicals attached to the forming macromolecule with small, mobile, initiator-derived radicals), and second order termination. The lower value of 0.29 for Acrylated Polyether HBP, compared to 0.35 for DPHA and 0.41 for Acrylated Boltorn H20, indicates that first order termination is more prevalent in Acrylated Polyether HBP, whereas the value of 0.41 for Acrylated Boltorn H20 indicates that in this case second order termination is more frequent. In Acrylated Boltorn H20, a high concentration of acrylate functions is not only present on the surface, but also in the core of the molecule, so that second order intramolecular termination is very likely. In contrast, the maximum attainable conversion increases moderately with increasing intensity.

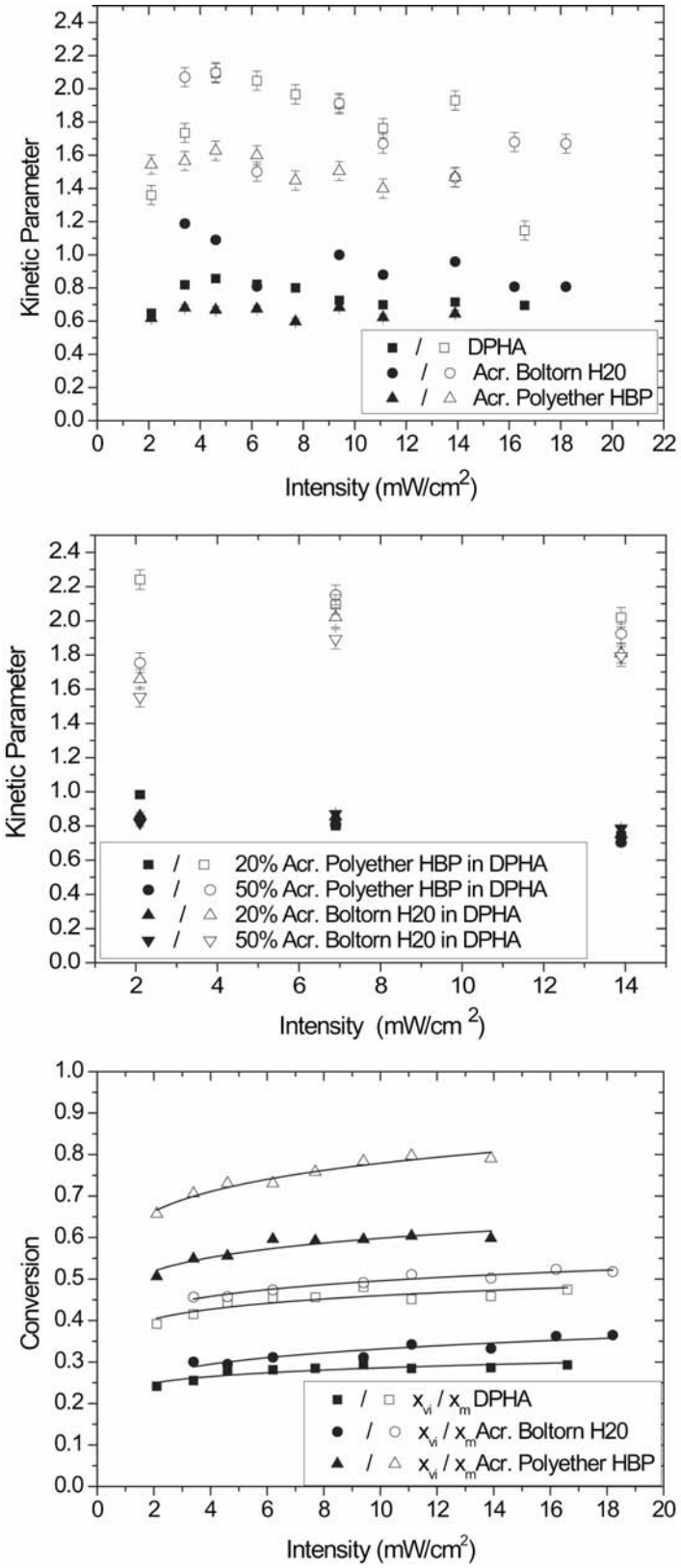

Figure 4-10 Influence of intensity on kinetic parameters (reaction order exponent: open symbols; autocatalytic exponent: filled symbols) for pure monomers (a), and their blends (b), and on conversion at vitrification and maximum conversion of the three materials (c). Lines are guides for the eye.

The intensity exponents for conversion at vitrification, β_2, and maximal conversion, β_3, were found to be in the range 0.05-0.13 (Table 4-1), indicating weak intensity dependence, as has already been found elsewhere, [2, 3] (ca. 0.09 and 0.1 for β_3). And again, final conversion was found to be close to 0.16 higher than the conversion at vitrification, independent of intensity.

Table 4-1 Rate constant exponent β_1, onset of vitrification-conversion exponent β_2, and ultimate conversion exponent β_3 for different materials.

Material	β_1	β_2	β_3
DPHA	0.37	0.084	0.081
Acr. Boltorn H20	0.42	0.127	0.086
20% Acr. Boltorn H20 in DPHA	0.41	0.093	0.061
50% Acr. Boltorn H20 in DPHA	0.41	0.110	0.057
Acr. Polyether HBP	0.25	0.088	0.087
20% Acr. Polyether HBP in DPHA	0.39	0.114	0.053
50% Acr. Polyether HBP in DPHA	0.41	0.101	0.047

4.5 Photopolymerization of Glass-Forming Systems

The above findings (weak intensity dependence of conversion at vitrification and maximum conversion, and conversion offset between vitrification and final conversion independent of composition and intensity) are related to the interplay between conversion, intensity and volume of the polymerizing substance, which is unable to keep up with the chemical conversion upon vitrification [23]. It is proposed to illustrate this structural recovery process during UV curing, analogous to the physical ageing of cured polymers, in the form of an isothermal V versus T/T_g diagram (Figure 4-11), where V stands for volume and T for temperature. This representation resembles the classic volume-temperature diagram for glass forming substances, although it is fundamentally different since T is constant, and T_g changes with conversion, so that the slopes in Figure 4-11 are not equal to the coefficients of thermal expansion of the liquid and glassy states. In this representation of isothermal cure the glass transition temperature increases from the glass transition temperature of the monomer $T_{g,m}$ to the glass transition temperature of the polymer $T_{g,p}$, which is a function of conversion, hence of intensity. When the polymer starts to cure, the mobility is high enough and the rate of volume shrinkage matches the conversion rate.

However, as soon as the curing polymer vitrifies, i.e., when the actual T_g becomes equal to the cure temperature (*T/Tg = 1*), excess volume appears as volume relaxation lags behind conversion [2, 3]. This excess volume increases with increasing intensity due to the higher conversion rate [23]. After vitrification, the polymer continues reacting until its mobility becomes small enough to stop diffusion. At a given volume, the polymer cured at the higher light intensity, I_2 ,will therefore have a higher ultimate conversion, being responsible for a higher T_g, compared to that cured under intensity I_1.

Increasing intensity is indeed generally used to reach higher conversions, although it is essentially useful to speed up the reaction. To reach a high ultimate conversion, further factors such as photoinitiator concentration and temperature (i.e., increased mobility) are therefore more effective, at least to a certain optimum, beyond which the maximum conversion decreases again [24].

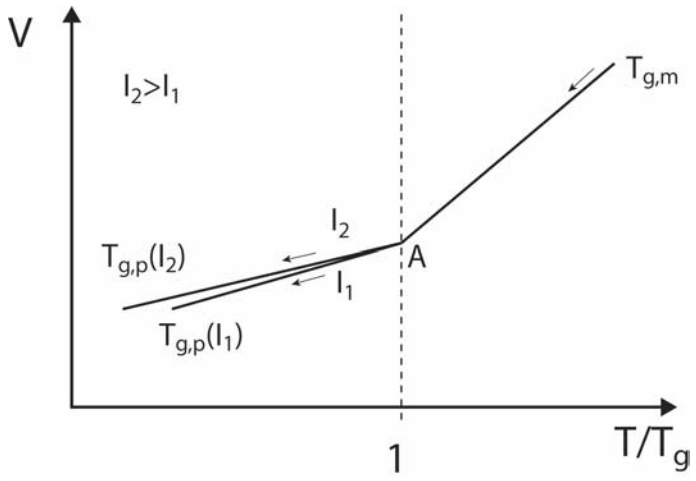

Figure 4-11 Representation of an isothermal curing cycle in a V versus T/Tg diagram for two different intensities (V is volume, T is temperature). See text for details.

4.6 Conclusions

The influence of intensity and vitrification on the UV curing behavior of DPHA, two acrylated HBPs, one with a stiff polyester and one with a flexible polyether structure, and DPHA/HBP reactive blends was investigated.

An autocatalytic model was used up to the onset of vitrification, which was determined from the conversion rate behavior, with a power-law intensity dependence of the reaction rate, conversion at vitrification, and ultimate conversion. It was found that the reaction order and autocatalytic exponents were independent of intensity and close to two and one, respectively, for all materials. The power law exponent

describing the influence of intensity on the reaction rate was about 0.4 for all compositions, thereby suggesting that the main termination mechanisms were a combination of second order and primary radical termination.

Ultimate conversion was found to be 0.16 higher than conversion at vitrification for all investigated materials and blends independent of UV intensity, which was argued to result from volume relaxation processes in the vitrifying acrylates.

4.7 References

1. Andrzejewska, E., *Photopolymerization kinetics of multifunctional monomers.* Progress in Polymer Science, 2001. **26**: p. 605-665.
2. Kloosterboer, J.G., *Network formation by chain crosslinking photopolymerization and its applications in electronics.* Advances in Polymer Science, 1988. **84**: p. 1-61.
3. Bowman, C.N. and N.A. Peppas, *Coupling kinetics and volume relaxation during polymerizations of multiacrylates and multimethacrylates.* Macromolecules, 1991. **24**: p. 1914-1920.
4. Schmidt, L.E., Y. Leterrier, J.-M. Vesin, M. Wilhelm, and J.-A.E. Månson, *Photorheology of fast UV curing multifunctional acrylates.* Macromolecular Materials and Engineering, 2005. **290**: p. 1115-1124.
5. Magnusson, H., E. Malmström, and A. Hult, *Synthesis of hyperbranched aliphatic polyethers via cationic ring-opening polymerization of 3-ethyl-3-(hydroxymethyl)oxetane.* Macromolecular Rapid Communications, 1999. **20**: p. 453-457.
6. Cook, W.D., *Thermal aspects of the kinetics of dimethacrylate photopolymerization.* Polymer, 1992. **33**(10): p. 2152-2161.
7. Kurdikar, D.L. and N.A. Peppas, *A kinetic model for diffusion-controlled bulk cross-linking photopolymerizations.* Macromolecules, 1994. **27**: p. 4084-4092.
8. Hayden, P. and S.H. Melville, *The kinetics of the polymerization of methyl methacrylate. II. The crosslinked and heterogeneous reaction.* Journal of Polymer Science, 1960. **43**: p. 215-227.
9. Dietz, E.J. and N.A. Peppas, *Reaction kinetics and chemical changes during polymerization of multifunctional (meth)acrylates for the production of highly crosslinked polymers used in information storage systems.* Polymer, 1997. **38**(15): p. 3767-3781.
10. Yu, Q., S. Nauman, J.P. Santerre, and S. Zhu, *Photopolymerization behaviour of di(meth)acrylate oligomers.* Journal of Materials Science, 2001. **36**: p. 3599-3605.
11. Chandra, R. and R.K. Soni, *Studies on kinetics of bulk polymerization of divinyl ester by radical-initiated thermal and photopolymerization.* Polymer International, 1993. **31**: p. 239-245.
12. Chandra, R., R.K. Soni, and S.S. Murthy, *Studies on the kinetics of radical initiated photocopolymerisation of Di(vinyl 2-hydroxy propanoate)ether of bisphenol-A and monomers.* Polymer International, 1993. **31**: p. 305-314.
13. Andrzejewska, E., M.B. Bogacki, and M. Andrzejewski, *The autocatalytic model of photopolymerization of dimethacrylates.* Polimery, 2001. **46**(7-8): p. 549-551.
14. Eom, Y., L. Boogh, V. Michaud, P. Sunderland, and J.-A.E. Månson, *Time-cure-temperature superposition for the prediction of instantaneous*

viscoelastic properties during cure. Polymer Engineering and Science, 2000. **40**(6): p. 1281-1292.
15. Teil, H., S.A. Page, V. Michaud, and J.-A.E. Månson, *TTT-cure diagram of an anhydride-cured epoxy system including gelation, vitrification, curing kinetics model, and monitoring of the glass transition temperature.* Journal of Applied Polymer Science, 2004. **93**: p. 1774-1787.
16. Andrzejewska, E., L.-Å. Lindén, and J.F. Rabek, *Modelling the kinetics of photoinitiated polymerization of di(meth)acrylates.* Polymer International, 1997. **42**: p. 179-187.
17. Kamal, M.R. and S. Sourour, *Kinetics and thermal characterization of thermoset cure.* Polymer Engineering and Science, 1973. **13**(1): p. 59-64.
18. Timpe, H.-J. and B. Strehmel, *Lichtinduzierte Polymer- und Polymerisationsreaktionen, 44: Zur Kinetik der radikalischen Photopolymerisation mehrfunktioneller Acrylate in polymeren Bindemitteln.* Makromolekulare Chemie - Macromolecular Chemistry and Physics, 1991. **192**: p. 779-791.
19. Schmidt, L.E., Y. Leterrier, D. Schmaeh, J.-A.E. Månson, and D. James. *Structural and residual stress analysis of UV curable hyperbranched acrylates*. in *RadTech Europe*. 2005. Barcelona.
20. Kou, H., A. Asif, and W. Shi, *Photopolymerization Kinetics of Hyperbranched Acrylated Aromatic Polyester.* Journal of Applied Polymer Science, 2003. **89**: p. 1500-1504.
21. Sangermano, M., G. Malucelli, R. Bongiovanni, A. Priola, A. Harden, and N. Rehnberg, *Hyperbranched polymers in cationic photopolymerization of epoxy systems.* Polymer Engineering and Science, 2003. **43**(8): p. 1460-1465.
22. Timpe, H.-J., B. Strehmel, F.H. Roch, and K. Fritzsche, *Lichtinduzierte Polymer- und Polymerisationsreaktionen, 29: Kinetische Studie der radikalinitiierten Photopolymerisation von Butandiol-1,4-dimethacrylat in Poly(vinylpyrrolidon)-Schichten mit einem isoperibolen Calorimeter.* Acta Polymerica, 1987. **38**(4): p. 238-244.
23. Cook, W.D., *Photopolymerization kinetics of dimethacrylates using the camphorquinone / amine initiator system.* Polymer, 1992. **33**(3): p. 600-609.
24. Lecamp, L., B. Youssef, and C. Bunel, *Photoinitiated polymerization of a dimethacrylate oligomer: 1. Influence of photoinitiator concentration, temperature and light intensity.* Polymer, 1997. **38**(25): p. 6089-6096.

5 Photorheology

The time resolution of the photorheology techniques as described in the state of the art restricts their use to UV intensities lower than ca. 50 mW/cm^2 for typical acrylate systems. One of the objectives of the present work was to improve both the dynamic range of detectable stress, and the time resolution of a photorheology set-up, in order to make it usable for low viscosity monomers. The goal was to investigate their structure and property build-up under higher UV intensities. To this end high-performance data acquisition hardware was combined with a tailored data processing algorithm, and this newly developed method was applied to a highly functional acrylate monomer and two different acrylated hyperbranched polymers.

5.1 Method

Based on a selection of key parameters, such as the monomers studied, the UV intensities used, and an estimate of the measurable stress range, Table 5-1 summarizes recent developments in photorheology. Since all four of the most recent studies were carried out on similar devices (Rheometric Scientific RDA-2, and Rheometric Scientific ARES) with similar transducers, an estimation of the measurable stress range is presented first in Table 5-1.

Table 5-1 Overview of recent developments in photorheology.

		ARES specification	Khan et al. [1]	Lee et al. [2]	Steeman [3]	Botella et al. [4]	present method
Year			1992	2000	2004	2004	2005
time resolution	**[s]**	1	NA	0.02	0.12	7	0.001
minimum stress	**[Pa]**	2000		200	1200	130	≈100
maximum stress	**[kPa]**	2000		2000	1200	130	2000
momomers studied			thiol	acrylates	acrylates	acrylate/ styrene	acrylates
UV intensity	**[mW cm^{-2}]**		pulses	15	28	0.15-1.36	9-80
tool diameter	**[mm]**		20	8	9.5	20	8
sample thickness	**[μm]**		100-600	150	100	500	100
coupling with FTIR		no	no	no	yes	yes	no
stiffness increase	**orders of magnitude**		4	4	3	3	5
duration of experiment	**[s]**		NA	5	5	500	5

The stress resolution of the standard equipment is equal to 2 kPa, with a tool diameter of 8 mm. Using a larger tool, Botella et al. [4] improved the stress resolution down to 130 Pa. This simply reflects the fact that the measured torque scales with the third power of the tool diameter. However, this also reduced the upper measurable shear modulus. The time resolution of the equipment which was initially 1 s had already been improved 50 fold by Lee et al. [2]. Our method, as described below, further improved this limit, thereby enabling very fast UV curing polymers to be accurately analyzed. Typically 100 independent measurement points per excitation cycle could be obtained, corresponding to a time resolution of 1 ms at an excitation frequency of 10 Hz, in contradiction with the classic assumption that an excitation frequency *f* can only result in data points with an approximate resolution of *1/f*. An overview of the of the different steps involved in rheological raw data treatment, namely oversampling, adaptative denoising, and extraction of the analytical signal through a Hilbert transform, is given in Table 5-1 and these steps are described in the following sections. Both the strain and the torque signal were treated independently according to this scheme.

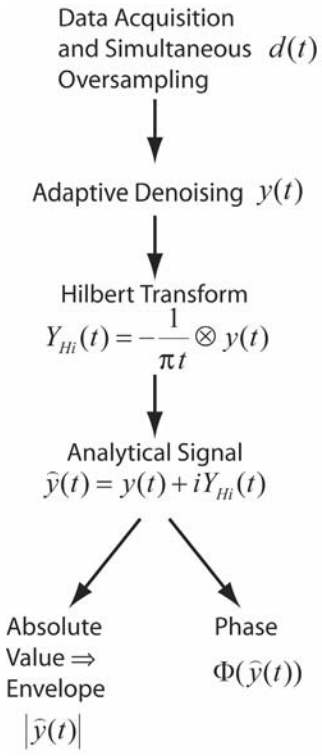

Figure 5-1 Overview of signal analysis and evaluation.

5.1.1 Oversampling

In a first step, the sinusoidal input signal (the deformation frequency is limited to 16 Hz by the hardware) and the corresponding output signal (torque) of the

rheometer were acquired at a very high sampling rate (e.g. 100 kHz per channel). The acquisition hardware used was a National Instruments NI 6052E card with a maximum sampling rate of 333 kS/s. The card was able to transfer measured data from its buffer, while continuously measuring new data. This gave the raw signal d(t). In a second step, an adjustable oversampling routine, that is averaging over multiple measurement points, as proposed by van Dusschoten and Wilhelm [5-7], was applied. Thereby the signal to noise ratio was increased by up to the square root of the number of oversampled points for the random noise contribution. Typically, oversampling was conducted over 100 raw data points (for an excitation frequency of 10 Hz and a sampling rate of 100 kHz). As depicted, for example, in Figure 5-2 in the case of di-pentaerythritol penta/hexaacrylate (DPHA), this method drastically improved the signal to noise ratio, and especially helped to filter out the random, stochastic noise.

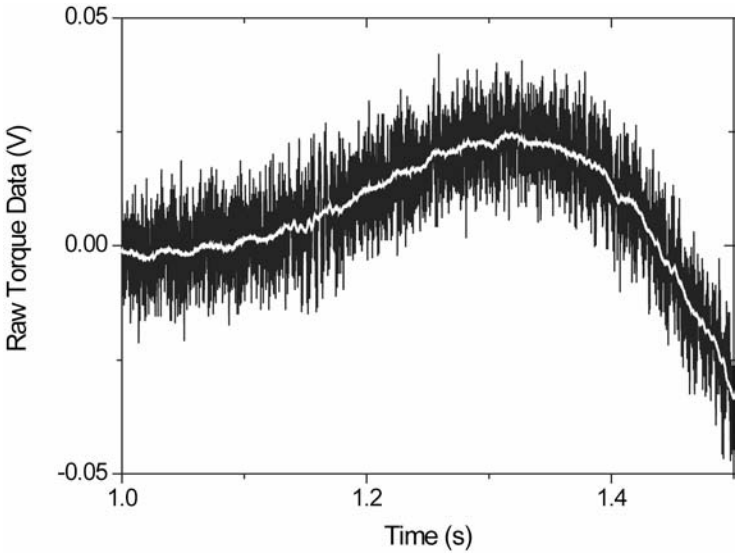

Figure 5-2 Segment of the raw torque data vs. time. The raw signal (black) and the oversampled signal (white) are shown. Oversampling over 100 data points leads to an approximately 10-fold improvement in accuracy.

5.1.2 Adaptive Denoising

For the Hilbert transform performed afterwards, it was essential to have a narrowband signal; therefore the signal *d(t)* was then subjected to adaptive denoising. The absolute value of the complex shear modulus and the phase angle between stress and strain signals were subsequently calculated from the resulting filtered analytical signal. The filtering not only extracts the noise, but also eliminates the DC offset by shifting the signal up to the zero-line, which facilitates later data handling.

Instead of using the common term “modulus” for the absolute value of a complex signal, the term “magnitude” is used in the following discussion, to avoid

confusion with the term “shear modulus”. Secondly the term “analytical signal” is a term typically used in signal processing. It does not indicate an analytic methodology. Using a conventional pass-band filter to enhance the signals leads to the usual problem of finding an acceptable trade-off between time and frequency resolution. If the pass-band is narrow, i.e. if the filter has a good frequency resolution, then its impulse response is long, and it responds slowly to changes. For this reason an adaptive notch-filtering scheme was used instead, based on the Least Mean Squares (LMS) adaptive algorithm. A detailed description can be found in the book by Widrow and Stearns [8]. The basic implementation of this scheme is presented in Figure 5-3, where *n* is the current sample index, and *f* is a normalized frequency, that is, the ratio f_a/f_s between the true oscillation frequency f_a (in Hz) and the sampling frequency f_s (in Hz).

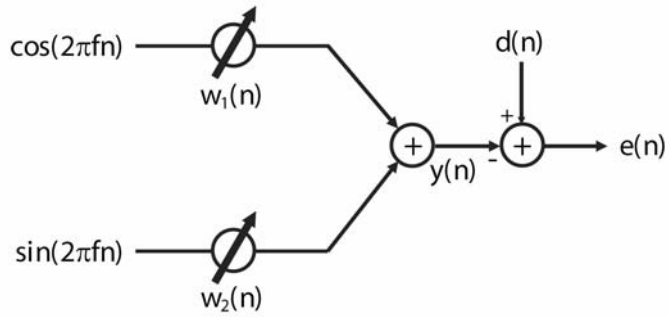

Figure 5-3 Principle of the adaptive notch filter. The signal of interest is d(n), f is the normalized frequency, y(n) is the filtered signal.

The signal *d(n)* is the signal of interest (the signal which needs to be filtered), e(n) is the error, and *y(n)* the filtered signal. The goal was to minimize the mean-square value $\langle e^2(n)\rangle$ of the difference between *d(n)* and the adaptive system output *y(n)*, which is nothing other than the weighted sum of a sine and cosine time function at frequency *f*. Consequently, *e(n)* has lost any component at frequency *f* that may have been present in *d(n)*. The output *y(n)* is thus exactly the component of *d(n)* at frequency *f*, which was used to enhance the torque and excitation signals at their operating frequency. LMS adaptation is a gradient search in which the gradient with respect to $\langle e^2(n)\rangle$, that is unavailable, is replaced by an instantaneous estimate, namely the gradient with respect to $e^2(n)$. System update is described by the four simple equations:

$$y(n) = w_1(n)\cos(2\pi fn) + w_2(n)\sin(2\pi fn) \tag{5.1}$$

$$e(n) = d(n) - y(n) \tag{5.2}$$

$$w_1(n+1) = w_1(n) + 2\mu e(n)\cos(2\pi fn) \tag{5.3}$$

$$w_2(n+1) = w_2(n) + 2\mu e(n)\sin(2\pi fn) \tag{5.4}$$

where μ is the gradient coefficient, and w_1, w_2 are the adaptive weights. Stability is assured for $0 < \mu < 1$. Of course, cancellation/enhancement is not perfect, in the sense that nearby frequencies are affected too. It can be shown [8] that in steady-state conditions the response bandwidth (normalized frequency) is μ/π. The method just described introduces a small delay, but the latter is identical for both enhanced signals, so it has no influence upon the phase difference between them.

To sum up, this approach presents advantages in terms of implementation (the only parameter to tune is μ), and of trade-off between time and frequency resolution. Figure 5-4 shows a segment of the unfiltered but already oversampled torque signal, the filtered signal, and the extracted noise. The difference between the unfiltered and the filtered signal is significant: The noise portion, which was not affected by the oversampling procedure, was removed largely by adaptive denoising.

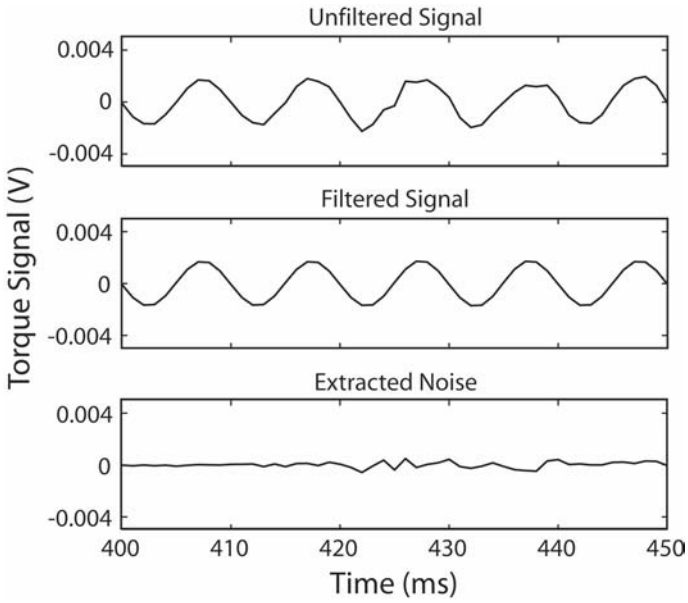

Figure 5-4 Segment of the torque signal subjected to adaptive filtering with a notch filter.

5.1.3 Evaluation of the Complex Shear Modulus via Hilbert Transform, and Extraction of the Phase Angle

The Hilbert transform of the filtered signal $y(t)$ was calculated, as follows:

$$Y_{Hi}(t) = \frac{1}{\pi}\int_{-\infty}^{\infty}\frac{y(\tau)}{\tau - 1}d\tau = -\frac{1}{\pi t} \otimes y(t) \tag{5.5}$$

From the Hilbert transform of the function *y*(t), which corresponds to the folding of -1/πt with *y(t)*, the so called "analytical signal" was calculated as the sum of the original signal and its Hilbert transform as imaginary part. A comprehensive description can be found in Bracewell's book [9] on the Fourier transformation:

$$\hat{y}(t) = y(t) + iY_{Hi}(t) \tag{5.6}$$

The magnitude of the analytical signal is the envelope from which the absolute value of the complex shear modulus can be calculated. As an example, a segment of the strain and the torque signals in the case of Acrylated Boltorn H20, a second generation polyester HBP, and the envelope of their analytical signals are plotted in Figure 5-5. The phase angle between stress and strain could subsequently be calculated by subtracting the phase angles of the two analytical signals.

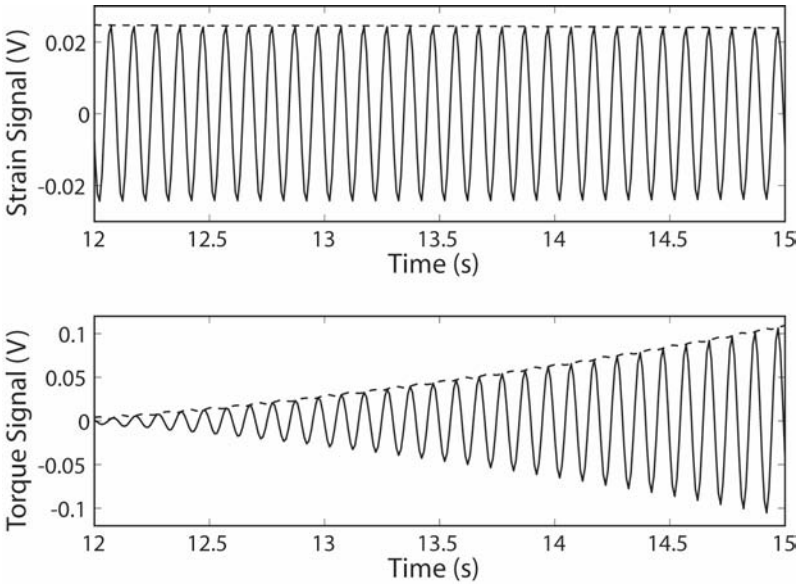

Figure 5-5 Filtered strain and torque signals and the magnitude of their analytical signals (dashed line).

In fact, this method is more suitable than performing a Fourier analysis with a moving window, since the amplitude changes drastically, even during one period. A Fourier analysis with a moving window would lead to the problem, already mentioned above, of the trade-off between time and frequency resolution. Since the amplitude of the torque signal changes drastically over time, a short window should be used to track this amplitude, but at the expense of reduced frequency resolution. The Hilbert transform is indeed the best approach to analyzing amplitude-modulated narrowband signals.

5.2 Limitations

The present technique is limited to monomers of viscosities higher than ca. 1 Pa·s, to polymerization durations in the range of seconds, and hence to UV intensities lower than 100 mW/cm^2 for most acrylate systems. The sensitivity of the measurement in the early stages of polymerization can be increased by using parallel plates with a larger diameter, since the torque scales with the third power of the tool diameter. The disadvantage is that this will drastically reduce the measurable maximum shear modulus. Using the 8 mm diameter parallel plate tool, a compromise between minimum sensitivity and maximum measurable shear modulus was found. Further restrictions included the limited excitation-frequency range of the rheometer; for instance, the upper threshold is approximately 16 Hz, which made it difficult to determine the gelpoint using the Winter-Chambon criterion [10, 11]. Moreover, the rheometer was unable to measure the dynamics of shrinkage during these fast UV curing reactions, since the control of the normal force used for this purpose did not respond fast enough. In addition, vibrations at the heating and cooling stages connected to the rheometer may have decreased the signal-to-noise ratio. Finally, another limitation is that the inhibition effect of oxygen, which is very important in coating applications of UV-curing, cannot be evaluated by this method, since the sample is laminated between a quartz and a metal plate. But it is therefore well suited for UV-curable adhesives and UV-glues.

5.3 Results and discussion

5.3.1 Sensitivity and Time Resolution

Figure 5-6 reproduces a typical result obtained in the case of the Acrylated Polyether HBP, during UV cure under an intensity of 9 mW/cm^2. According to the manufacturer, the transducer is able to measure torque in the range of $2 \cdot 10^{-4}$-0.2 N·m. For the chosen experimental conditions, tool geometry, and sample thickness, this corresponded to a measurable stress range between 2 kPa and 2 MPa.

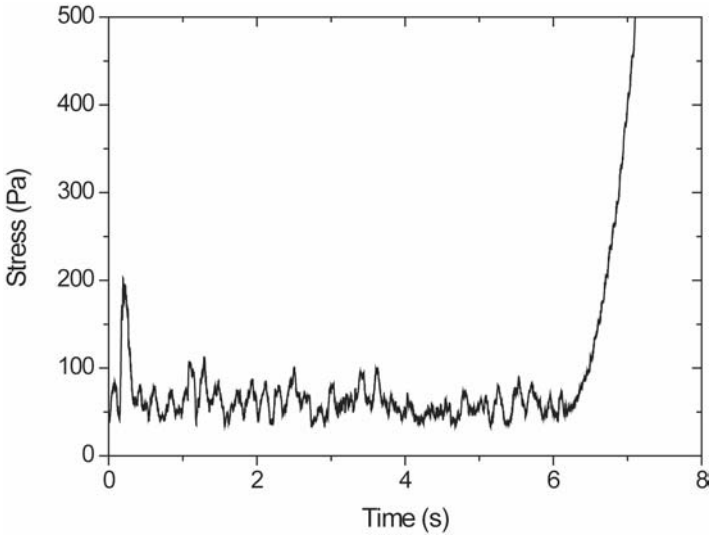

Figure 5-6 Segment of the stress measured during UV curing of the Acrylated Polyether HBP with an 8 mm diameter tool, a sample thickness of 0.1 mm, and a strain of 10%. The figure shows that a lower stress resolution of the equipment of about 100 Pa could be reached with the proposed data treatment procedure, time zero: exposure start.

It is clear that following the enhanced data treatment procedure described in the previous section, the stress resolution was better than 100 Pa, a 20-fold improvement in fact (as seen in Figure 5-6) compared to the standard set-up. Moreover, this increase in stress resolution was achieved without reducing the maximum measurable torque. The time resolution of this experiment, and all experiments reported in the following section, was equal to 1 ms, independent of the excitation frequency.

5.3.2 Linear Viscoelastic Range

Figure 5-7 shows the complex shear modulus of the Acrylated Polyether HBP during cure, under 1% and 10% strain. Whereas the build-up of modulus could not be resolved during the initial 700 ms of illumination, it is clear that the two curves superimposed during the remaining cure process. In the following experiments, the 10% strain amplitude was therefore used for improved sensitivity, without exceeding the linear viscoelastic range.

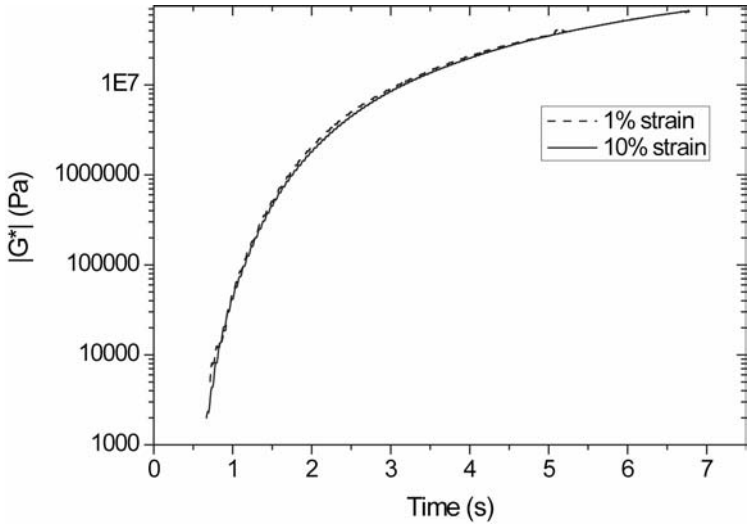

Figure 5-7 Absolute value of the complex shear modulus for DPHA with 1 w% Irgacure 184 cured at an intensity of 80 mW/cm^2 measured for different strains, time zero: exposure start.

After reaching a modulus of about 70 MPa the rheometer was no longer able to track any further increase for the chosen tool geometry, sample thickness, and applied strain. To be able to measure even higher moduli, it would be necessary to either reduce the tool diameter or the strain. The first option would have required an improvement of the measurement hardware, whereas the second option would have clearly reduced the sensitivity at early polymerization stages.

5.3.3 Gelation

Gelation corresponds to the transition from a viscous liquid to an elastic solid. Two criteria are generally used to determine the occurrence of gelation: either the crossover of storage and loss moduli expressed in the tangent of the phase angle being equal to one, or the point at which the phase angle is independent of frequency [10, 11]. Figure 5-8 shows the phase angle between loss and storage moduli of Acrylated Boltorn H20 for three frequencies. The viscosity of this monomer was high enough for the whole cure process to be captured, from the onset of illumination. During the first second of illumination, the Acrylated Boltorn H20 remained purely viscous. Whether this period corresponded or not to a true induction time, during which part of the initiator radicals were consumed by oxygen dissolved in the monomer [12], should be checked by means of photo DSC or real-time FTIR. After this initial induction time, the phase angle dropped, and the three curves lay close together up to about 2.5 s, indicating the occurrence of gelation. In fact, no intersection point between the three curves could be identified within the limited frequency range accessible with the rheometer. Nevertheless the values are very close. Steeman at al. [3] came to the same

conclusion when discussing whether a superposition of sine-waves of different frequencies, as proposed by Chiou et al. [13], would be applicable for fast UV curing acrylates (a so called multiwave test). Therefore, in the following discussion, the time where the phase angle equals $\pi/4$ = 0,79 (tan $\delta = 1$) will be used as a gelpoint criterion. Using this criterion in the case of Acrylated Boltorn H20 under 80 mW/cm^2 showed that gelation occurred after 2.4 s of illumination. Interestingly, at this time the phase angle vs. time curves changed slope significantly, which might indicate that further network formation was slowed down because the propagation mechanism became diffusion-controlled, (so called autodeceleration [14]). A kinetic analysis would be useful to correlate the above findings with structural information, using, for example;. photo DSC or real-time FTIR, preferably simultaneously with the photorheology experiment [3, 4].

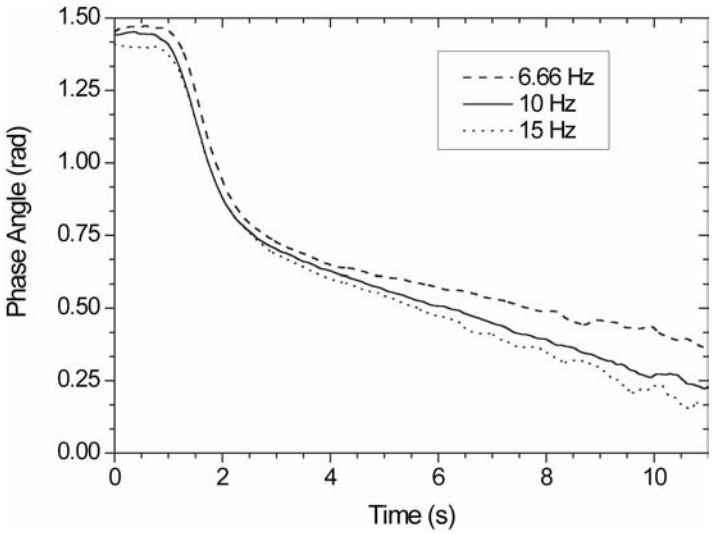

Figure 5-8 Phase angle between strain and stress signals for the Acrylated Boltorn H20 (polyester HBP) during UV curing at 80 mW/cm^2 with 1 wt.-% of Irgacure 184 as photoinitiator. Time zero: exposure start.

A comparison of the gelling of DPHA and Acrylated Boltorn H20 under UV intensity equal to 9 mW/cm^2 is shown in Figure 5-9. Even though the initial transformation of DPHA could not be resolved, due to insufficient viscosity, an initial liquid-like period of approximately 8 s was detected, followed by a steep decrease of phase angle, and gelation after 9.2 s of UV illumination. In this case, the time resolution of the present method was necessary to capture the fast change from a viscous liquid to a viscoelastic solid. The network formation of Acrylated Boltorn H20 was more gradual, and gelation occurred after 17.2 s.

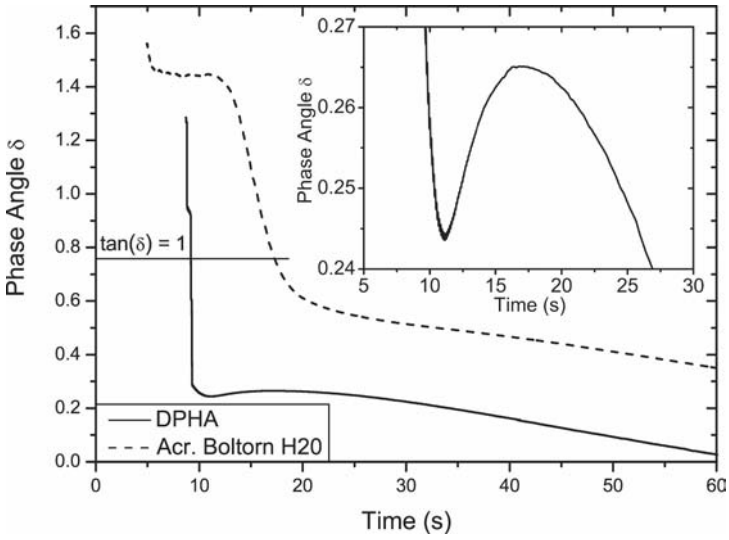

Figure 5-9 Phase angle between strain and stress signals for different acrylate monomers during UV curing at 9 mW/cm^2 with 1wt.-% of Irgacure 184 as photoinitiator, excitation frequency: 10 Hz, strain: 10%.

The remarkable difference between Acrylated Boltorn H20 and DPHA can be explained considering the structure of Acrylated Boltorn H20, which allowed intramolecular reactions to happen. These would not have contributed to the overall gelation of the network and, consequently, a higher conversion would have been necessary to reach gelation in the case of the hyperbranched polymer.

5.3.4 Vitrification

One criterion proposed to detect vitrification during cure, is the occurrence of a peak in the tan δ or δ plotted versus curing time [15]. Whereas no such peak could be observed in the case of Acrylated Boltorn H20, a broad local maximum was measured for DPHA (inset in Figure 5-9), showing that the present refined method was able to resolve even such subtle changes. Lange et al. [16] stated that gelation and vitrification are not distinguishable for acrylates and chain-wise reacting systems in general, which is the reason for the DPHA peak being rather weak. In fact, vitrification in acrylates is a gradual process happening over a wide conversion range, mainly due to the inhomogeneous network formation of chain-wise reacting systems. It is important to point out that for both Acrylated Boltorn H20 and DPHA systems, the cure temperature was below the T_g of the cured networks (Chapter 3). The T_g of DPHA was equal to 68°C (at 73% conversion), that is, approximately 40°C above the cure temperature, so that vitrification at cure temperature occurred at a rather high conversion, and was indeed detected. By contrast, the T_g of Acrylated Boltorn H20 was equal to 126°C (also at 73% conversion), and its vitrification at cure temperature

occurred at a lower conversion, and could not be distinguished from gelation. It should be pointed out that the evolving heat and resulting temperature rise during photopolymerization were not measured, and that this could have contributed to the observed behavior and explained the high T_g values obtained.

5.3.5 Influence of Intensity

The influence of UV intensity on the mechanical properties of DPHA during cure is depicted in Figure 5-10. Increasing the intensity is very effective in reducing the initial liquid-like stage, and the overall polymerization time. Under 80 mW/cm^2 the complex shear modulus reached high values in less than 10 s, approximately 10 times faster than under 9 mW/cm^2. For the first time, the set-up presented here enabled this fast process to be monitored with a time resolution of about 1 ms. The modulus of the sample tested under 40 mW/cm^2 dropped after it reached 1 MPa, most likely as a consequence of material failure during the experiment. In several cases the samples strongly adhered to the rheometer tools and had to be burned off, an indication that oxygen inhibition did not occur on the sample tool interface, which otherwise would have led to incorrect torque measurement.

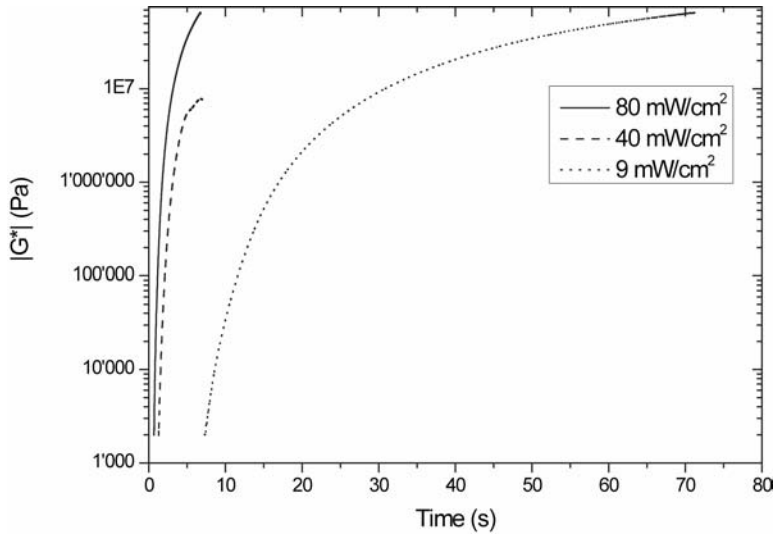

Figure 5-10 Magnitude of the complex shear modulus for DPHA with 1w% Irgacure 184 measured for different intensities at 10 Hz excitation frequency and 10% strain, time resolution 1 ms, time zero: exposure start.

5.3.6 Influence of Composition

Figure 5-11 compares the complex shear modulus of DPHA, Acrylated Boltorn H20 (polyester HBP), and Acrylated Polyether HBP during photopolymerization under an UV intensity of 9 mW/cm^2. The induction period for DPHA and the

Acrylated Polyether HBP was approximately 7 s, and this increased to 12 s for Acrylated Boltorn H20. The modulus of Acrylated Polyether HBP leveled off at a value equal to 15 MPa, indicative of a rubbery behavior, or, in other terms, of a glass-transition temperature of the cured polymer, which was below the cure temperature. The T_g of cured Acrylated Polyether HBP was found to be equal to 26°C (at 83% conversion, cured at 40 mW/cm^2), and it is expected that the T_g of Acrylated Polyether HBP polymerized at 9 mW/cm^2 was lower than this value.

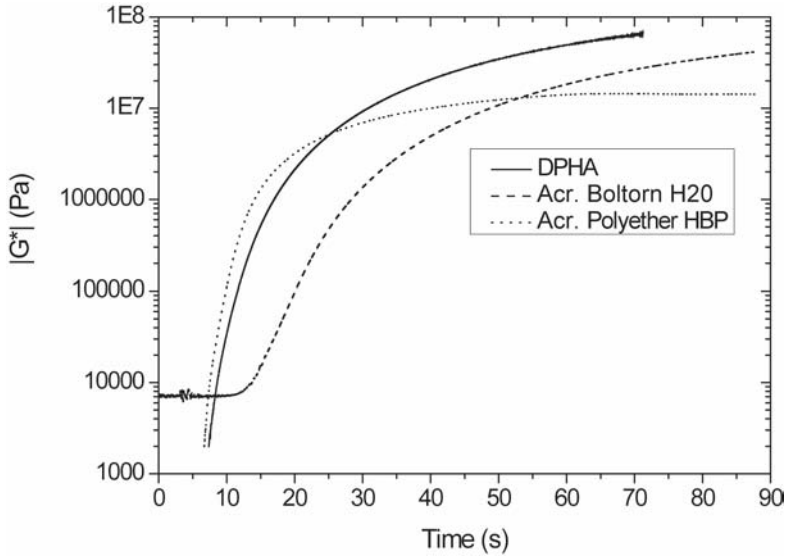

Figure 5-11 Magnitude of the complex shear modulus as a function of time for different acrylate monomers during UV curing at 9 mW/cm^2 with 1wt.-% of Irgacure 184 as photoinitiator at an excitation frequency of 10 Hz, time resolution 1 ms, time zero: exposure start.

Figure 5-12 compares the phase angle between strain and stress signals for DPHA, Acrylated Boltorn H20 and two reactive blends, cured at 20 mW/cm^2. As already found for a lower UV intensity, the gelation of Acrylated Boltorn H20 was delayed compared to that of DPHA. For both reactive blends containing 20 wt.-% and 50 wt.-% Acrylated Boltorn H20, this was not the case.

However, a significant difference was observed for the further course of the phase angle δ. For DPHA a peak of tan δ was found, which was attributed to vitrification [15, 17]. Adding Acrylated Boltorn H20 erased the vitrification peak, presumably because of the increase of the glass-transition temperature of HBP blends (Chapter 4). Acrylated Boltorn H20 and the two reactive blends kept their viscoelastic characteristics up to a higher reaction level, which should help in relaxing the stress, and hence reducing the final internal stress level. In thermoset processing, this

enhanced viscoelastic behavior is effectuated by choosing low cooling rates after crosslinking [18].

As shown in Figure 5-13 the modulus build-up of Acrylated Boltorn H20 and its reactive blends with DPHA was retarded compared to that of pure DPHA, which should also contribute to a further reduction of internal stress.

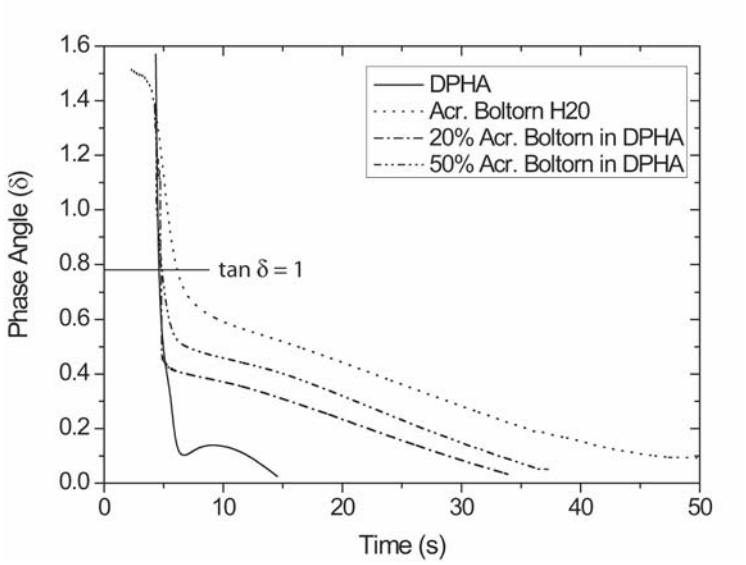

Figure 5-12 Phase angle as a function of time for pure DPHA, Acrylated Boltorn H20, and their blends, cured at 20 mW/cm^2.

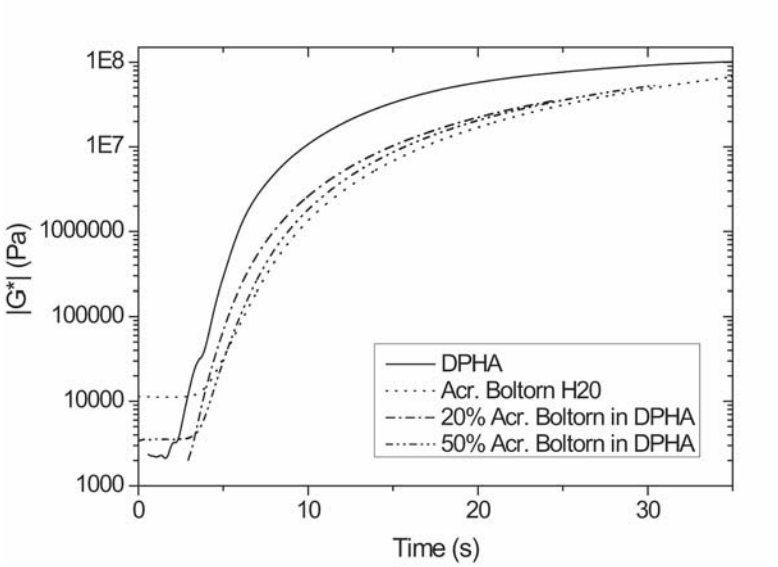

Figure 5-13 Absolute value of the complex shear modulus as a function of time for pure DPHA, Acrylated Boltorn H20, and their blends, cured at 20 mW/cm^2.

Equivalent information for reactive blends of DPHA and Polyether HBP were plotted in Figure 5-14 and Figure 5-15. The stiffness build-up happened earlier for the two reactive blends. In order to judge whether this led to higher internal stresses, one has to look at the conversion at gelation and the conversion at vitrification. Unlike

Acrylated Boltorn H20 blends, the introduction of Polyether HBP reduced the gelling and vitrification times, with resulting earlier modulus build-up compared to that of pure DPHA. The differences in the final level of Young's modulus result from changes in the ultimate conversion and glass transition temperatures of the cured materials, as discussed later.

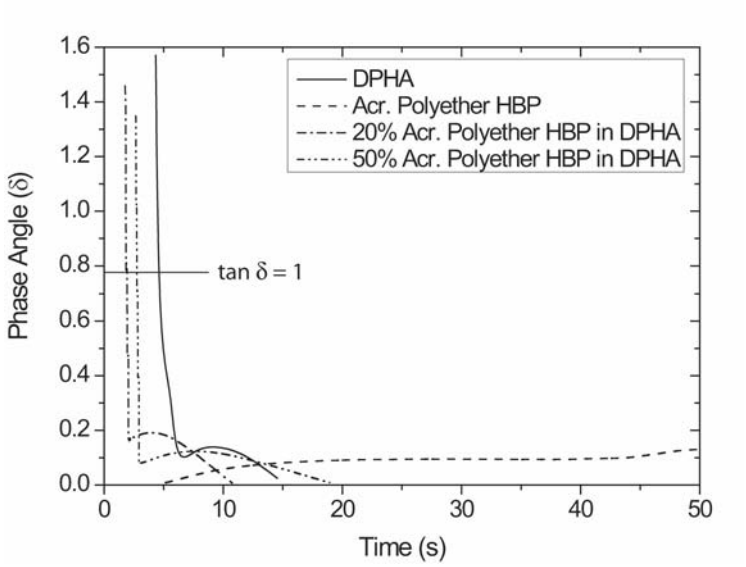

Figure 5-14 Phase angle as a function of time for pure DPHA, Acrylated Polyether HBP, and their blends, cured at 20 mW/cm^2.

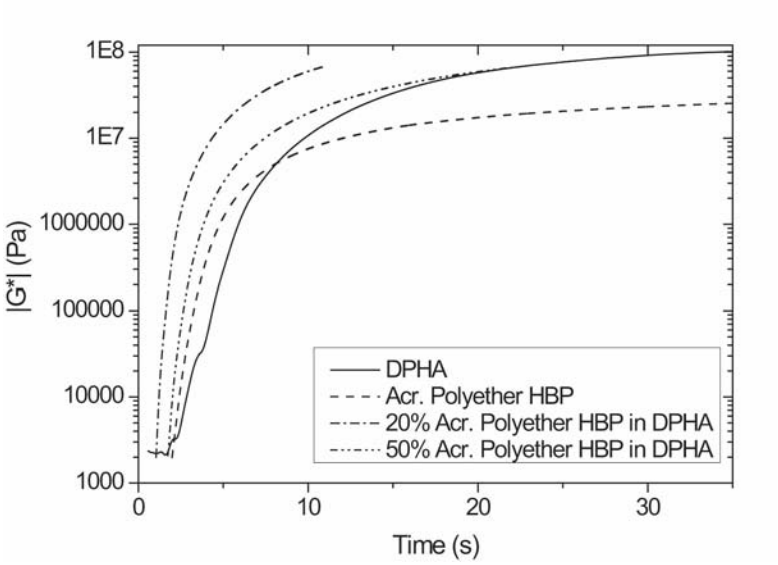

Figure 5-15 Absolute value of the complex shear modulus as a function of time for pure DPHA, Acrylated Polyether HBP, and their blends, cured at 20 mW/cm^2.

5.3.7 Microgelation and Microvitrification

Figure 5-16 illustrates the development of the magnitude of the shear modulus as a function of the phase angle. Interestingly enough, both DPHA and Acrylated Boltorn H20 have a modulus of about 100 kPa at gelation. For thermally curing/cured methacrylates a modulus at gelation of the order of 10 Pa was found [19]. One hypothesis for the higher modulus would be the occurrence of microgelation [20, 21] and/or microvitrification [22], before the actual gelation sets in, as illustrated in Figure 5-17. A possible cause could be intramolecular cyclization reactions. Percec et al. [23] and Chu et al. [24] stated that intramolecular cyclization during the synthesis is very likely to occur, especially in HBPs with flexible chains. It should be noted that the term microgel is normally used for intramolecular crosslinked macromolecular molecules in solution. In the present case, the solvent would be an unreacted monomer.

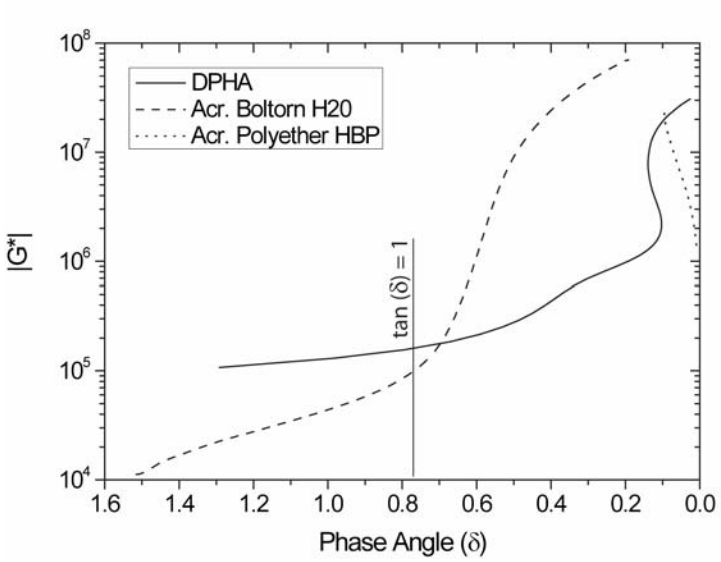

Figure 5-16 Absolute value of the complex shear modulus as a function of the phase angle for different acrylate monomers during UV curing at 20 mW/cm^2.

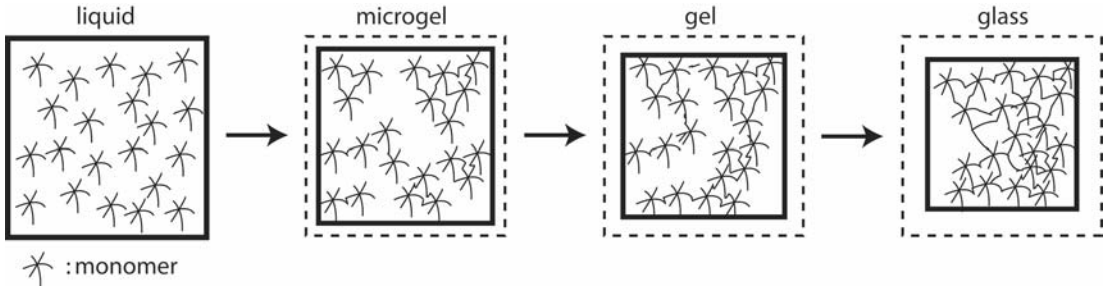

Figure 5-17 Schematic of acrylate shrinkage during UV polymerization from a liquid to a glassy solid, including microgel formation and macrogelation.

5.3.8 Influence of HBPs on Conversion at Gelation and at Vitrification

In Figure 5-18, conversion at the onset of gelation, determined from the tan $\delta = 1$ data in Figure 5-12 and Figure 5-14, conversion at vitrification, and maximum conversion, determined from photo DSC (Chapter 4), are plotted as a function of HBP concentration in DPHA. Gelation was not delayed to higher conversions by introducing HBPs. Instead, a slight shift of conversion at vitrification was detected: from 32% for DPHA to 36% for a 50/50 DPHA / Acrylated Boltorn H20 blend, and to 43% for a 50/50 DPHA / Acrylated Polyether HBP blend. Delayed vitrification in HBP reactive blends should in principle reduce the internal stress, although the dependence of the ultimate glass transition temperature T_g^{∞} of the blends on their composition may counteract this reduction since higher conversion may be reached when curing at a temperature close to T_g^{∞}, which was indeed the case for the Acrylated Polyether blends.

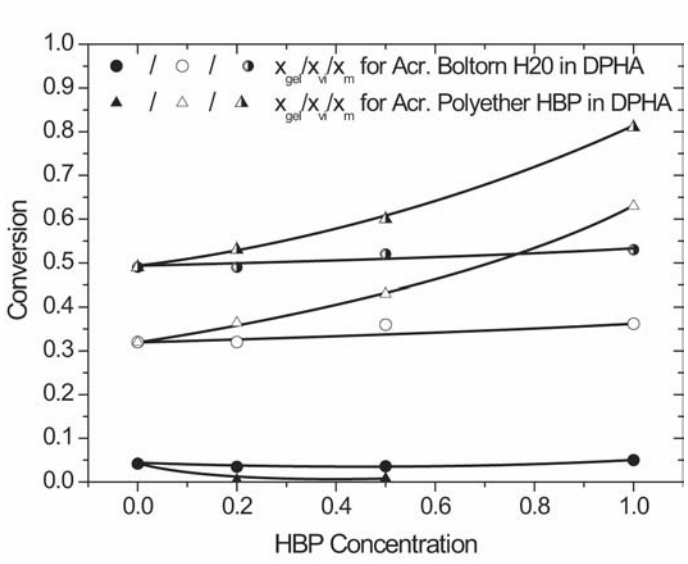

Figure 5-18 Dependence on composition of the conversion at gelation x_{geb}, at vitrification x_{vi} and the maximum conversion; determined from photo DSC and photorheology. Lines are guides for the eye.

Figure 5-19 finally elucidates how the shear modulus develops as a function of conversion. DPHA shows the earliest modulus build-up, followed by Acrylated Boltorn H20 and the Acrylated Polyether HBP. It is clear that a significant modulus already develops in the rubbery state, although the major share of the modulus develops after vitrification for DPHA and Acrylated Boltorn H20. For the Acrylated Polyether HBP this is not the case, since vitrification happened at a very high conversion.

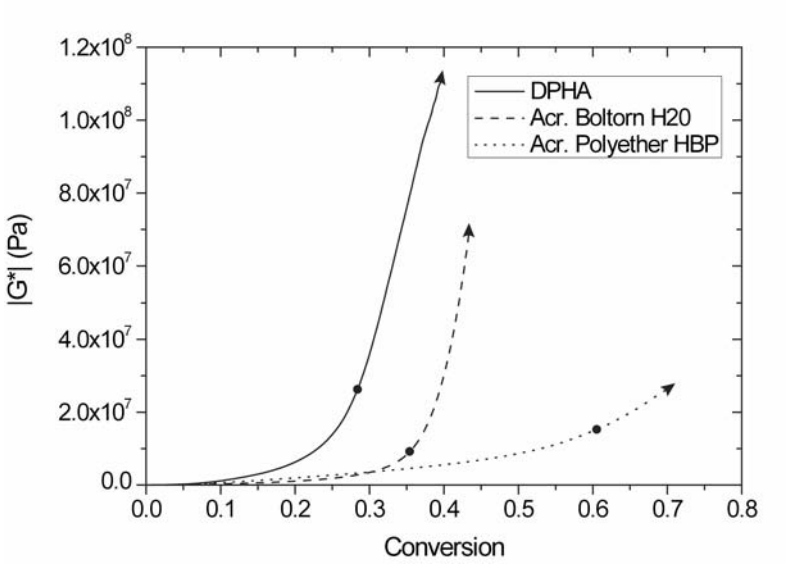

Figure 5-19 Evolution of the magnitude of the shear modulus for the three acrylates cured at 20 mW/cm^2 as a function of conversion. The points mark vitrification onset and the arrowheads illustrate that the reaction is not completed.

5.4 Time-Intensity-Transformation Diagrams

The conversion data and modeled iso-conversion curves are combined with gelation and vitrification in the form of time-intensity-transformation diagrams depicted in Figure 5-20 to Figure 5-22, for DPHA, Acrylated Boltorn H20, and Acrylated Polyether HBP, respectively. The iso-conversion curves were only plotted up to vitrification, since the autocatalytic model only was able to follow the measured conversion profile up to this point, as discussed in the precedent Chapter. It is clear that intensity has a considerable influence on conversion [25], and that the intensity dependence of conversion and vitrification is different, as represented by the different slopes of iso-conversion and the vitrification lines. For very low intensities, it is expected, that high conversions, can not be reached, even at very long exposure times, due to the absent excess volume effect, which was found for higher intensities [26]. For very high intensities, the iso-conversion lines should become vertical, since there is a maximum intensity, beyond which the reaction does not accelerate further [25].

For all three materials it is also obvious that vitrification was shifted to higher conversions for higher intensities. The implication of the shift in vitrification on internal stress is discussed in the following Chapter.

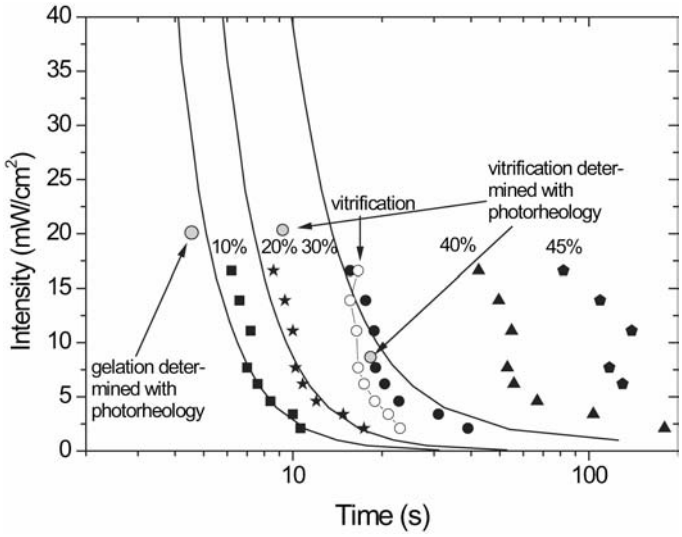

Figure 5-20 Time-intensity-transformation diagram of DPHA. See text for details.

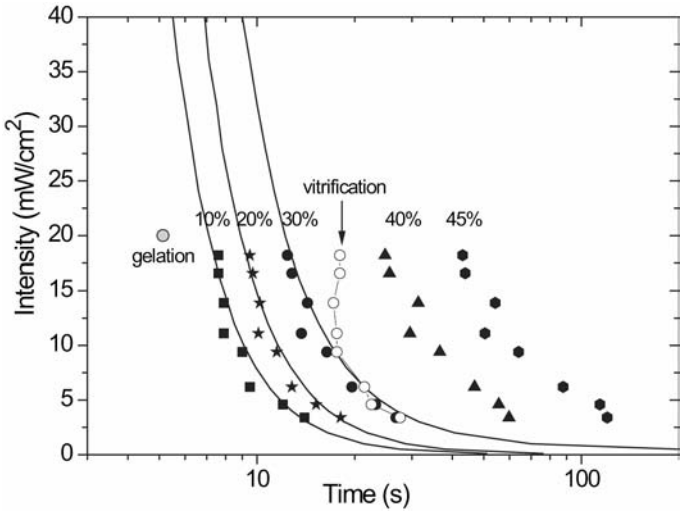

Figure 5-21 Time-intensity-transformation diagram of Acrylated Boltorn H20. See text for details.

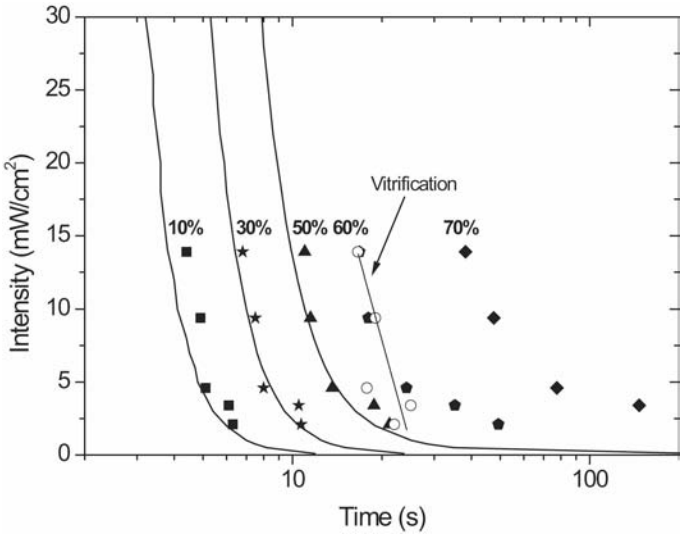

Figure 5-22 Time-intensity-transformation diagram of Acrylated Polyether HBP. See text for details.

5.5 Conclusions

A novel data treatment approach was devised to improve photorheology of fast-curing acrylate systems. The methodology, based on oversampling and adaptive denoising, was particularly efficient in increasing the stress sensitivity to 100 Pa and reducing the time resolution of the rheometer down to 1 ms, independent of the excitation frequency. It enabled accurate measurements to be made of gelation and vitrification of the multifunctional acrylates, as well as the influence of UV intensity on the stiffness build-up in these monomers, and it is therefore a powerful complement to the widely used real-time Fourier transform infrared spectroscopy. A 5 order of magnitude increase in shear modulus within 10 s could be monitored in 1 ms increments. Gelation and vitrification were detected as distinct events in the case of DPHA, which was related to the relatively low glass transition of the cured acrylate network. In contrast, no such distinction could be made for the second generation hyperbranched polyester Acrylated Boltorn H20, presumably due to its high ultimate T_g. The influence of reactive blends on gelation and vitrification was also investigated. It was found that adding Acrylated Boltorn H20 to DPHA retarded the stiffness build-up, whereas adding Acrylated Polyether HBP accelerated the stiffness build-up. However adding HBPs did not shift gelation to higher conversions, but it did move vitrification onset to higher conversions.

Time-temperature-transformation diagrams were compiled based on conversion data and modeled iso-conversion curves, showing that conversion increases for higher intensity, and that conversion and vitrification have different intensity dependence.

5.6 References

1. Khan, S.A., I.M. Plitz, and R.A. Frantz, *In situ technique for monitoring the gelation of UV curable polymers.* Rheologica Acta, 1992. **31**: p. 151-160.
2. Lee, S.S., A. Luciani, and J.-A.E. Månson, *A rheological characterisation technique for fast UV-curable systems.* Progress in Organic Coatings, 2000. **38**: p. 193-197.
3. Steeman, P.A.M., A.A. Dias, D. Wienke, and T. Zwartkruis, *Polymerization and network formation of UV-curable systems monitored by hyphenated real-time dynamic mechanical analysis and near-infrared spectroscopy.* Macromolecules, 2004. **37**: p. 7001-7007.
4. Botella, A., J. Dupuy, A.-A. Roche, H. Sautereau, and V. Verney, *Photo-rheometry/NIR spectrometry: An in situ technique for monitoring conversion and viscoelastic properties during photopolymerization.* Macromolecular Rapid Communications, 2004. **25**: p. 1155-1158.
5. Wilhelm, M., *Fourier-Transform Rheology.* Macromolecular Materials and Engineering, 2002. **287**: p. 83-105.

6. van Dusschoten, D. and M. Wilhelm, *Increased torque transducer sensitivity via oversampling.* Rheologica Acta, 2001. **40**: p. 395-399.
7. Hilliou, L., D. van Dusschoten, M. Wilhelm, H. Burhin, and E.R. Rodger, *Increasing the force torque transducer sensitivity of an RPA 2000 by a factor 5 - 10 via advanced data acquisition.* Rubber Chemistry and Technology, 2004. **77**(1): p. 192-200.
8. Widrow, B. and S.D. Stearns, *Adaptive signal processing*. 1985, Englewood Cliffs, New Jersey: Prentice-Hall Inc. 316-323.
9. Bracewell, R.N., *The fourier transform and its applications*. 3rd edition ed. 2000, Singapore: McGraw-Hill Book Co. 359-367.
10. Winter, H.H. and F. Chambon, *Analysis of linear viscoelasticity of a crosslinking polymer at the gel point.* Journal of Rheology, 1986. **30**(2): p. 367-382.
11. Winter, H.H. and M. Mours, *Rheology of polymers near liquid-solid transitions.* Advances in Polymer Science, 1997. **134**: p. 165-233.
12. Decker, C., D. Decker, and F. Morel, *Light intensity and temperature effect in photoinitiated polymerization,* in *Photopolymerization: fundamentals and application*, A.B. Scranton, C.N. Bowman, and R.W. Pheiffer, Editors. 1997, American Chemical Society: Washington. p. 63-80.
13. Chiou, B.-S., R.J. English, and S.A. Khan, *Rheology and photo-cross-linking of thiol-ene polymers.* Macromolecules, 1996. **29**: p. 5368-5374.
14. Dietz, E.J. and N.A. Peppas, *Reaction kinetics and chemical changes during polymerization of multifunctional (meth)acrylates for the production of highly crosslinked polymers used in information storage systems.* Polymer, 1997. **38**(15): p. 3767-3781.
15. Lange, J., N. Altmann, C.T. Kelly, and P.J. Halley, *Understanding vitrification during cure of epoxy resins using dynamic scanning calorimetry and rheological techniques.* Polymer, 2000. **41**: p. 5949-5955.
16. Lange, J. and J.-A.E. Månson, *Build-up of structure and viscoelastic properties in epoxy and acrylate resins cured below their ultimate glass transition temperature.* Polymer, 1996. **37**(26): p. 5859-5868.
17. Schmidt, L.E., Y. Leterrier, J.-M. Vesin, M. Wilhelm, and J.-A.E. Månson, *Photorheology of fast UV curing multifunctional acrylates.* Macromolecular Materials and Engineering, 2005. **290**: p. 1115-1124.
18. Clifford, S.M., N. Jansson, W. Yu, V. Michaud, and J.-A.E. Månson, *Thermoviscoelastic anisotropic analysis of process induced residual stress and dimensional stability in real polymer matrix composite components.* Composites Part A - Applied Science and Manufacturing, 2006. **37**: p. 538-545.
19. Lange, J., M. Johansson, C.T. Kelly, and P.J. Halley, *Gelation behaviour during chainwise crosslinking polymerization of methacrylate resins.* Polymer, 1999. **40**: p. 5699-5707.
20. Funke, W., *Reactive microgels - polymers intermediate in size between single molecules and particles.* British Polymer Journal, 1989. **21**: p. 107-115.
21. Kil, S.B., Y. Augros, Y. Leterrier, and J.-A.E. Månson, *Rheological properties of hyperbranched polymer/poly(ethylene terephtalate) reactive blends.* Polymer Engineering and Science, 2003. **43**(2): p. 329-343.
22. Lange, J., R. Ekelöf, and G.A. George, *Indications of micro-vitrification during chainwise cross-linking polymerisation.* Polymer, 1999. **40**: p. 3595-3598.
23. Percec, V., P. Chu, and M. Kawasumi, *Toward "willowlike" thermotropic dendrimers.* Macromolecules, 1994. **27**: p. 4441-4453.

24. Chu, F., C.J. Hawker, P.J. Pomery, and D.J.T. Hill, *Intramolecular cyclization in hyperbranched polyesters.* Journal of Polymer Science Part A-Polymer Chemistry, 1997. **35**(9): p. 1627.
25. Decker, C., B. Elzaouk, and D. Decker, *Kinetic study of ultrafast photopolymerization reactions.* Journal of Macromolecular Science, Part A - Pure and Applied Chemistry, 1996. **A33**(2): p. 173-190.
26. Kloosterboer, J.G., *Network formation by chain crosslinking photopolymerization and its applications in electronics.* Advances in Polymer Science, 1988. **84**: p. 1-61.

6 Shrinkage and Internal Stress

The aim of this chapter is to investigate the dynamics of the internal stress, and its relation to the shrinkage and modulus build up during UV polymerization. The particular objective was to identify the effect of gelation and vitrification on internal stress paying special attention to the influence of intensity.

6.1 Shrinkage

6.1.1 Reliability of the Method

The method is described in detail in Chapter 3. A typical measurement of a 100 μm DPHA film, cured under 300 mW/cm^2 is plotted in Figure 6-1. The graph shows the laser intensity measured at photodetector 1 (see Chapter 3), which is a superposition of the signal reflected from the top side of the coating and from the coating-substrate interface. UV exposure starts at t = 0 s. At about 0.2 s the measured intensity at photodetector 1 drops from 6.7 to 3.2 V and oscillations start. The first few oscillation are not well resolved since their frequency is of the range of the acquisition frequency (100 Hz), leading to a diminished acquired amplitude. The significant increase of the oscillation period from 0.02 to 100 s during the course of

the reaction indicates the massive slow-down of the shrinkage rate with polymerization.

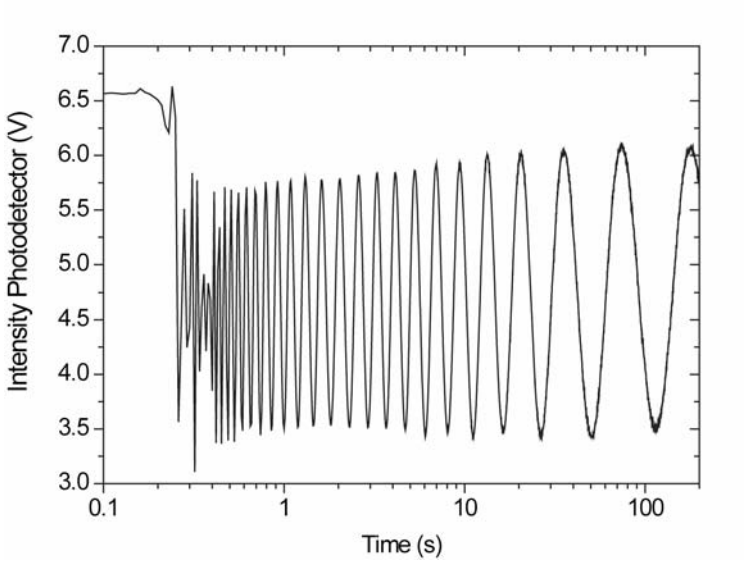

Figure 6-1 Laser Intensity measured at photodetector 1 during UV exposure. The sample used was a 100 μm DPHA film cured under 300 mW/cm^2. Exposure time 180 s.

Figure 6-2 shows the linear shrinkage for DPHA, measured four times under equal conditions, in order to estimate the experimental scatter. An error of about ±10% was found.

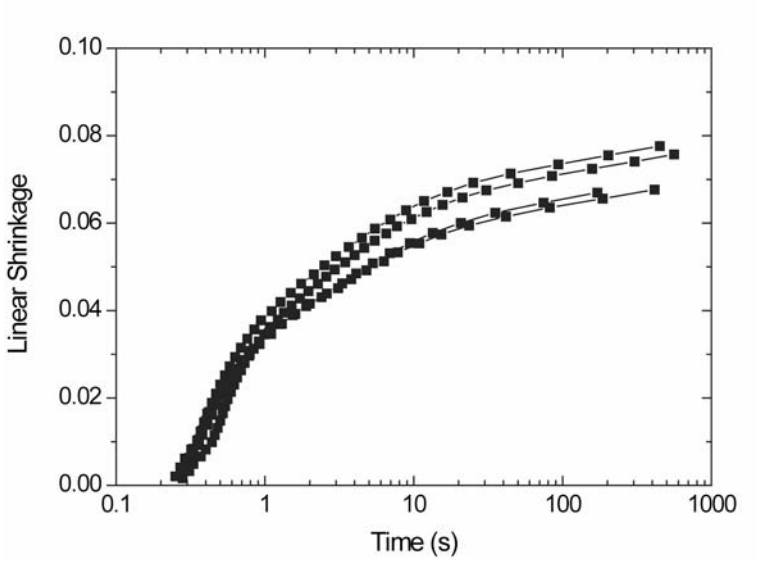

Figure 6-2 Linear shrinkage of 4 DPHA films cured at an intensity of 300 mW/cm^2. Exposure time 180 s.

6.1.2 Shrinkage for Different Acrylates

The linear shrinkage for the different acrylates studied is plotted in Figure 6-3. Both hyperbranched materials shrink by approximately 5%, whereas DPHA shrinks

by more than 6%, which was confirmed elsewhere [1]. The shrinkage is therefore about 50% higher compared with epoxies [2] and about double the shrinkage of thiol-ene systems [3].

Kou et al. [4] measured a reduction in linear shrinkage from 10% to 2% by incorporating an acrylated HBP into a standard acrylate resin. These findings were not confirmed by the present study. Presumably, the shrinkage measurement using a quartz glass capillary is less precise, compared with the method in the present study, which could explain the different results. Also Klee et al. [5] found a shrinkage reduction from about 4% to about 1.5% by replacing the dental composites with functionalized HBPs, which is lower compared to the results in Figure 6-3 due to the presence of fillers.

All samples measured in Figure 6-3 were exposed to UV light for only 180 s. It is remarkable that after 1000 s DPHA still shrank, whereas the for the two HBPs, the shrinkage rate is neglectable already after about 400 s. This again is explained by the retarded modulus build-up for the HBPs (see Chapter 5), which allows more relaxation, and hence more shrinkage to happen during the course of the reaction. In Figure 6-3 b also vitrification determined from photo DSC is added. For all three acrylates, the linear shrinkage decelerated significantly at the onset of vitrification, which is consistent with the findings of de Boer et al. [6]. More interestingly, only 40% of the total shrinkage occurred before gelation in the case of DPHA, but above 60% for both HBPs, which should lead to lower internal stresses of the HBPs.

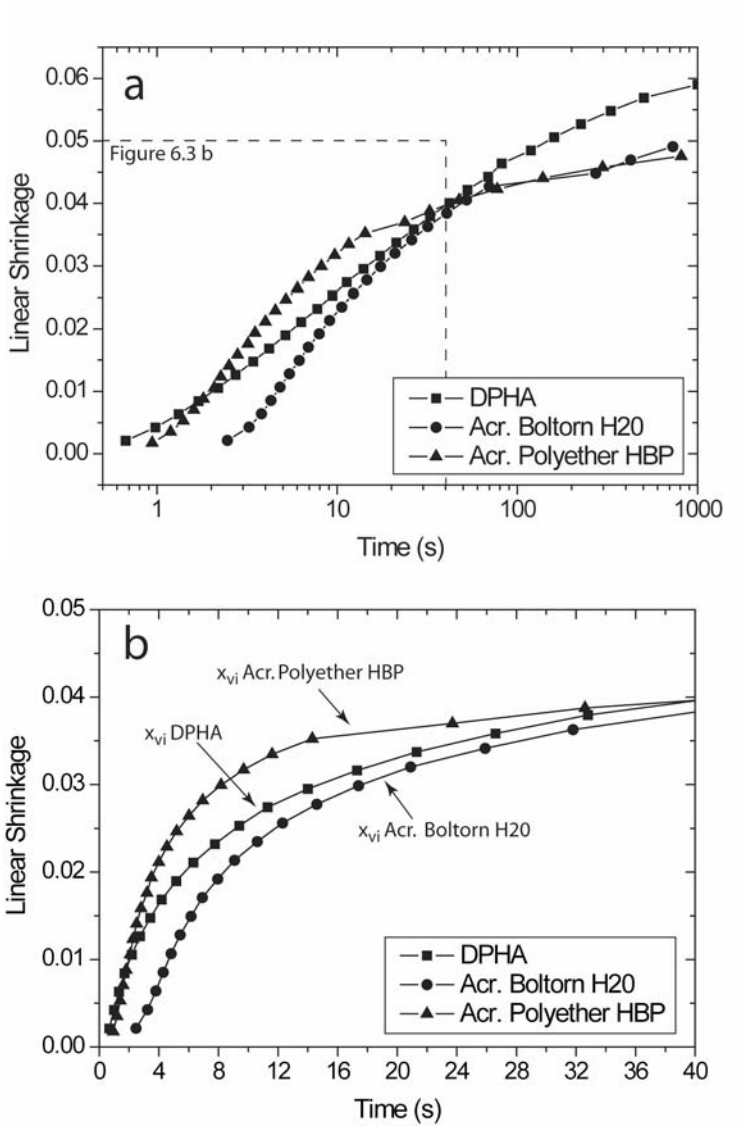

Figure 6-3 a) Linear shrinkage for DPHA, Acrylated Boltorn H20, and Acrylated Polyether HBP cured at 9 mW/cm^2. Exposure time 180 s. b) Segment of a) with vitrification points, determined from photo DSC included.

6.1.3 Impact on Internal Stress

As introduced in Chapter 1, a low stress material should show reduced shrinkage and delayed build up of modulus. The former phenomenon is demonstrated in Figure 6-3 in the case of acrylated HBPs. The latter was shown in Chapter 5 also for both HBPs. The combination of these two phenomena should significantly contribute to stress reduction.

Figure 6-4 shows the magnitude of the complex shear modulus plotted versus the linear shrinkage during UV polymerization at 9 mW/cm^2. It is clear that the stiffness build-up was retarded in the two HBPs relative to DPHA. For a higher UV intensity of 20 mW/cm^2 the behavior was different (Figure 6-5 and Figure 6-6): no

clear difference between DPHA and the two HBPs was observed. However, for a reactive blend of 50 wt.-% Acrylated Boltorn H20 and DPHA, the modulus build-up was once again shifted to a higher shrinkage. The following section discusses these results, as a consequence of the interplay between UV intensity, conversion and vitrification.

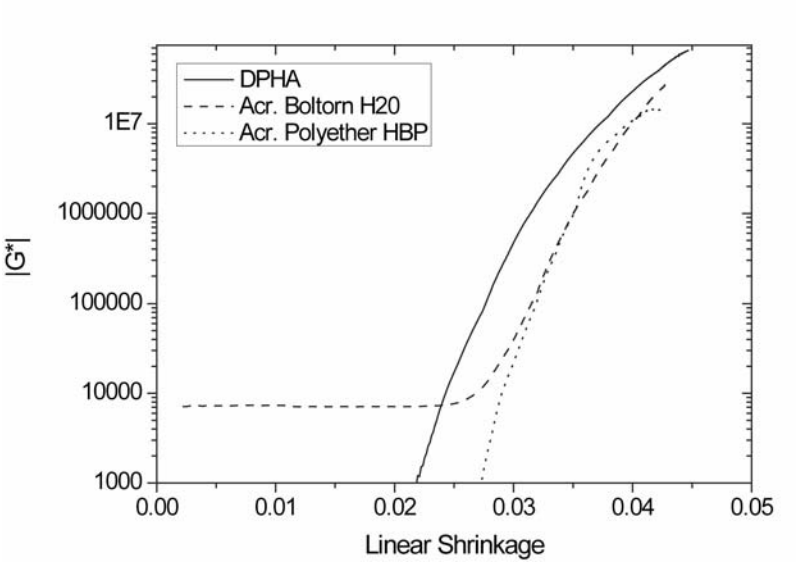

Figure 6-4 Magnitude of the complex shear modulus, plotted as a function of conversion for the three different acrylates. Photocuring was carried out at 9 mW/cm^2. Exposure time 180 s.

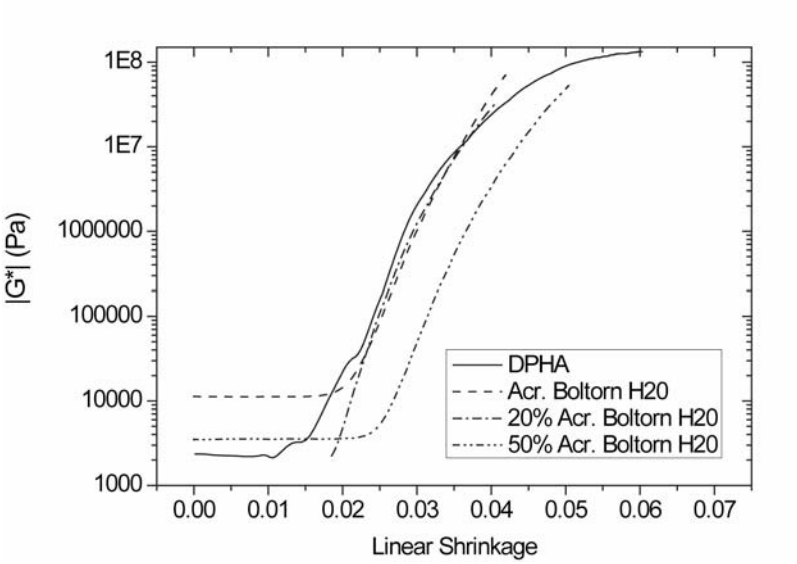

Figure 6-5 Magnitude of the complex shear modulus, plotted as a function of conversion for DPHA, Acrylated Boltorn H20 and two reactive blends. Photocuring was carried out at 20 mW/cm^2. Exposure time 180 s.

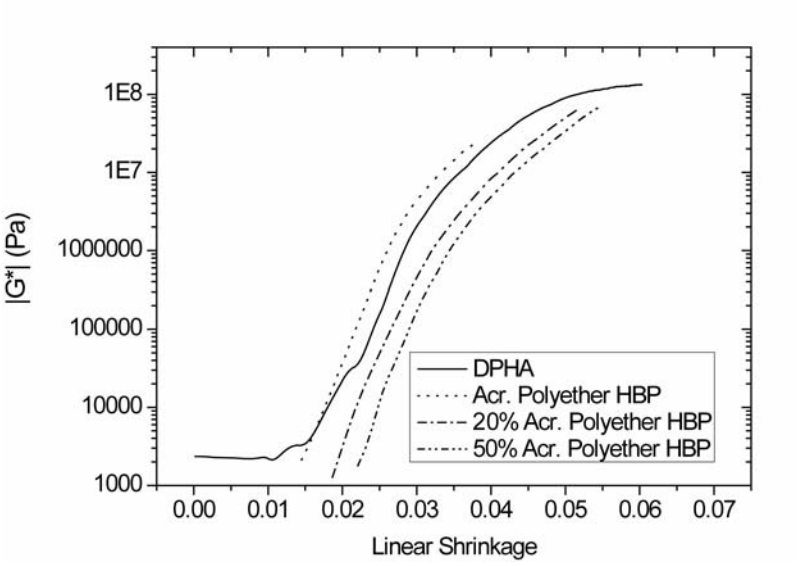

Figure 6-6 Magnitude of the complex shear modulus, plotted as a function of conversion for DPHA, Acrylated Polyether HBP and two reactive blends. Photocuring was carried out at 20 mW/cm^2. Exposure time 180 s.

6.2 Internal Stress

The knowledge of internal stress of polymer coatings is vital, since it has an important influence on the adhesion properties of the coating [7, 8]. Phenomena having a substantial influence on these process-induced internal stress are gelation and vitrification. Chapter 4 and 5 discussed the fact that adding HBPs to DPHA would not shift gelation to higher conversions, but it delayed vitrification from 32% conversion for DPHA to 36% for a 50/50 DPHA / Acrylated Boltorn H20 blend, and to 43% for a 50/50 DPHA / Acrylated Polyether HBP blend.

Figure 6-7 and Figure 6-8 compare the internal stress and Young's modulus of pure DPHA, and HBPs and their blends cured at 40 mW/cm^2. Of the three pure acrylates, DPHA showed the highest internal stress (6.7 MPa) and a Young's modulus equal to 3.2 GPa. In contrast, the internal stress in the cured acrylated Boltorn H20 was reduced by 30%, compared to that in DPHA, while at the same time it had the highest Young's modulus of all three materials (3.9 GPa). A comparable stress reduction was reported, by introducing 14 wt.-% epoxy-functional HBP in a tetraglycidyl-4,4'-methylene dianiline based epoxy resin [9]. Adding 20 wt.-% of Acrylated Boltorn H20 to DPHA led to a drastic increase of internal stress to 10.2 MPa, presumably due to the high modulus of this blend, equal to 5.7 GPa.

An outstanding result was reported in the case of a blend of 50 wt.-% Acrylated Boltorn H20 in DPHA. This material combined low internal stress, (approximately

half of that of DPHA), and a Young's modulus as high as 5 GPa, i.e., more than 50% higher than that of DPHA. For this composition, the delayed modulus build-up compared to its two components shown in Figure 6-5, largely contributed to this result.

The contrasted values of Young's modulus and internal stress of the different blends reflect the dependence on composition of the conversion at vitrification x_{vi} and at maximum conversion x_m and this is discussed in the next section.

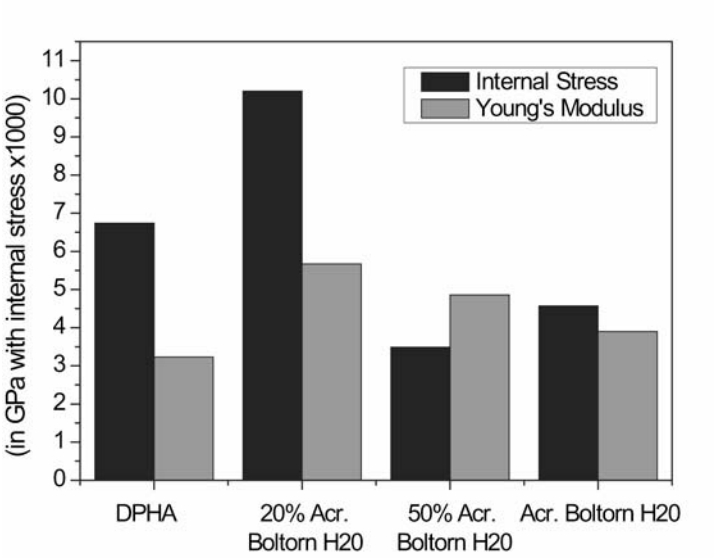

Figure 6-7 Internal stress level and Young's modulus of cured films of DPHA, Acrylated Boltorn H20, and their reactive blends, cured 40 mW/cm^2.

The polyether HBP was most favorable in terms of internal stress (2.4 MPa), but this large stress reduction was obtained at the expense of the elastic properties, with a Young's modulus equal to 1.1 GPa (Figure 6-8). For a blend of 20 wt.-% of Acrylated Polyether HBP in DPHA an internal stress of 11.2 MPa was measured, compared to 6.7 MPa for DPHA, and 2.4 GPa for Acrylated Polyether HBP. The blend of 50 wt.-% Acrylated Polyether HBP in DPHA was more beneficial, with a 46% reduction of internal stress and only a 10% reduction in stiffness compared to that of pure DPHA. Again, the composition dependence of Young's modulus on internal stress is discussed in the next section.

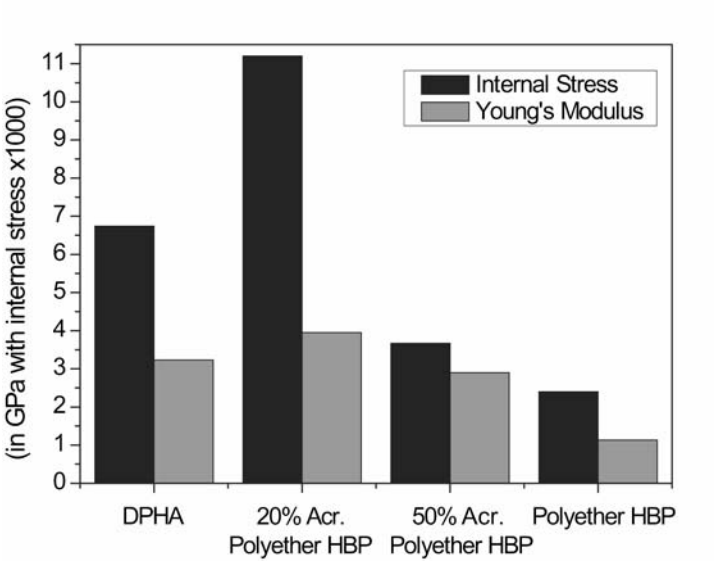

Figure 6-8 Internal stress level and Young's modulus of cured films of DPHA, Acrylated Polyether HBP, and their reactive blends, cured at 40 mW/cm^2.

6.2.1 Influence of UV Intensity on the Dynamics of Internal Stress

Figure 6-9 compares the development of internal stress under two different light intensities, plotted versus conversion and taking into account vitrification. At a low intensity (6 mW/cm^2), significant stresses already built up prior to vitrification. Similar behavior was observed by Lange et al. in the case of acrylate and epoxy thermosets [10]: In acrylates, about half of the stress already developed above T_g, whereas in epoxies this was not the case. In the case of acrylates, this result was attributed to the occurrence of micro-vitrification, in other words the presence of small highly cross-linked domains in the rubbery matrix [11].

In contrast, at a high intensity (40 mW/cm^2), significantly less internal stress was built up before the material started vitrifying. This was a consequence of volume relaxation processes lagging behind network formation, the more, the higher the intensity [12]. Again, the higher final internal stress level obtained for films cured at higher intensities was caused by their higher ultimate conversion. The above findings indicate that stress dynamics result from competing processes: Firstly, enhanced viscoelastic behavior (hence stress relaxation) in cases where there was high acrylate equivalent weight and high intensity, the rate of which depend on $T_g{}^{\infty}$-T_{cure}, and secondly, modulus build-up (hence stress increase) upon vitrification up to final conversion, which also depends on $T_g{}^{\infty}$-T_{cure}, and, moreover, increases with increasing intensity.

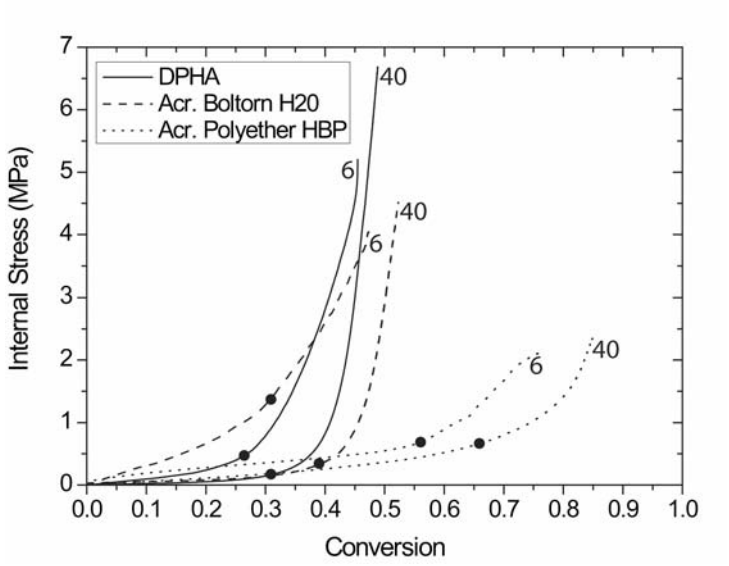

Figure 6-9 Internal stress versus conversion. For each curve the intensity is indicated in mW/cm^2. The bold points mark the onset of vitrification.

For very fast reacting systems, where internal stress is already measurable at early stages, Wen et al. [13] defined vitrification as the point when the stress exceeded the linear extrapolation of the stress of the early reaction by 0.1 MPa. Following this approach, as listed in Table 6-1, the conversion at vitrification x_{vi} was found to be equal to 31% for DPHA, 34% for Acrylated Boltorn H20 and 52% for Acrylated Polyether HBP. These values are very close to the values derived from the photo-DSC data described above (using the criterion proposed in Chapter 4) and from photorheology as described in Chapter 5. The remarkable deviation in the case of Acrylated Polyether HBP results from the limited slope of the stress-conversion cure.

Table 6-1 Comparison of the conversion at vitrification x_{vi} determined with photo DSC, with beam-bending according to Wen et al. [13] and with photorheology.

	Intensity (mW/cm^2)	**x_{vi} (photo DSC)**	**x_{vi} (Wen [13])**	**Photorheology**
DPHA	9	0.28	-	0.30
DPHA	20	0.30	-	0.25
DPHA	40	0.32	0.32	-
Acr. Boltorn H20	40	0.34	0.38	-
Acr. Polyether HBP	40	0.52	0.67	-

As depicted in the time-intensity-transformation diagrams in Chapter 5, vitrification shifts to higher conversions for higher intensities. This explains the shape

of the stress versus conversion curves as measured in Figure 6-9, and illustrated in Figure 6-10. Curing at a low intensity (A), leads to both earlier vitrification, hence earlier internal-stress build-up, but also to limited maximum conversion and therefore limited final stress. Curing at a higher intensity (B) leads to later stress build-up but higher final stress.

The reduced stress for the Acrylated Boltorn H20 results partly from delayed vitrification, but is also a direct consequence of its higher acrylate equivalent weight compared to that of DPHA. The bulk of the internal stress build-up happens in the vitreous state: Adding 20 wt.-% of Acrylated Boltorn H20 to DPHA already increases the maximum conversion x_m by 0.03, which is in agreement with a study by Payne et al. [14, 15], suggesting that a slight increase in conversion in the vitrified state has a considerable impact on the internal stress. The lower internal stress of a 50/50 DPHA / Acrylated Boltorn H20 blend also results from delayed vitrification, as discussed in Chapter 5, allowing for more stress relaxation during isothermal photo-polymerization. The higher Young's modulus of the 50/50 DPHA/Acrylated Boltorn H20 blend is related to its higher ultimate conversion (Chapter 4).

The high conversion levels of Acrylated Polyether HBP result from curing close to its $T_g{}^{\infty}$, in other words they are due to late vitrification. As seen from the vitrification data (Chapter 4), adding 50 wt.-% of Acrylated Polyether HBP to DPHA shifted vitrification to a 0.13 higher conversion, whereas for a blend of 20% of Acrylated Polyether HBP in DPHA the conversion at vitrification was not affected. The resulting fast increase in Young's modulus in the vitrified state together with increased ultimate conversion explains the high level of stress of this blend.

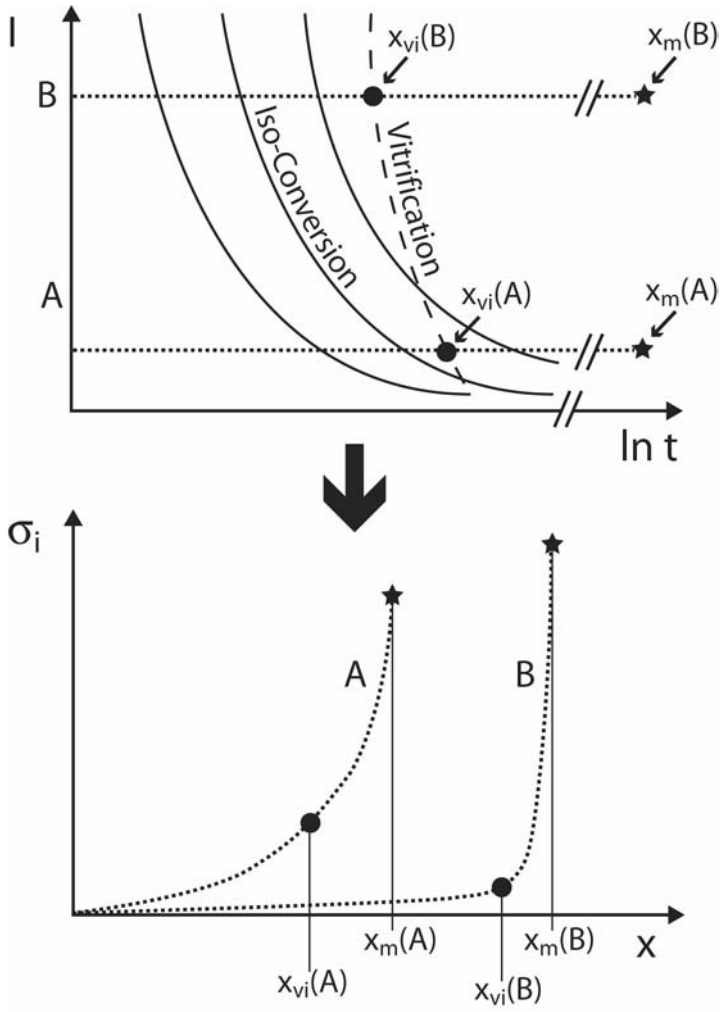

Figure 6-10 Illustration of the dynamics of internal stress: Curing at a low intensity (A) leads both to earlier vitrification at lower conversion x_{vi}, which in turn results in earlier internal-stress build-up, but also to limited maximum conversion x_m and thus to limited final stress; whereas curing at a higher intensity (B) leads to later stress build-up but higher final stress.

6.2.2 Comparison of the Internal Stresses of Acrylates and SU-8

The internal stress of SU-8 was also calculated using Stoney's and Inoue's equations, based on curvature measurements of SU-8 coated silicon wafers after post-exposure baking, as performed by Lorenz et al. [16]. The results are listed in Table 6-2. The wafer was 380 μm thick and the coating thickness varied from 6.75 to 200 μm; stresses larger than 25 MPa were found. Li et. [17] carried out an FE-analysis of SU-8 curing and measured an up to 70% stress reduction, by decreasing the post-exposure baking temperature form 95 to 55 °C, also they did not discuss the impact of the changed curing cycle on the mechanical properties of the crosslinked SU-8.

Compared to the internal stress of SU-8, all acrylate polymers had substantially lower internal stress, ranging from 2.4 MPa for the polyether HBP, over 4.5 MPa for the Acrylated Boltorn H20, to 6.7 MPa for DPHA [18].

Table 6-2 Wafer deflection measurement [7] and internal stress calculated using the Stoney and the Inoue model (biaxial case). The wafer used was a 380 μm thick silicon wafer and the deflection was measured between two 40 mm distant supports. For SU-8 the modulus was set to 3 GPa [10] and the Poisson's ratio to 0.33 [11], and for the Si wafer the modulus was assumed to be 170 GPa and the Poisson's ratio 0.26 [12].

Material	Thickness (μm) [16]	Residual Stress (Stoney, MPa)	Residual Stress (Inoue, MPa)
SU-8	6.75	29.1	27.8
SU-8	19	26.2	25.0
SU-8	200	19.6	13.3
DPHA	280	6.7	5.1
Acr. Boltorn H20	220	4.5	3.6
Acr. Polyether HBP	500	2.4	1.4

6.3 Conclusions

The internal stress of the acrylated HBPs was considerably reduced compared to that of the DPHA. Moreover, in the case of Acrylated Boltorn H20, and of 50/50 reactive blends with DPHA, stress reduction was obtained combined with an increase of Young's modulus. The increased Young's modulus resulted from an increased conversion, while the reduced stress was a consequence of the later onset of macroscopic vitrification.

It was found, that for a higher intensity, higher final internal stresses develop, inspite of being delayed during the polymerization. This is firstly due to a shift of vitrification to higher conversions, and secondly by the lag of volume relaxation behind network formation, hence a higher level of conversion reached.

6.4 References

1. Klang, J.A., *Radiation curable hyperbranched polyester acrylates*. 2006, Sartomer Company, Inc.: Exton, Pennsylvania. p. 1-7.
2. Eom, Y., L. Boogh, V. Michaud, and J.-A.E. Månson, *Internal stress control in epoxy resins and their composites by material and process tailoring.* Polymer Composites, 2002. **23**(6): p. 1044-1056.

3. Carioscia, J.A., H. Lu, J.W. Stansbury, and C.N. Bowman, *Thiol-ene oligomers as dental restorative materials.* Dental Materials, 2005. **21**(12): p. 1137-1143.
4. Kou, H.-G., A. Asif, and W.-F. Shi, *Hyperbranched acrylated aromatic polyester used as a modifier in UV-curable epoxy acrylate resins.* Chinese Journal of Chemistry, 2003. **21**: p. 91-95.
5. Klee, J.E., C. Schneider, D. Hölter, A. Burgath, H. Frey, and R. Mülhaupt, *Hyperbranched polyesters and their application in dental composites: monomers for low shrinking composites.* Polymers for Advanced Technologies, 2001. **12**(6): p. 346-354.
6. de Boer, J., R.J. Visser, and G.P. Melis, *Time-resolved determination of volume shrinkage and refractive index change of thin polymer films during photopolymerization.* Polymer, 1992. **33**(6): p. 1123-1126.
7. Perera, D.Y., *On adhesion and stress in organic coatings.* Progress in Organic Coatings, 1996. **28**: p. 21-23.
8. Negele, O. and W. Funke, *Internal stress and wet adhesion of organic coatings.* Progress in Organic Coatings, 1996. **28**: p. 285-289.
9. Mezzenga, R., L. Boogh, and J.-A.E. Månson, *A review of dendritic hyperbranched polymer as modifiers in epoxy composites.* Composites Science and Technology, 2001. **61**: p. 787-795.
10. Lange, J., S. Toll, J.-A.E. Månson, and A. Hult, *Residual stress build-up in thermoset films cured above their ultimate glass transition temperature.* Polymer, 1995. **36**(16): p. 3135-3141.
11. Lange, J., R. Ekelöf, and G.A. George, *Indications of micro-vitrification during chainwise cross-linking polymerisation.* Polymer, 1999. **40**: p. 3595-3598.
12. Kloosterboer, J.G., *Network formation by chain crosslinking photopolymerization and its applications in electronics.* Advances in Polymer Science, 1988. **84**: p. 1-61.
13. Wen, M., L.E. Scriven, and A.V. McCormick, *Differential scanning calorimetry and cantilver deflection studies of polymerization kinetics and stress in ultraviolet curing of multifunctional (meth)acrylate coatings.* Macromolecules, 2002. **35**: p. 112-120.
14. Payne, J.A., L.F. Francis, and A.V. McCormick, *The effects of processing variables on stress development in ultraviolet-cured coatings.* Journal of Applied Polymer Science, 1997. **66**: p. 1267-1277.
15. Francis, L.F., A.V. McCormick, D.M. Vaessen, and J.A. Payne, *Development and measurement of stress in polymer coatings.* Journal of Materials Science, 2002. **37**: p. 4717-4731.
16. Lorenz, H., M. Despont, N. Fahrni, J. Brugger, P. Vettiger, and P. Renaud, *High-aspect-ratio, ultrathick, negative-tone near-UV photoresist and its applications for MEMS.* Sensors and Actuators A-Physical, 1998. **64**: p. 33-39.
17. Li, B., M. Liu, and Q. Chen, *Low-stress ultra-thick SU-8 UV photolithography process for MEMS.* Journal of Microlithography, Microfabrication, and Microsystems, 2005. **4**(4): p. 043008-1 - 043008-6.
18. Schmidt, L.E., Y. Leterrier, D. Schmaeh, J.-A.E. Månson, and D. James. *Structural and residual stress analysis of UV curable hyperbranched acrylates*. in *RadTech Europe*. 2005. Barcelona.

7 Low-Stress Polymer Microstructures

The main limitations for the development and fabrication of polymer microstructures are shrinkage and related stress, and processing time. During fabrication of SU-8, a very frequently used epoxy, two mechanisms contribute to shrinkage; firstly the evaporation of solvent during the soft-baking step, and secondly the chemical shrinkage during UV and thermal crosslinking in the exposure and post-exposure, or hard baking, steps. Cooling down after the post-exposure bake and hard bake leads to further stresses due to a mismatch in the coefficients of thermal expansion of SU-8 and the substrates, typically Si.

Not only the baking steps, but also the development of the microstructures is very time-consuming. It can be accelerated firstly, by stirring the development solution in order to increase diffusion [1], although stirring at high rates can harm microstructures. Secondly, putting the substrate upside down helps the exchange of developer solution if the density of the developer solution is lower than that of the unreacted polymer [2]. Thirdly, sonic agitation [1] increases the development rate, but should be carried out well above the resonance frequencies of the microstructure, i.e. in the megasonic frequency range.

The objective of this chapter is to evaluate the potential of highly functional solvent-free acrylates as photoresists for thick polymer microstructures with combined reduction of internal stress and processing time. This is especially challenging since decreasing processing time allows less viscoelastic relaxation to occur thus leading to higher internal stresses.

7.1 Fabrication

The polymer microstructures were produced in a so-called photolithographic process, in which the monomer was exposed to UV light through a so-called photomask carrying an absorber pattern, which is the negative of the microstructure to be formed. The mask used was a glass mask with a chromium layer as absorber pattern. It was divided in 1x2 cm^2 rectangular areas containing patterns of columns of different sizes with square and round cross sections, channels open on the top side only, and channels open on three sides (see Appendix) . As depicted in Figure 7-1 the mask enabled various key parameters to be determined including resolution, shape fidelity, that is the accuracy of the produced structure compared with the design, as well as the development and undercut as a result of scattering. These parameters allowed given fabrication conditions and materials to be evaluated.

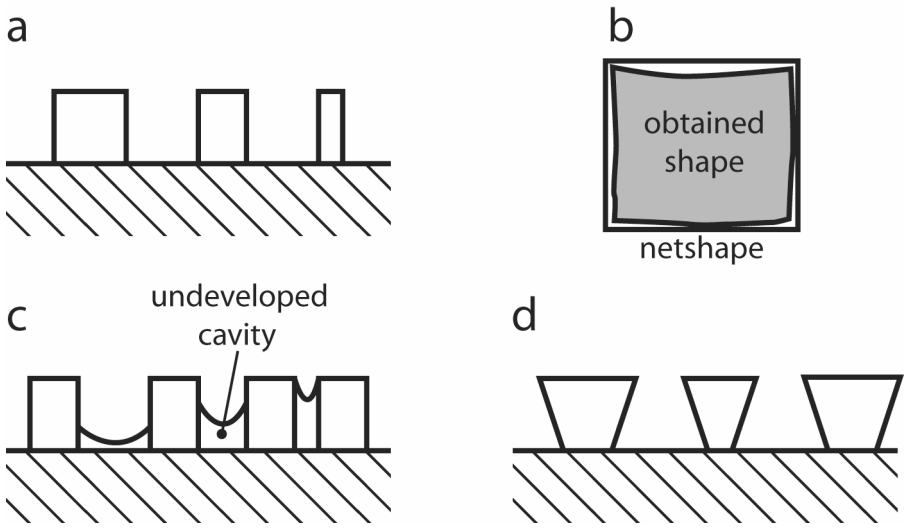

Figure 7-1 Parameters for evaluation of the suitability of material and processing conditions in a photolithographic process: a) Resolution or smallest feature size and spacing, b) shape fidelity, c) development, and d) undercut.

7.1.1 SU-8

The SU-8 reference structure was produced according to the specifications of the supplier. The maximum obtainable thickness, using a standard one-layer process was 105 μm. Due to the high internal stresses, a 1.5 mm thick Si wafer was used to limit the resulting curvature. Processing included dehydration of the wafer for 15 min at 200 °C, spin coating of SU-8 2100 (Microchem, US) at 500 rpm for 10 s, and at 1000 rpm for 30 s. The solvent in the SU-8 was then removed by soft baking at 65 °C for 30 min, and at 95°C for 90 min. Subsequently, the wafer was exposed to UV light for 30 s at an intensity of 20 mW/cm^2 at the 365 nm peak (Hg i-line), which corresponded approximately to an UV-A intensity of 50 mW/cm^2. The wafer was baked again at 65 °C for 1 min and at 95 °C for 20 min, and finally developed in 1-Methoxy-2-propyl acetate for 20 min and rinsed with 2-propanol for 15 s.

7.1.2 Acrylates

In the case of acrylates, which are liquid at room temperature, the following method was used: in a first step, to improve adhesion between the polymer and the glass or silicon substrate a physical vapour deposition of hexamethyl disilazane (HMDS, CAS 999-97-3) was carried out at 170 °C for 30 min at ambient pressure. In order to further improve adhesion, a thin layer of the acrylate (about 30 μm) was spincoated onto the substrate in a second step (1500 rpm for 10 s, and 3000 rpm for 30 s) and cured (exposure for 60 s, RT, intensity: 20 mW/cm^2 at the 365 nm Hg i-line). The microstructures were produced in a third step, using glass spacers to control the thickness of the liquid monomer and a 12 μm polyethylene terephthalate (PET) film placed between mask and monomer to protect the mask (Figure 7-2). The polymer thickness investigated was between 150 and 1000 μm, and the exposure time between 15 s and 60 s. After exposure, the mask and PET film and the spacer were removed carefully and the device was placed in the development solution (1-Methoxy-2-propyl acetate; CAS 108-65-6). In order to improve development, the solution was stirred and the sample was put upside down into the solution (density of 1-methoxy-2-propyl acetate 0.970 g/cm^3; density of the acrylate monomers > 1.1 g/cm^3).

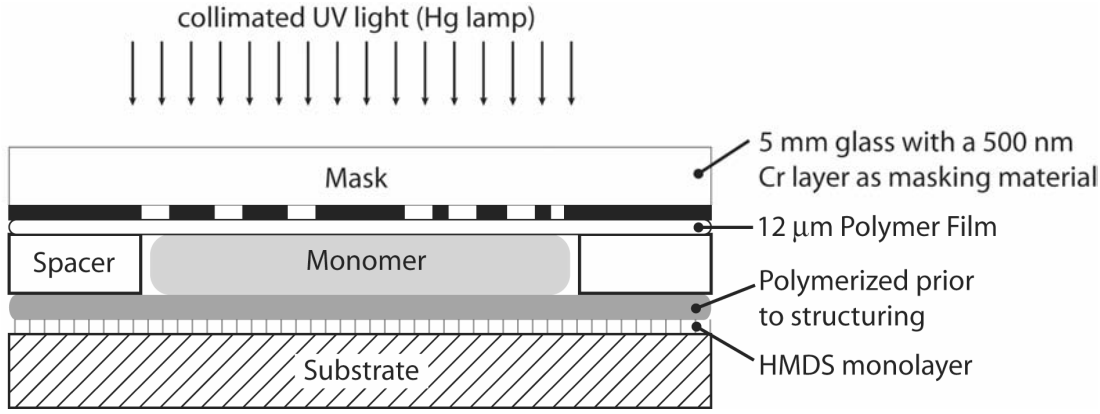

Figure 7-2 Photolithographic fabrication method. The collimated UV light was produced from an Hg lamp with an intensity maximum at 365 nm (Hg i-line).

7.2 Results of Fabrication

7.2.1 Development process of microstructures

As shown in Figure 7-3, in the case of Acrylated Polyether HBP neither increasing the development time by a factor of 11 nor using ultrasonic agitation improved the development significantly. This investigation revealed that rather than stripping unreacted monomer, overexposure is the crucial issue. Reducing the exposure time from 15 s to 10 s does not change the development progress for small channels, but it does change the minimum channel width for entirely developed channels from 100 to 76 µm. For shorter exposures, the scattering angle φ, at which the UV dose is large enough to lead to gelation, becomes smaller. Firstly, it was found that the gelled polymer was not soluble in the developer and secondly, that the adhesion between gel and the cured polymer (of which there is also a thin layer on the substrate) was weak. Gel can therefore be removed during the development process, if the developer can attack this interface.

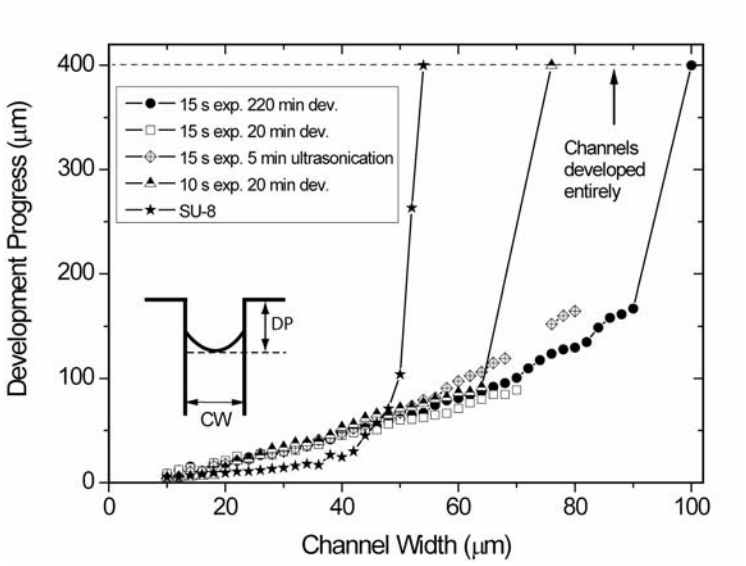

Figure 7-3 Influence of the development conditions on the development progress DP (see inset) for an Acrylated Polyether HBP microstructure, with varying exposure times (10 s and 15 s), and development conditions (time, and agitation). The development progress is compared to a reference structure fabricated from SU-8.

Figure 7-4 a shows a segment of a microstructure made from Acrylated Polyether HBP: A microtip was used to scratch in the partially developed channel. It was found that the residue was not the remains of liquid monomer, due to insufficient development, but a soft gel. Since acrylates react in a chain-wise manner, gelation happens at low conversions, normally in the range of 1-15%, whereas for step-wise reacting epoxies gelation sets in between 30% and 70% conversion [3]. For the present HBP, conversion at gelation could not be determined experimentally, but was assumed to be below 5% (Chapter 5), which would explain why scattering and diffraction of UV light also led to partial polymerization in the unexposed parts of the structure.

In the case of SU-8 the development was not limited by scattering. Figure 7-4 b shows a channel which should have been entirely developed from bottom to top. But what was found was a continuous decrease in the channel depth from bottom to top until the channel was fully developed throughout. In contrast, for the Acrylated Polyether HBP (Figure 7-4 a) the channel depth of the partially developed area was constant and only diminished at the very edge of the channel. This finding can be explained by the step-wise reaction mechanism of SU-8, with gelation at high conversion. The limiting factor in the development of SU-8 is the diffusioncontrolled nature of the process.

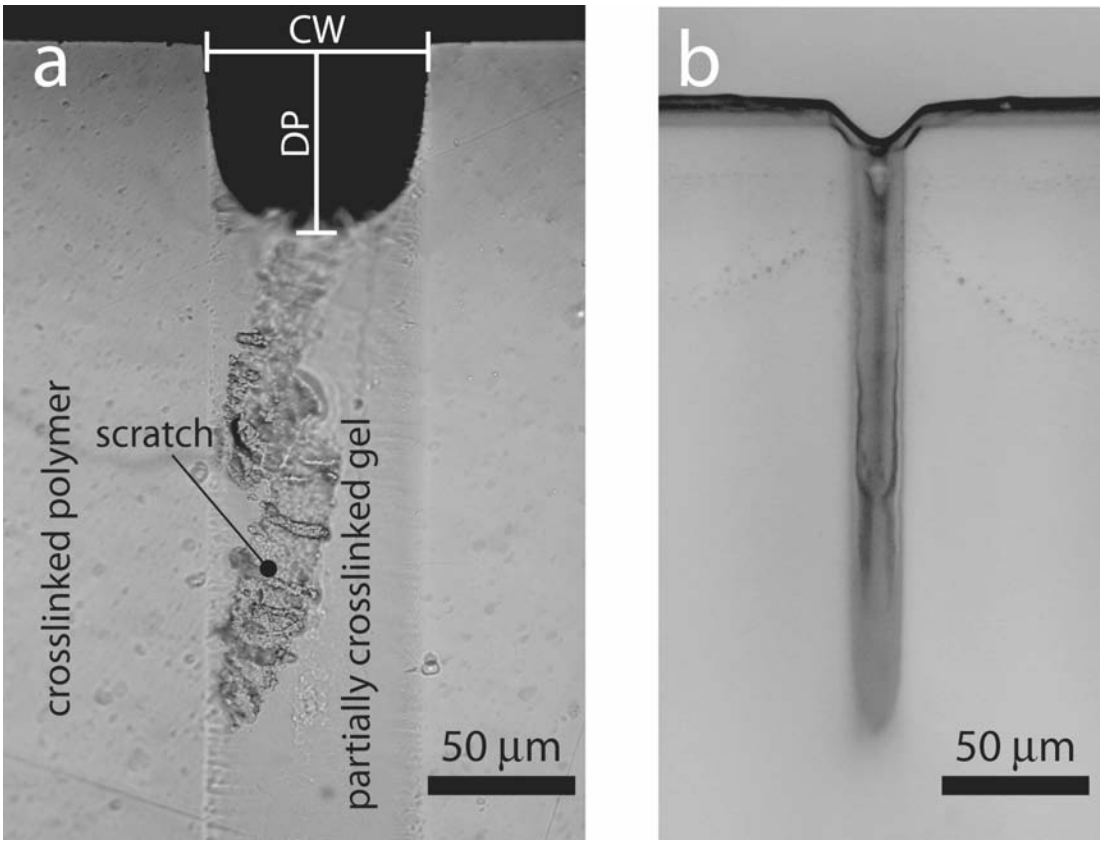

Figure 7-4 Microchannel fabricated a) from Acrylated Polyether HBP (75 µm wide), and b) from SU-8 (26 µm wide).

7.2.2 Defects

Figure 7-5 shows cracks in DPHA and SU8 structures, respectively, originating from high internal stresses. In the Acrylated Polyether HPB and the Acrylated Boltorn H20 no cracks were detected. In the case of SU-8, cracks mainly emerged at the sharp corners surrounding an open cavity. This crack formation is a well known phenomenon for SU-8 [4, 5], which was shown to be overcome by a so-called hard-baking step after development [6]; however, such a process increases internal stress [7], which is somewhat contradictory. One possible explanation is that during the hard-baking step, due to thermal expansion of SU-8, these cracks are closed and that residual epoxy groups react at the crack interface.

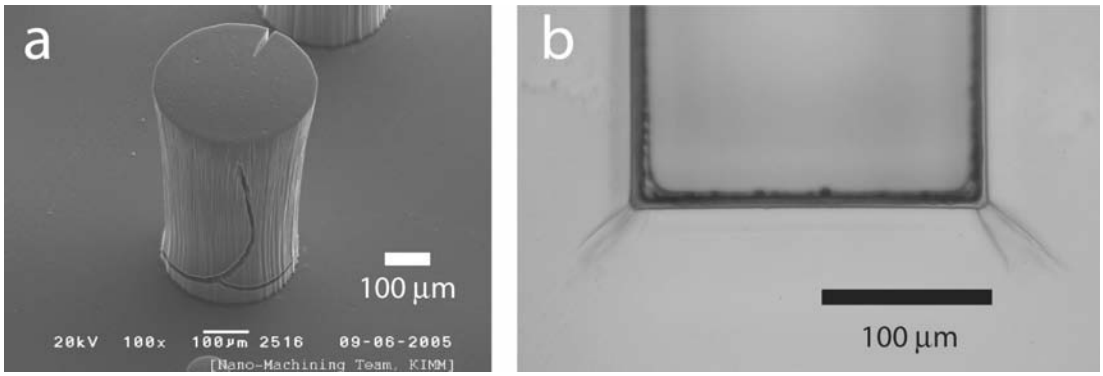

Figure 7-5 Defects due to internal stress in a) a 400 µm tall micropillar produced from DPHA, and b) at the edges of open cavities fabricated from SU-8.

7.2.3 Shape Fidelity

The shape fidelity SF was defined as:

$$SF = LA\left(1 - \frac{\chi}{10°}\right) \tag{7.1}$$

where *LA* is the length accuracy, that is actual length divided by target length, and χ is the angle deviation of the 90° angle of L-shaped structures as seen in Figure 7-6. The structure produced from the acrylated polyether HBP shows an angle deviation of 0.7°, for Acrylated Boltorn H20 it is 2.2°, and for DPHA it is 4.8°, due to the higher internal stresses. For SU-8 an angle deviation of 1.0° was measured, indicating that SU-8 does not release internal stress by deformation, but by cracking.

The length accuracy *LA*, which is determined by polymerization shrinkage and solvent attack during the development step, was determined by relating the actual length of one side of the L-shaped structure to the target length of 400 µm. For the polyether HBP a shape accuracy of 95.6% was measured, for the acrylated Boltorn H20 it was 94.9%, and for the DPHA it was 92.9%, respectively. Compared to the acrylates, SU-8 had a higher shape accuracy of 98.6%.

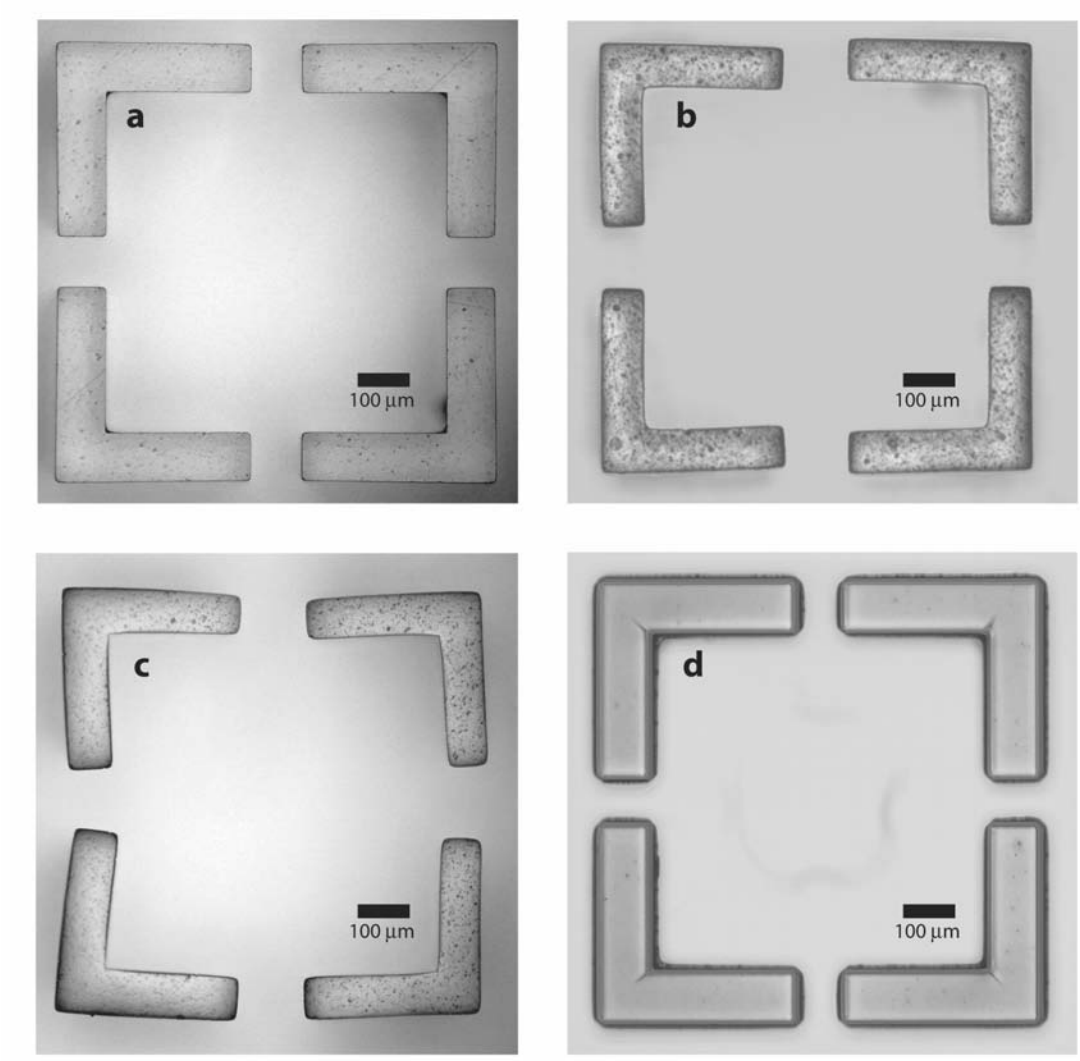

Figure 7-6 Top view of a a) 420 µm high structure fabricated from the polyether HBP, b) 500 µm Acrylated Boltorn H20, c) 400 µm DPHA, and d) 105 µm SU-8 2100 . Due to internal stresses the DPHA and the acrylated Boltorn H20 is deformed, whereas the polyether HBP has good shape accuracy. In SU-8 the internal stress did not cause deformation, but resulted in cracks in corners, and delamination.

7.2.4 Distortion of vertical walls

Negative type photoresists normally show some degree of distortion of vertical walls, also termed undercut. Smith attributed the undercut to oxygen inhibition by ingress of oxygen from unexposed areas [8]. Due to a higher polymerization rate in the top layer, less oxygen diffusion from the unexposed into the exposed areas is possible compared with the bottom layer. The undercut angle (deviation of the edge of a column from the normal to the wafer surface) was found to be 3.41° for Acrylated Polyether HBP; for DPHA it was 2.65°; whilst the lowest value, 1.04°; was determined for the Acrylated Boltorn H20 and for SU-8 2.15° was measured.

7.2.5 Aspect ratio of free standing columns

One measure of photoresist performance is the maximum aspect ratio of produced microstructures. It was defined, in the present case, as the height to width ratio of a square column and evaluated with a pattern of columns designed in such a way that the width of the column increased by 2 μm for every row (Figure 7-7). The first row of straight, undeformed columns was used to calculate the aspect ratio.

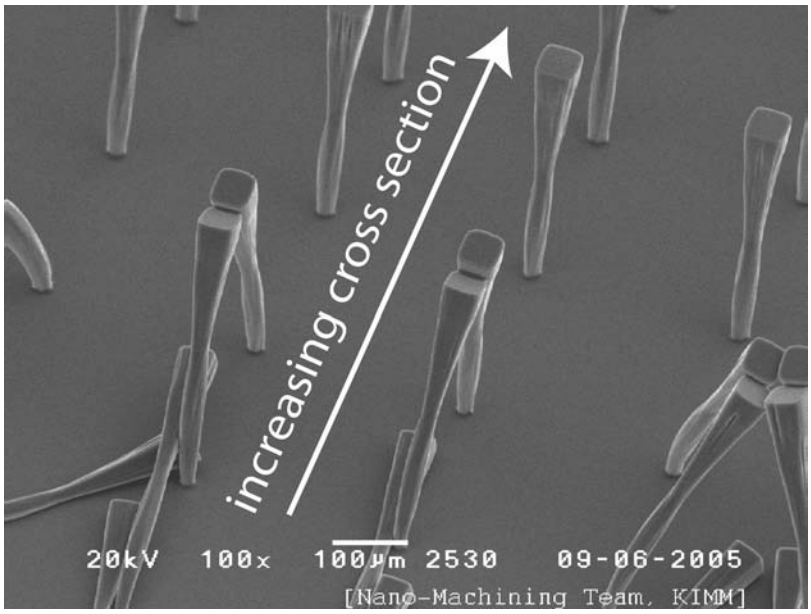

Figure 7-7 Micropillar array produced from Acrylated Polyether HBP with increasing pillar cross section (two micron steps) and a height of 420 μm (15 s exposure at 20 mW/cm^2).

Among the three acrylates, the polyether HBP showed the highest aspect ratios. For a layer thickness of 420 μm (Figure 7-8) it was 7.7, and for a layer thickness of 850 μm it was 6.0. The acrylated Boltorn H20 had a maximum aspect ratio of 3.3 (for a 500 μm thick layer) which was similar to that of DPHA (3.1 for a 400 μm thick layer). For SU-8 aspect ratios up to 10.5 could be obtained, although with thickness limited to 105 μm (Figure 7-9), and at the expense of increased processing time. Elsewhere aspect ratios up to 18 where found [7].

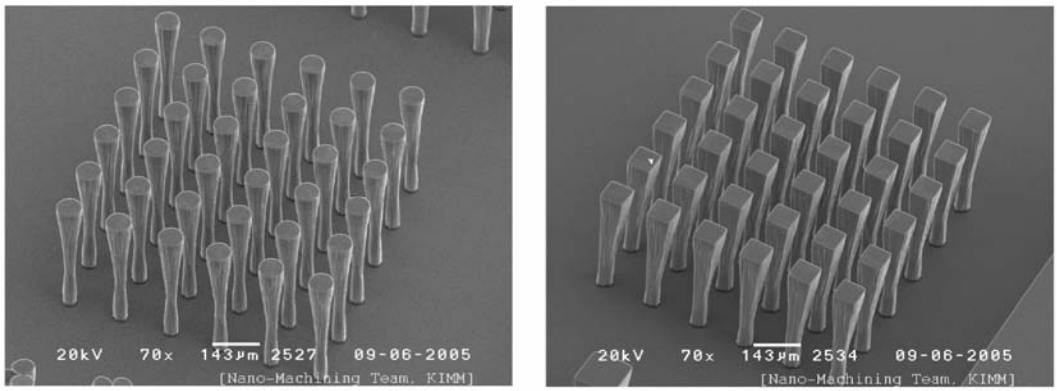

Figure 7-8 Array of round and square columns fabricated in a photolithographic process from Acrylated Polyether HBP (15 s exposure at 20 mW/cm^2).

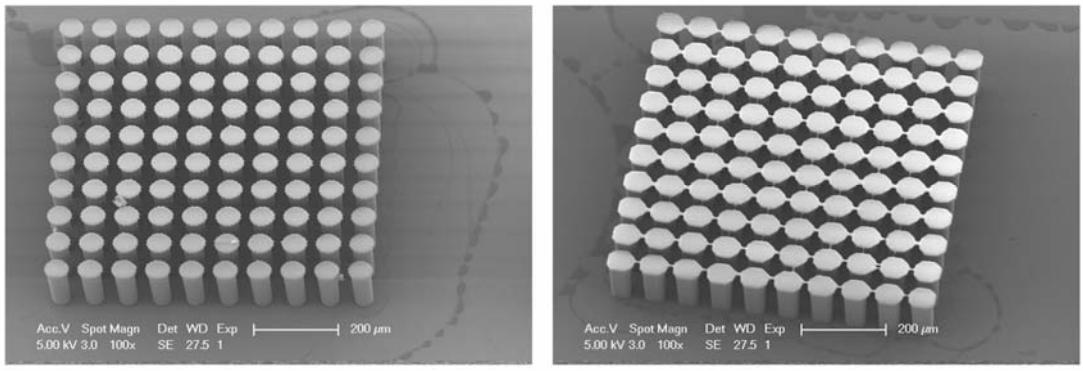

Figure 7-9 Array of round and square columns fabricated in a photolithographic process from SU-8.

Table 7-1 gives an overview of the obtained results for different materials and processing conditions. To facilitate the comparison of different materials for the fabrication of thick polymeric microstructures for microfluidic devices, a figure of merit (FOM) is defined:

$$FOM = \frac{AR \cdot SF}{\sigma_i \cdot D_{Ch} \cdot t_{Fab}} * 1000 \qquad (7.2)$$

where *AR* is the highest aspect ratio obtained with square columns, *SF* the shape fidelity (comparing the cross section of the actual feature with the target cross section), σ_i is the internal stress, D_{Ch} the width of the slimmest entirely developed channel closed on both ends, and t_{Fab} the fabrication time. An FOM of 30 was calculated for the Acrylated Polyether HBP, 11 for the Acrylated Polyester HBP, 8 for DPHA and 4 for SU-8 . These results confirm that low-stress Acrylated HBPs are promising materials for producing ultra-thick, high aspect ratio polymer microstructures.

Table 7-1 Overview of the performance of different photoresists. The aspect ratio was determined as the height of the smallest square column divided by its width. The internal stress for the acrylates was taken from [1]. The angle deviation was determined as the deviation of the 90° angle of structure with an L-shapedcross-section. The length accuracy was determined by comparing actual and target lengths of a feature with a rectangular cross-section.

Resist	Layer Thickn (µm)	Aspect Ratio	Smallest Dev. Channel (µm)	Angle Deviation (°)	Length Accuracy	Undercut Angle (°)	Internal Stress (MPa)	Processing Time (min)	FOM
Polyether HBP	420	7.7	145	0.7	95.6%	3.41	2.4	30	30
Polyether HBP	850	6.0	190				2.4	30	
DPHA	400	3.1	85	4.8	92.9%	2.65	6.7	30	8
Acr. Boltorn H20	500	3.3	70	2.2	94.9%	1.04	4.5	30	12
SU-8	105	10.5	65	0.58	98.6%	2.15	>13	240	4

7.3 Outlook and Conclusions

In collaboration with the Korea Advanced Institute of Science and Technology a micro battery was fabricated, as a sample device as shown in Figure 7-10. Based on these preliminary results, the process could be optimized and the sample device will then undergo fluidic tests.

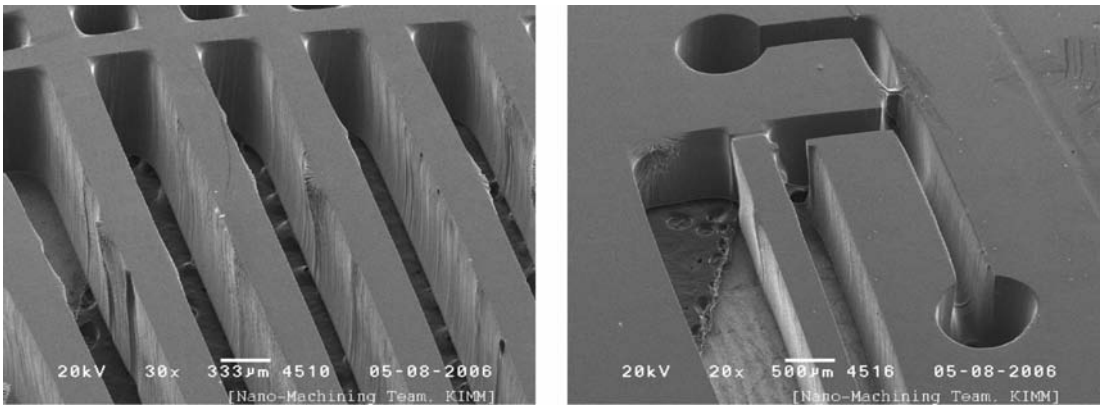

Figure 7-10 Sample device (micro battery) fabricated from Acrylated Polyether HBP. Layer thickness 1.7 mm.

Novel materials were proposed as negative tone photoresists for photolithography of ultra-thick layers. The materials included a range of acrylate monomers, having low to high internal stresses. These materials were compared to the widely used negative tone photoresist SU-8. It was found that internal stress is the key limiting factor for producing thick micropatterns.

In the case of acrylates, light scattering was found to limit the development of narrow channels, whereas in the case of SU-8 the development was diffusion-controlled.

The acrylated polyether HBP, showed the best performance: comparatively high shape fidelity, layer thicknesses up to 850 μm, and aspect ratios up to 7.7 could be produced in a simple single-layer process. The processing time was reduced 8-fold compared to SU-8. These findings suggest that future developments should focus on liquid, solvent-free photoresists, polymerizing entirely during UV exposure.

7.4 References

1. Williams, J.D. and W. Wang, *Using megasonic development of SU-8 to yield ultra-high aspect ratio microstructures with UV lithography*. Microsystem Technologies, 2004. **10**: p. 694-698.
2. Cheng, C.-M. and R.-H. Chen, *Development behaviours and microstructure quality of downward-development in deep x-ray lithography.* Journal of Micromechanics and Microengineering, 2001. **11**: p. 692-696.
3. Lange, J., M. Johansson, C.T. Kelly, and P.J. Halley, *Gelation behaviour during chainwise crosslinking polymerization of methacrylate resins.* Polymer, 1999. **40**: p. 5699-5707.
4. Tseng, F.-G. and C.-S. Yu, *High aspect ratio ultrathick micro-stencil by JSR THB-430N negative UV photoresist.* Sensors and Actuators A - Physical, 2002. **97-98**: p. 764-770.
5. Li, B., M. Liu, and Q. Chen, *Low-stress ultra-thick SU-8 UV photolithography process for MEMS.* Journal of Microlithography, Microfabrication, and Microsystems, 2005. **4**(4): p. 043008-1 - 043008-6.
6. Rabarot, M., J. Bablet, M. Ruty, M. Kipp, I. Chartier, and C. Dubarry. *Thick SU-8 photolithography for BioMEMS*. in *Micromachining and Microfabrication Process Technology VIII*. 2003: SPIE.
7. Lorenz, H., M. Despont, N. Fahrni, J. Brugger, P. Vettiger, and P. Renaud, *High-aspect-ratio, ultrathick, negative-tone near-UV photoresist and its applications for MEMS.* Sensors and Actuators A-Physical, 1998. **64**: p. 33-39.
8. Smith, D.K., *A mathematical model of photomeric oxygen consumption in photopolymer*. Photographic Science and Engineering, 1968. **12**(5): p. 263-266.

8 Conclusions

8.1 Summary

The dynamics of microstructure and internal stress build-up in a penta/hexa-acrylate monomer (DPHA) and in two different acrylated hyperbranched polymers during crosslinking under ultraviolet (UV) light were investigated with special attention paid to composition and UV intensity. The hyperbranched polymers included a second generation hyperbranched polyester and a third generation hyperbranched polyether. Specifically, the chemical network formation, stiffness build-up, and structural transitions, such as gelation and vitrification were examined.

Chemical conversion was investigated by means of photo differential scanning calorimetry. Three main stages of polymerization were identified. In the first stage, the reaction was autoaccelerating, due to the diffusion-controlled nature of the termination up to a maximum in conversion rate, which was found to be independent of UV intensity for DPHA and Acrylated Polyester HBP. For the Acrylated Polyether HBP, a slight shift of the maximum to higher conversions was observed. In the second stage, the propagation mechanism became diffusion-controlled, leading to autodeceleration. The final stage was only pronounced in the case of DPHA and Acrylated Polyester HBP, both being cured below their ultimate T_g. Curing these materials above their ultimate T_g erased this third stage. Based on the occurrence of a third stage, a criterion was therefore proposed to identify vitrification directly from photo DSC measurements. This criterion was correlated to photorheology

measurements in the case of DPHA, where vitrification was identified from a peak in the evolving phaseangle. The conversion profiles were analyzed using an autocatalytic model. It was shown that the reaction order and the autocatalytic exponent were independent of UV intensity, whereas the rate constant showed strong intensity dependence, and the maximal conversion reached showed weak intensity dependence. For all three materials, the main termination mechanisms could be identified as second order and primary radical termination.

Ultimate conversion was found to be 0.16 higher than conversion at vitrification for all investigated materials and blends, independent of UV intensity, which was argued to result from volume relaxation processes in the vitrifying acrylates. The intensity behavior was found to be similar for both conversion at vitrification and final conversion. This important result indicates that vitrification rather than gelation, controls the final conversion in UV curing acrylates [1].

The transition from a viscous liquid to a viscoelastic solid was analyzed with photorheology. The sensitivity of the commercial rheometer was improved several-fold, by a combination of an adaptive filter algorithm and improved data treatment, using a powerful oversampling acquisition hardware [2]. The novel set-up was capable of monitoring up to a 5 order of magnitude increase in shear modulus within short experiment timescales (about 10 s). The improvement in sensitivity and acquisition rates enabled induction time, gelation, and vitrification of the multifunctional acrylates to be determined. In the case of the penta/hexa-acrylate system, gelation and vitrification were detected as distinct events, in contrast to the second-generation hyperbranched polyester, for which vitrification could not be identified. These findings were related to the difference in the glass transition temperature of the cured networks. The results of the photo DSC and the photorheology study were synthesized in the form of time-intensity-transformation diagrams [3], which clearly revealed a markedly different influence of intensity on conversion and vitrification.

Curing at low intensity led to lower conversion at vitrification, limiting the final conversion. Curing at high intensity led to later vitrification and to higher final conversion.

The implication of these findings on the development of internal stress during photopolymerization was studied by performing beam-bending experiments: The tensile internal stress of the acrylated HBPs (4.5 MPa for Acrylated Polyester HBP and 2.4 MPa for Acrylated Polyether HBP), having a thickness between 200 and 500

μm, was greatly reduced compared to that of the DPHA (6.7 MPa). Moreover, in the case of Acrylated Polyester HBP and a 1/1 reactive blend with DPHA, the stress reduction was obtained with a combined increase of Young's modulus [4] (from 3.2 GPa for DPHA to 5 GPa for the reactive blend). The stress reduction was explained by retarded vitrification in the blend (0.03 higher conversion compared to DPHA), whereas the increase in stiffness resulted from a higher final conversion (0.04 higher compared to DPHA). For reactive blends of 20 wt.-% of either of the HBPs with DPHA, the internal stress doubled due to the high modulus of the blends. It is therefore essential to optimize both material composition and process conditions such as UV intensity, to produce low stress acrylates with high stiffness.

In addition the influence of UV intensity on the internal stress build-up was studied. Increasing intensity by a factor of 7 increased internal stresses up to 20 %, depending on the monomer. These results were analyzed based on the time-intensity-transformation diagrams. Curing at a lower intensity led to earlier vitrification, hence earlier internal-stress build-up, but limited maximum conversion thus limiting final stress. On the contrary, curing at a higher intensity led to delayed vitrification, hence later stress build-up, but higher final conversion and higher final stresses.

Shrinkage development during exposure to UV light was analyzed with an interferometry-based method. The linear shrinkage of DPHA was found to be above 6%, and approximately 5% for the two HBPs. This method revealed the drastic slow down of shrinkage during vitrification. In other words, only 40% of the total shrinkage occurred before gelation in the case of DPHA, but above 60% for both HBPs.

The different acrylate materials were used to fabricate polymer microstructures and compared with standard negative epoxy photoresist SU-8. It was demonstrated that acrylated hyperbranched polymers offer interesting possibilities for the production of large-scale microdevices, such as microfluidic devices [5]. Internal stresses for the engineering material SU-8 were reported to be larger than 20 MPa, compared to 2.4 MPa measured of the Acrylated Polyether HBP. This low level of internal stress enabled the fabrication of defect free resist layers up to 850 μm in thickness, having a good adhesion and shape fidelity. In addition, the fabrication time was much shorter (reduced from 240 to 30 min) compared to that of conventional SU-8, and the production of thicker layers was possible even on standard substrates (500 μm Si wafer), due to the low level of internal stress.

8.2 Concluding Discussion

The development of shrinkage and internal stress of UV crosslinking acrylates is related to the interplay between conversion, UV intensity and volume of the polymerizing substance, lagging back behind conversion. After exposure start, there is a short induction time, typically below 0.5 s, where the photoinitiator molecules are decomposed, and chaingrowth is initiated. During the course of reaction the liquid monomer starts forming microgels, particularly for the highly branched structures, with high functionality in a small volume. The microgels react further to macrogels, hence only a small amount of modulus build-up occurs, allowing the crosslinking polymer to shrink relatively freely. As the reaction proceeds, the network forms a gel and vitrifies, leading to a drastic slowdown of reaction combined with a steep increase in stiffness and internal stress. The following behavior is observed:

- Curing at higher UV intensities leads to a higher conversion rate, hence increased mobility, shifting vitrification to higher conversion, and enabling higher final conversion to be reached.
- At the onset of vitrification the volume is no longer able to follow conversion. This effect increases by a higher UV intensity. This leads to lower internal stresses during the course of the reaction for curing at higher intensities. The final stress level is however higher, since the excess volume allows for more conversion to take place.
- In comparison to the reference penta/hexa-acrylate monomer, for HBPs, vitrification is not resolved by photorheology, indicating that vitrification spans over a wider conversion range. This in fact allows for more viscoelastic relaxation to happen, leading to lower internal stresses. In thermoset curing, this principle is used by choosing low cooling rates [6].

This work demonstrates that the combination of UV-curing and highly functional polymers based on hyperbranched architectures is effective in producing low stress materials. UV curing enables shrinkage to be reduced compared to thermal curing, and the shrinkage of HBPs was found to be lower than that of standard acrylate. HBPs moreover form microgels that shrink in absence of modulus build-up, thereby delaying the generation of internal stress.

8.3 Outlook

The limited long-term stability of polymers hinders their application, specifically due to uncontrolled levels of process-induced internal stress. In the case

of UV-curing acrylate, the present study addressed a selection of key factors influencing internal stress, such as molecular architecture and UV intensity. Important aspects not discussed include curing temperature and air moisture [7]. The approach for reducing internal stresses included the use of hyperbranched polymers, a concept already verified for thermally curing epoxies [8]. Recent studies discuss the introduction of mineral fillers, to increase both the mechanical properties [9], and reduction of permeation of small molecules [10, 11], hence improved barrier properties. Various methods for preparing UV-curable acrylate nanocomposites based on silicates have been reported [12, 13], either through a silicon alkoxide route, or via mixing with dense silicate nanoparticles. In the case of acrylates, grafting of trialkoxysilanes onto silica nanoparticles enabled good dispersion up to 35 wt% [14]. In these studies devoted to UV-curable nanocomposites, the influence of the nanofiller on the rheological behavior and stress build-up was, however, not considered. Moreover HBPs were found to ensure homogeneous dispersion of nano-fillers, both in thermoset [15] and photosetting polymers [16].

Stansbury et al. [17] point out that, especially in the field of dental composites, comprehensive work was carried out on composites containing fillers for shrinkage reduction, but little effort was devoted to study the effect of filler on the internal stress. No clear consensus about the implication of fillers on the internal stress level has been reached. The results obtained so far have suggested either an increase [18] or decrease of the internal stress [17]. It has been suggested that in particular the quality of adhesion between reinforcement and matrix has a considerable effect [19, 20].

A further unclarified question is whether stress-induced cavitation arises, as reported for drying coatings [21] and crosslinking thermosets [22], and how it influences the final stress level. Stress induced at defects may relax through microcracking. Incorporating HBPs in thermosets has led to reaction-induced phase separation and toughening of the thermoset [23-26]. However, it is not yet known, whether reaction-induced phase separation [27, 28] can occur during the short experimental time-scale in the case of UV curing.

8.4 References

1. Schmidt, L.E., Y. Leterrier, D. Schmäh, J.-A.E. Månson, D. James, E. Gustavsson, and L.S. Svensson, *Conversion analysis of acrylated hyperbranched polymers UV-cured below their ultimate glass transition temperature.* submitted to Journal of Applied Polymer Science.

2. Schmidt, L.E., Y. Leterrier, J.-M. Vesin, M. Wilhelm, and J.-A.E. Månson, *Photorheology of fast UV curing multifunctional acrylates.* Macromolecular Materials and Engineering, 2005. **290**: p. 1115-1124.
3. Schmidt, L.E., D. Schmäh, Y. Leterrier, and J.-A.E. Månson, *Time-intensity-transformation and internal stress in UV-curable hyperbranched acrylates.* submitted to Rheologica Acta.
4. Schmidt, L.E., Y. Leterrier, D. Schmaeh, J.-A.E. Månson, and D. James. *Structural and residual stress analysis of UV curable hyperbranched acrylates*. in *RadTech Europe*. 2005. Barcelona.
5. Jin, Y.-H., L.E. Schmidt, Y. Leterrier, Y.-H. Cho, and J.-A.E. Månson. *Fabrication process of low-stress UV-curable hyperbranched polymers for microfluidic applications*. in *NanoTech 2005, The 9th annual European conference on micro- & nanoscale technologies for the biosciences*. 2005. Montreux.
6. Clifford, S.M., N. Jansson, W. Yu, V. Michaud, and J.-A.E. Månson, *Thermoviscoelastic anisotropic analysis of process induced residual stress and dimensional stability in real polymer matrix composite components.* Composites Part A - Applied Science and Manufacturing, 2006. **37**: p. 538-545.
7. Payne, J.A., *Stress Evolution in Solidifying Coatings*, in *Department of Chemical Engineering and Materials Science*. 1998, University of Minnesota: Twin Cities.
8. Eom, Y., L. Boogh, V. Michaud, and J.-A.E. Månson, *Internal stress control in epoxy resins and their composites by material and process tailoring.* Polymer Composites, 2002. **23**(6): p. 1044-1056.
9. Huang, J.-c., C.-b. He, Y. Xiao, K.Y. Mya, J. Dai, and Y.P. Siow, *Polyimide/POSS nanocomposites: interfacial interaction, thermal properties and mechanical properties.* Polymer, 2003. **44**: p. 4491-4499.
10. LeBaron, P.C., Z. Wang, and T.J. Pinnavaia, *Polymer-layered silicate nanocomposites: an overview.* Applied Clay Science, 1999. **15**: p. 11-29.
11. Sangermano, M., G. Malucelli, E. Amerio, A. Priola, E. Billi, and G. Rizza, *Photopolymerization of epoxy coatings containing silica nanoparticles.* Progress in Organic Coatings, 2005. **54**: p. 134-138.
12. Etienne, P., J. Phalippou, and R. Sempere, *Mechanical properties of nanocomposite organosilicate films.* Journal of Materials Science, 1998. **33**: p. 3999-4005.
13. Decker, C., L. Keller, K. Zahouily, and S. Benfarhi, *Synthesis of nanocomposite polymers by UV-radiation curing.* Polymer, 2005. **46**: p. 6640-6648.
14. Bauer, F., H.-J. Gläsel, U. Decker, H. Ernst, A. Freyer, E. Hartmann, V. Sauerland, and R. Mehnert, *Trialkoxysilane grafting onto nanoparticles for the preparation of clear coat polyacrylate systems with excellent scratch performance.* Progress in Organic Coatings, 2003. **47**: p. 147-153.
15. Rodlert, M., C.J.G. Plummer, L. Garamszegi, Y. Leterrier, H.J.M. Grünbauer, and J.-A.E. Månson, *Hyperbranched polymer/montmorillonite clay nanocomposites.* Polymer, 2004. **45**: p. 949-960.
16. Fogelström, L., P. Antoni, E. Malmström, and A. Hult, *UV-curable hyperbranched nanocomposite coatings.* Progress in Organic Coatings, 2006. **55**: p. 284-290.
17. Stansbury, J.W., M. Trujillo-Lemon, H. Lu, X. Ding, Y. Lin, and J. Ge, *Conversion-dependent shrinkage stress and strain in dental reasins and composites.* Dental Materials, 2005. **21**: p. 56-67.

18. Condon, J.R. and J.L. Ferracane, *Assessing the effect of composite formulation on polymerization stress.* Journal of the American Dental Association, 2000. **131**: p. 497-503.
19. Condon, J.R. and J.L. Ferracane, *Reduction of composite contraction stress through non-bonded microfiller particles.* Dental Materials, 1998. **14**: p. 256-260.
20. Condon, J.R. and J.L. Ferracane, *Reduced polymerization stress through non-bonded nanofiller particles.* Biomaterials, 2002. **23**: p. 3807-3815.
21. Vaessen, D.M., A.V. McCormick, and L.F. Francis, *Effects of phase separation on stress development in polymeric coatings.* Polymer, 2002. **43**: p. 2267-2277.
22. Eom, Y., L. Boogh, V. Michaud, P. Sunderland, and J.-A.E. Månson, *Stress-initiated void formation during cure of a three-dimensionally constrained thermoset resin.* Polymer Engineering and Science, 2001. **41**(3): p. 492-503.
23. Boogh, L., B. Pettersson, and J.-A.E. Månson, *Dendritic hyperbranched polymers as toughening for epoxy resins.* Polymer, 1999. **40**: p. 2249-2261.
24. Plummer, C.J.G., R. Mezzenga, L. Boogh, and J.-A.E. Månson, *Phase separation in epoxy resing-reactive dendritic hyperbranched polymer blends.* Polymer Engineering and Science, 2001. **41**: p. 43-52.
25. Mezzenga, R., C.J.G. Plummer, L. Boogh, and J.-A.E. Månson, *Morphology build-up in dendritic hyperbranched polymer modified epoxy resins: modelling and characterization.* Polymer, 2000. **42**: p. 305-317.
26. Mezzenga, R., A. Luciani, and J.-A.E. Månson, *Phase separation and gelation of epoxy resin/hyperbranched polymer blends.* Polymer Engineering and Science, 2002. **42**(2): p. 249-257.
27. Kinkelaar, M., B. Wang, and L.J. Lee, *Shrinkage behaviour of low-profile unsaturated polyester resins.* Polymer, 1994. **35**(14): p. 3011-3021.
28. Huang, Y.-J. and C.-M. Liang, *Volume shrinkage characteristics in the cure of low-shrink unsaturated polyester resins.* Polymer, 1996. **37**(3): p. 401-412.

Appendix A – List of Symbols

Symbol	Unit	Meaning
a		ratio of Young's modulus of coating and substrate $(a=E_c/E_s)$
b		ratio of coating and substrate thickness $(b=h_c/h_s)$
c		thickness contraction
c_c		thickness contraction between gelation and final conversion
d		acquired and oversampled signal
e		Eulers number (2.718)
e		signal error
f	Hz	normalized frequency
f_a	Hz	true oscillation frequency
f_s	Hz	sampling frequency
g	m	deflection
h_c	m	coating thickness
$h_{c,fi}$	m	final coating thickness after UV curing
h_s	m	substrate thickness
n		sample index
n_c		refractive index of coating
n_s		refractive index of substrate
p		reaction order exponent
q		autocatalytic exponent
r	m	radius of curvature
r_c		refractive index of coating
r_e		ratio of the reflected to the incident amplitude of light
r_s		refractive index of substrate
s		thickness contraction
t	s	time
t_c	s	time, where cure is finished
t_{fab}	s	fabrication time
t_g	s	time at gelation
t_{vi}	s	time at vitrification onset
w_1		adaptive weight
w_2		adaptive weight
x		double bond conversion
x_m		maximum conversion
x_{vi}		conversion at the starting point of vitrification
y		filtered signal
$\hat{y}$		analytical signal
y_0	m	distance of the neutral axis from the y-axis
z	m	sample depth

AR		aspect ratio
AEW	$g \cdot mol^{-1}$	acrylate equivalent weight
C	mol^{-1}	constant $(c=(4/3)\ \pi N_A)$
CW	m	channel width
D_{Ch}	m	width of the smallest entirely developed channel
$DB_{Frechet}$		degree of branching (Fréchet)
DB_{Frey}		degree of branching (Frey)
DP	m	development progress
E_c	Pa	Young's modulus of the coating
E_s	Pa	Young's modulus of the substrate
FOM		figure of merit
G	Pa	shear modulus
G^*	Pa	complex shear modulus
G_r	Pa	stress relaxation modulus
I	$W \cdot m^{-2}$	light intensity
I_0	$W \cdot m^{-2}$	incident light intensity
I_m	$W \cdot m^{-2}$	intensity amplitude
I_O	$W \cdot m^{-2}$	intensity offset
K	s^{-1}	rate constant
L	m	distance between bearings
LA		length accuracy
M	$g \cdot mol^{-1}$	molecular weight
M_n	$g \cdot mol^{-1}$	number average molecular weight
N_A	mol^{-1}	Avogadro's number $(6.022 \cdot 10^{23})$
N_D		number of dendritic units
N_L		number of linear units
N_{MM}		number of minima and maxima
N_T		number of terminal units
R_{LL}	$m^3 \cdot mol^{-1}$	molar refraction
S_L		linear shrinkage
S_V		volumetric shrinkage
SF		shape fidelity
T	°C or K	temperature
T_c	°C or K	cure temperature
T_f	°C or K	final temperature at the end of cool down after cure
T_g	°C or K	glass transition temperature
T_g^∞	°C or K	ultimate glass transition temperature of the fully cured polymer
V	m^3	Volume
Y_{Hi}		Hilbert transform of y

α	$m^3 \cdot mol^{-1}$	polarizability
α_m	$m^3 \cdot mol^{-1}$	polarizability of the monomer
α_p	$m^3 \cdot mol^{-1}$	polarizability of the polymer
α_s	K^{-1}	coefficient of thermal expansion of the substrate
β_1		rate constant intensity exponent
β_2		conversion-at-vitrification intensity exponent
β_3		maximum-conversion intensity exponent
δ		phase shift
ε_t	$mol \cdot m^{-4}$	molar extinction coefficient
η	Pa·s	viscosity
μ		gradient coefficient
λ	m	radiation wavelength
λ_L	m	laser wavelength
ν_c		Poisson's ratio of the coating
ρ	$g \cdot m^{-3}$	density
ρ_m	$g \cdot m^{-3}$	monomer density
σ	$N \cdot m^{-2}$	in-plane stress
σ_i	$N \cdot m^{-2}$	internal stress
τ	s	time
χ		angle accuracy
φ		scattering angle
[M]	$mol \cdot l^{-1}$	monomer concentration
[PI]	$mol \cdot l^{-1}$	photoinitiator concentration
$\otimes$		folding

Appendix B – Resolution Pattern

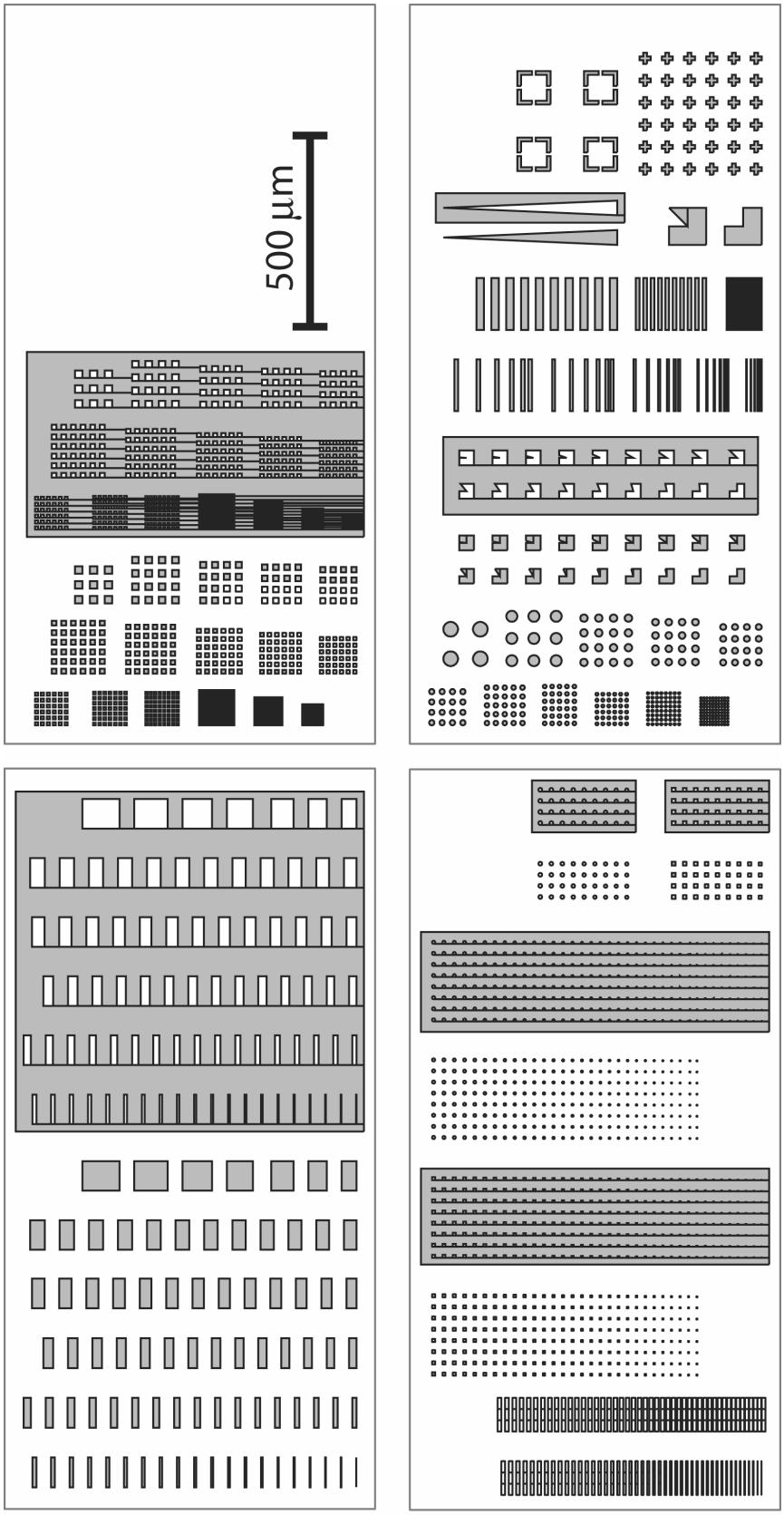

Figure A - 1 Resolution pattern – Grey surfaces will be exposed during photolithography.

Publications Related to this Thesis

Journal Papers

Schmidt L. E., Leterrier Y., Vesin J.-M., Wilhelm M., Månson J.-A. E., **"Photorheology of fast UV curing multifunctional acrylates"**, *Macromolecular Materials and Engineering*, 290 (2005) 1115-1124 (Accepted as feature publication with illustration on the journal's title page)

Schmidt L. E., Leterrier Y., Schmäh D., Månson J.-A. E., James D., Gustavsson E., Svensson L. S., **"Conversion analysis of acrylated hyperbranched polymers UV-cured below their ultimate glass transition temperature"**, submitted to *Journal of Applied Polymer Science*

Schmidt L. E., Schmäh D., Leterrier Y., Månson J.-A. E., **"Time-intensity-transformation and internal stress in UV-curable hyperbranched acrylates"**, submitted to *Rheologica Acta*

Jin Y.-H., Schmidt L. E., Leterrier Y., Cho Y.-H., Månson J.-A. E, **„Fabrication process of low-stress UV-curable hyperbranched polymers and its application to microfluidic devices"**, to be submitted to *Lab on a Chip*

Schmidt L. E., Yi S., Jin Y. H., Leterrier Y., Cho Y. H., Månson J.-A. E., **"Acrylated Hyperbranched Polymer Based Photoresist for Ultra-Thick High Aspect Ratio Micropatterns",** to be submitted

Conferences

Schmidt L. E., Leterrier Y., Schmaeh D., Månson J.-A. E., James D., **"Structural and residual stress analysis of UV curable hyperbranched acrylates"**, in *RadTech Europe*. 2005. Barcelona

Schmidt L. E., Leterrier Y., Vesin J.-M., Wilhelm M., Månson J.-A. E., **„Photorheology of fast UV curing multifunctional acrylates"**, in *Annual European Rheology Conference*. 2006, Heronisos, Greece.

Patent

Patent pending: **"Fabrication Process of Low-stress UV-curable Hyperbranched Polymers for Microfluidic Applications"**

Curriculum Vitae

Lars Erik Schmidt

Date of Birth: 19th April 1977

Nationality: German

Rue Couchirard 9

1004 Lausanne

Phone: 079 761 63 24

Email: larserik@gmx.de

Education

10/1997 – 06/2002	MSc, ETH Zürich
11/2001 – 04/2002	University of California, Santa Barbara Graduate thesis: “Superhydrophobic Alumina Covered Glass Surfaces”
08/2000 – 07/2001	Royal Institute of Technology, Stockholm Exchange student (ERASMUS scholarship)

Professional Experience

10/2002 – present	Ecole Polytechnique Fédérale de Lausanne (EPFL), Laboratory of Polymer and Composite Technology, Prof. Jan-Anders Månson Ph.D. thesis: “Low Stress Acrylated Hyperbranched Polymers”
04/2005 – 09/2005	Korean Advanced Institute of Science and Technology Research Exchange: “Microstructuring of UV curable polymer for microfluidic applications”
05/2002 – 07/2002	Alu Menziken Industrie AG Internship in Technology Department Metallurgical examinations of cast Aluminum billets